PERFORMANCE OF A BRIDGE DECK WITH GLASS FIBER REINFORCED POLYMER (GFRP) BARS AS THE TOP MAT OF REINFORCEMENT

By

Kimberly A. Phillips

Thesis submitted to the Faculty of the Virginia Polytechnic Institute and State University in partial fulfillment of the requirements for the degree of

MASTERS OF SCIENCE
In
CIVIL ENGINEERING

Carin L. Roberts-Wollmann, Chairperson

Thomas E. Cousins

John J. Lesko

December 2004
Blacksburg, Virginia

Keywords: fiber reinforced polymer (FRP) bars, bridge decks, reinforced concrete, degradation, field investigation, long-term performance

Performance of a Bridge Deck with Glass Fiber Reinforced Polymer (GFRP) Bars as the Top Mat of Reinforcement

By

Kimberly A. Phillips

(ABSTRACT)

The purpose of this research was to investigate the effectiveness and durability of GFRP bars as reinforcement for concrete decks. Today's rapid bridge deck deterioration is calling for a replacement for steel reinforcement. The advantages of GFRP such as its high tensile strength, light weight, and resistance to corrosion make it an attractive alternative to steel.

The first objective of this research was to perform live load testing on a bridge deck reinforced with GFRP in one span and steel in the other. The results were compared to the findings from the initial testing performed one year earlier. The strains and deflections of the bridge deck were recorded and the two spans compared. Transverse stresses in the GFRP bars, girder distribution factors, and dynamic load allowances were calculated for both spans. From the live load tests, it was concluded that the GFRP-reinforced span results were within design parameters. The only concern was the increased impact factor values.

The second objective was to perform live load tests on a slab reinforced with GFRP installed at a weigh station. Two live load tests were performed approximately five months apart. Peak strains in the GFRP and steel bars were recorded and compared. The peak stresses had increased over time but were within design allowable stress limits.

The third objective of this research was to investigate the long term behavior and durability of the GFRP reinforcing bars cast in a concrete deck. The strain gauges, vibrating wire gauges, and thermocouples in the bridge deck were monitored for approximately one year using a permanent data acquisition system. Daily, monthly, and long term fluctuations in temperature and stresses were examined. It was concluded that the vibrating wire gauges were more reliable than the electrical resistance strain gauges. It was further observed that the main influence over strain changes was temperature fluctuations.

Acknowledgements

I would like to extend my deepest gratitude to everyone that helped me and supported me throughout the research process. First, thank you to my advisor, Dr. Carin Roberts-Wollmann, who always had her door open and was always willing to lend a hand when I needed help. I also would like to express my appreciation towards my other two committee members, Dr. Tommy Cousins and Dr. Jack Lesko. Thank you to VDOT and VTRC for assisting me in the live load testing of the Gills Creek Bridge. The students in the SURP program also were a huge help during the live load testing at the bridge. I would like to thank all of my friends and collegues who helped me with my testing, and Brett Farmer and Dennis Huffman for their assistance with any lab work that I performed. Thank you to Matt Harlan for helping me with any questions I had about the bridge and his thesis. Thank you to Nick Amico for helping me with the live load testing performed on his weigh station slab, assisting me with questions on analyzing the data collected, and his encouragement and friendship. Thank you also to Jeremy Lucas for always giving me helpful advice, helping me with learning and operating the new data acquisition system, the CR9000, and being an incredible friend.

Lastly, I would like to thank my parents for being a never-ending source of love and encouragement all of my life. They always have believed in me. Without them, I would not have made it this far.

Table of Contents

List of Figures

List of Tables

List of Equations

Chapter 1 - Introduction

1.1 Background

Engineers are always looking for more efficient methods and materials for design. Recently, bridge designers have been faced with the challenge to remedy the increasing number of deteriorating bridge decks. According to an article from *Concrete International*, "Concrete bridge decks deteriorate faster than any other bridge components because of direct exposure to the environment, deicing chemicals, and ever-increasing traffic loads" (Benmokrane et al. 2004). In the United States, 100 billion dollars per year is wasted due to corrosion alone (Chong 1998).

One solution is the use of an increasingly popular material, fiber reinforced polymer (FRP) reinforcing bars. FRP bars are made of fibers pulled longitudinally that are held together by a resin. There are three commonly used types of fibers: glass (GFRP), carbon (CFRP), and aramid (AFRP). A new more experimental fiber material is basalt (BFRP). As a replacement for typical steel reinforcement, FRP has many advantages. It is a lighter material, so it is easier to transport and install in construction. FRP has a higher tensile strength than steel. It also is neutral to electrical and magnetic disturbances that may be caused by utilities and other elements on or near a bridge deck. Most importantly, FRP does not corrode like steel (Benmokrane et al. 2004). This makes FRP bars a nice alternative for the upper mat of reinforcement of bridge decks. Particularly in the northern states, salt and other chemicals that are used for deicing can permeate the deck and corrode the reinforcing bars. Even the freeze and thaw cycles can accelerate corrosion by causing water that gets into the cracks in the deck to freeze and expand, widening the crack and exposing the reinforcing bars to the environment.

To investigate the effectiveness and durability of GFRP bars as reinforcement for concrete decks, the Virginia Department of Transportation (VDOT) and the Virginia Transportation Research Council (VTRC) with funding provided through the FHWA's Innovative Bridge Research and Construction (IBRC) program worked with Virginia Tech to construct the Route 668 Bridge over Gills Creek located in Franklin County, Virginia. The bridge was completed in July 2003 and is pictured in Figure 1.1. The deck of one span is reinforced with GFRP bars as the top mat and steel rebar as bottom mat.

The other two spans are reinforced with steel bars as the top and bottom mat. VDOT also funded the construction and placement of a concrete deck with GFRP reinforcement in the top mat located in the roadway of a weigh station on Interstate 81 near the Troutville exit. The concrete deck at the weigh station is pictured in Figure 1.2.

Figure 1.1: Route 668 Bridge Over Gills Creek

Figure 1.2: I-81 Weigh Station Slab

The reason VDOT chose to use steel as the lower mat reinforcing (the tension side of the deck) is the uncertainties of GFRP. VDOT wanted a proven material as the bottom mat. GFRP has a low modulus of elasticity which could lead to excess deflections and cracking. There is no conclusive research on the extent of deflection and cracking that would occur in an all GFRP-reinforced concrete deck. VDOT was especially concerned with the deck's long term durability. Research has been done on durability, but only with accelerated lab testing which could have extreme results and is not truly representative of the actual conditions in the field. The long term durability of GFRP reinforced concrete decks is a serious issue that needs to be further explored to ensure the longevity of bridges.

During construction, the bridge was instrumented with devices to measure the temperature within the deck and the changes in strain of the GFRP bars. One of the all-steel reinforced spans was instrumented for comparison. The concrete slab at the weigh station also has instrumentation for measuring temperature and strain changes of the GFRP bars. The instrumentation of the two structures has been and continues to be used to perform short-term testing and long-term monitoring. Using the data collected, the changes in stress will be evaluated and compared to the design standards. Also, the long-term changes in stress will be used to identify significant changes in the deck condition or possibly reinforcing bar properties.

1.2 Objectives

1.2.1 Objective One

The first objective of this research was to perform live load testing on the Gills Creek Bridge and compare the results to the initial testing done by Matthew Harlan (Harlan 2003) one year earlier. The initial live load test was performed shortly after the pouring of the deck. The follow-up live load testing was performed approximately one year after the initial testing.

A comparison of the results gives an indication of the changes in strains the GFRP bars are experiencing and if the deck is behaving differently than when first installed. The results are compared to the design standards specified by the American Concrete

Institute (ACI) in the "Guide for the Design and Construction of Concrete Reinforced with FRP Bars" to see that the stresses in the deck are within the specified limits (2003).

1.2.2 Objective Two

The second objective was to perform live load tests on the slab reinforced with GFRP built and installed by Ross Amico on March 2, 2004 at the weigh station along Interstate 81. Live load tests were performed approximately two months and seven months after installation. The strains in the GFRP caused by the passing truck traffic were recorded. The recorded strains were converted to stresses to compare to the limits in the design standards. Only trucks that were weighed on the scales were used in the analysis. The results from the two tests were compared to detect any changes in the GFRP reinforcing bars.

1.2.3 Objective Three

The third objective of this research was to investigate the long term behavior and durability of the GFRP reinforcing bars cast in a concrete deck. To accomplish this goal, the bridge deck over Gills Creek was monitored for approximately one year using a permanent data acquisition system. The bridge deck has strain gauges, vibrating wire gauges, and thermocouples installed at specified locations within the slab. A permanent data acquisition system was also installed at the weigh station to monitor the strain gauges and thermocouples embedded in the concrete slab. The topics of interest include daily, monthly, and long term fluctuations in temperature and stresses in the bar and whether any slip or degradation of the GFRP bars may be occurring.

1.3 Thesis Organization

This thesis is organized into five chapters. Chapter 2 presents the literature review investigating previous research on FRP in bridge decks. Chapter 3 describes the materials used in the tests and the methods followed. Chapter 4 presents the results found from the two live load tests and the long-term data collection. Lastly, Chapter 5 discusses the conclusions on the durability of the GFRP reinforcing bars and recommendations for future research.

Chapter 2 - Literature Review

Although FRP does not corrode like steel, it can deteriorate due to the effects of the environment and extreme loads or conditions that are not considered in design (Chong 1998). FRP can degrade over time due to the high alkalinity and moisture content of the surrounding concrete. Accelerated methods have been developed in order to examine the long-term durability of FRP. This chapter presents an overview of the durability of the materials used in FRP, the performance of FRP cast in concrete members, and finally some research studying bridges in service that utilize FRP as reinforcement.

2.1 Materials

The durability of the materials that make up the bar is detrimental to the bar's overall resistance to deterioration. The three main types of fibers used in FRP are glass, carbon, and aramid (Benmokrane et al. 2004). The common types of resins used to bind together the fibers are isopthalic polyester, vinylester, and epoxy resins. Isopthalic polyester is not recommended for use in direct contact with Portland cement concrete since it does not protect the fibers as well as vinylester does from moisture and alkaline attack (Gentry et al. 2002).

The advantages of vinylester were shown in a study performed by Valter Dejke in Sweden (2001). Four different GFRP bars were used in the experiment: FIBERBAR (E-glass/vinyl ester), Grey bar (E-glass/vinyl ester), Yellow bar (AR-glass/vinyl ester), and Green bar (AR-glass/polyester). The bars were exposed to concrete, an alkaline solution, and water at elevated temperatures of 20, 40, 60, and 80^{o}C to accelerate the degradation process.

Table 2.1 displays the GFRP bars' strength retention after being in a saturated concrete condition at a temperature of 60^{o}C. From the results, it can be concluded that the GFRP bars with E-glass and vinyl ester are more durable than the other bars tested. For the GFRP bars with the E-glass and vinyl ester, the fibers have less resistance to the environment than the polymer matrix. In fact, the GFRP bars that had an undamaged outer polymer layer did not display any alkali ingress. This suggests that if the polymer layer remains intact, it could serve as a barrier to the adverse environmental conditions

that cause the fibers in the GFRP to deteriorate. It was also noted that the modulus of elasticity of the bars was not significantly reduced from the adverse environment.

Table 2.1: GFRP Strength Retention

	Tensile strength retention (after 1.5 years)	Interlaminar shear strength retention (after 1.0 years)
FIBERBAR	41%	90%
Grey bar	57%	96%
Yellow bar	45%	37%
Green bar	53%	0%

Porter and Barnes also investigated GFRP reinforcement durability (1998). They accelerated the aging process by exposing the glass fiber to a high pH (12.5-13.0) in a water bath to simulate concrete porewater for two to three months, the equivalent of 50 years in the field. The porewater was at high temperature of 60^{o}C. Polyester and vinyl ester resin was used. The bars that were submerged for 19 days had a 29.0 to 60.7 % loss in tensile strength, and bars submerged for 81 days had 47.6 to 65.8% loss in tensile strength. It was concluded that the accelerated processes may be too severe to accurately model the actual behavior of GFRP in concrete structures and needs to be verified in long-term conditions.

The materials used in FRP were examined in the first two steps of a five step program conducted by Clarke and Sheard (1998). First, they worked to optimize the materials used in the rebar itself, particularly the resin used to bind together the fibers. Second, the durability of the rebar was then tested using an accelerated method of immersing the FRP in a simulated concrete pore fluid solution with a pH of 13.5. Temperatures of 20, 50, and 80^{o}C were used. Duration of immersion, effect of pH, effect of temperature, influence of stress, and effect of ionic content of the solution were the five variables examined. This test was run for two years. It was found that the carbon rebar was affected more by the alkaline environment. Accelerated tests on reinforced concrete showed no significant deterioration of the reinforcement. A microscopic examination of the FRP showed no damage from corrosion, and a chemical analysis of the FRP showed no leaching out of metallic ions from glass reinforced bars indicating it had withstood the alkaline solutions.

The studies described are just a few of the many studies performed on FRP reinforcing bars. Bhise (2002) summarizes the durability results from 9 authors of the testing of GFRP (E-glass) bars under an unstressed condition. Each used a variation of vinyl ester, polyester, or both as the resin and some kind of alkaline solution. The pH ranged from 11 to 13.5 with an average pH of approximately 12.6. The duration of the saturation process ranged from 21 to 203 days and temperatures were from 20 to 80°C. The strength reduction was as high as 53% but was mostly around 20-30%.

Bhise's findings indicate that there is no standardized method for testing durability of GFRP, making it difficult to compare the results from different researchers. The results did indicate that the GFRP bars experienced significant degradation, especially more with the polyester resin than the vinyl ester resin. The strength degradation of the GFRP bars follows an Arrhenius relationship (Bhise 2002). The Arrhenius model assumes that with increased temperature, the rate of a given chemical degradation is accelerated using the following equation:

$$r(T) = Ae^{\frac{-E_{act}}{RT}} \qquad \textbf{Equation 2-1}$$

where r is the rate of degradation, T is the temperature in Kelvin, and A, E_{act}, and R are constants (Gentry et al. 2002).

In terms of the moisture absorption of the bars, the initial weight gain of the GFRP bars exhibited a Fickian behavior and the long-term exposure resulted in non-Fickian behavior (Bhise 2002). The diffusion of moisture is Fickian if the heat transfer can be described by Fourier's law, the moisture diffusion is a form of Fick's law, energy (Fourier) and mass transfer (Fick) equations are decoupled, and thermal conductivity and mass diffusivity are depend only on temperature and are independent of the stress levels in the core or moisture concentration. Fourier's law is

$$\rho C \frac{\partial T}{\partial t} = \frac{\partial}{\partial x} K_x \frac{\partial T}{\partial x} \qquad \textbf{Equation 2-2}$$

where ρ is density, C is specific heat, T is temperature, t is time, x is distance, K_x is thermal conductivity. Fick's law is

$$\frac{\partial c}{\partial t} = \frac{\partial}{\partial x} D_x \frac{\partial c}{\partial x} \qquad \textbf{Equation 2-3}$$

where c is moisture concentration, D_x is the diffusion coefficient, x is distance, and t is time. The diffusion is non-Fickian when there are cracks in the material or delamination leading to an altered structural representation or the moisture propagation is dominated by the fiber-matrix interface (Vijay et al. 1998).

2.2 FRP Performance in Concrete

The third step in Clarke and Sheard's program was to test concrete reinforced with the FRP bars (1998). Pull out strengths were measured. The variables of the test included three levels of alkalinity and temperatures of 20 and 38^{o}C. Each specimen was also subjected to wet and dry cycles, a high chloride content, and carbonation. The rebar tested was reinforced with 1st Generation glass and aramid and 2nd Generation glass and carbon. Second generation glass was developed through a quality control program making it a more reliable and consistent material. Field testing on laboratory specimens was performed to compare to the testing done in the laboratory. Finally, four structures were constructed with FRP reinforcing to see the effects of the environment on the FRP.

The results of the testing showed a reduction in bond strength after two years. The specimens from the site exposure showed no sign of corrosion. Testing on the four structures had not been performed at the time the research had been published (Clarke and Sheard 1998).

To examine the cause of bond degradation, Nanni et al. (1998) also performed accelerated degradation tests. They focused on two causes of bond degradation: sustained loading (mechanical conditioning) and exposure to alkaline solutions (environmental conditioning). Concentric pullout testing was used to determine the effects of the conditioning. For the environmental conditioning, they conditioned the bars in two different ways: one by saturating the naked bar with a calcium hydroxide solution and the other by casting the unconditioned bar in concrete and then immersing the entire specimen in the solution. It was found that the sustained loading conditioning did not accelerate the deterioration of the FRP-concrete bond, but the exposure to the alkaline environment did. It was further concluded that the FRP degradation due to its environment is not easily modeled. With increased temperatures, the degradation was

more severe (lower pullout strengths). Finally, the carbon/vinyl ester rods were more resistant to the environmental conditioning and had higher shear stiffness than the glass/vinyl ester rods.

To compare the performance of FRP bars versus steel bars, ten full-size concrete slabs were tested by Salakawy and Benmokrane (2004). Five of the slabs had GFRP reinforcing bars, three had CFRP bars, and two had steel bars. Four-point bending tests were performed with a clear span of 8.20 ft that was simply supported. The GFRP bars had fiber content of 73% (by weight) with a vinyl ester resin. The average ultimate tensile strength of the bars was 86.6 ksi, and the average modulus was 5800 ksi. The GFRP-reinforced slabs had No. 16 bars. Electrical resistance strain gauges were installed on the reinforcement bars and on the concrete surface at midspan. Deflections at midspan were measured with two linear variable differential transformers (LVDTs) on either side of the slab.

Each slab was loaded until failure. The slabs reinforced with GFRP (0.18 to 0.26 in.) had more deflection than the CFRP slabs (0.15 to 0.25 in.). The steel-reinforced slabs had slightly less deflection (0.13 to 0.19 in.). The strains in the FRP-reinforced slabs varied linearly after cracking until failure. However, the maximum measured strains never reached the ultimate strains of the FRP bars. It was discovered that the number of cracks, crack spacing, crack penetration depth, and crack width of the GFRP slabs were similar to the steel slabs. The FRP slabs experienced shear failures; however, in the steel slabs the steel yielded and the concrete crushed. For FRP, an increase of reinforcement ratio decreased the strains in the bars and the concrete. Specifically for GFRP, a larger reinforcement ratio increased the flexural stiffness of the slab.

Long-term deflections of GFRP-reinforced concrete beams were examined by Hall and Ghali in 2000. Their main objective was to determine if the long-term deflection prediction methods used for steel could be applied to FRP. Four concrete beams were loaded at the third points: two reinforced with GFRP and two reinforced with steel. Each beam was 11 in. wide, 7 in. thick, and 11 ft-6 in. long with a simply supported span of 10 ft-6 in. The beams were subjected to a sustained load for approximately 8 months. It was determined that GFRP-reinforced concrete beams deflect 1.7 times more than steel due to the long-term effects of creep and shrinkage.

Temperature effects were investigated by Elbadry et al. in 2000. Three different types of stresses that develop in the concrete due to temperature were examined: self-equilibrating stresses, continuity stresses, and stresses due to the transverse thermal expansion of the reinforcing bars. Self-equilibrating stresses are caused by the reinforcing bars having a different coefficient of thermal expansion than the concrete and by uneven distribution of temperature. Fortunately, GFRP has a very similar longitudinal coefficient of expansion to concrete (≈10-11 με/°C). Continuity stresses are caused by the concrete member ends being restrained externally. Finally, stresses can result from the difference in transverse coefficients of thermal expansion between the bars and the concrete. The transverse coefficient for GFRP is 5 to 8 times greater than that of concrete.

Seven concrete beams were tested using different thermal gradients. Three of the beams were reinforced with GFRP (E-glass/polyester) and two with CFRP. The other two beams were reinforced with a hybrid of four different fiber types: E-Glass, Carbon, Aramid, and a combination of Carbon and E-Glass. The tests were compared to prior testing of steel-reinforced concrete beams. End moments were applied to the beam to cause initial cracking. Heat bulbs were placed on one side of the beam to cause a thermal gradient. The temperature was increased steadily to the highest temperature of 160^{o}C. The cool face was 40^{o}C, resulting in a temperature difference of 120^{o}C.

It was determined that the GFRP-reinforced concrete beams displayed high bursting stresses in the concrete near the GFRP bars at high temperatures. This is due to the high transverse coefficient of thermal expansion of GFRP. The stresses cause the bond between the concrete and GFRP to weaken leading to lower tension stiffening in the concrete and higher deflections. The CFRP performed better than the GFRP and steel. The crack widths of all the specimens displayed no significant differences.

2.3 Long-term Monitoring

To determine long-term performance of FRP, four bridges were reinforced with FRP bars (Benmokrane et al. 2004). One had CFRP grids as the top reinforcement layer and steel as the bottom. Two of the bridges had GFRP bars at the top and CFRP bars at the bottom. The final bridge had GFRP bars at the top and the bottom. The bridges were

instrumented with fiber optic sensors (FOS) to collect internal temperature and strain data.

The first three bridges were live load tested with both dynamic and static field tests. Maximum strains in the FRP, steel reinforcement, and the concrete were measured. Gauges were placed in the concrete at both the top and bottom layer of reinforcement. The concrete gauges displayed only a 12 με change. The concrete surface strains at the top and bottom could be calculated as a maximum of 10 and 25 με, respectively. There was a strain change of 4 με in the top GFRP bars and 18 με in the bottom CFRP bars of the two bridges (less than 0.16% of ultimate strain of the material). As expected, the strains decreased when further away from the wheel load. The strain changes in the steel bars at top and bottom were 4 με and 14 με, respectively. The deflections of the bridge deck and girders were less than 0.2 and 0.4 in., respectively.

After testing, the bridges were monitored using a fiber optic sensor data acquisition system using a modem and a phone line. After five years of monitoring, it was concluded that "temperature is the most prominent factor influencing strain variation in the bridge deck." The range of strain change recorded for the bridge with CFRP and steel was -520 to 440 με. One of the bridges with GFRP and CFRP ranged from -420 to 360 με. These strains from temperature changes were 25 to 30 times that induced by the truckloads (3 to 4% ultimate strain of the material). It was noted, however, that deck slabs are still designed for wheel loads since thermal strains are independent of slab thickness or reinforcement ratios.

From the field tests and long-term monitoring, it was concluded that concrete deck reinforced with FRP bars had similar serviceability to a typical steel-reinforced slab. The bridges showed no signs of additional cracking during severe service conditions such as the use of deicing salts, freeze-thaw cycles, and times of high temperatures and heavy traffic loads. Overall, FRP bars could be a competitive material against steel reinforcing bars.

Chong (1998) referred to a futuristic composite bridge that included an ultraviolet protective coating, dampers, a deck that uses geothermal energy to deice the deck, and structural controls. The control systems in the bridge could be used to reduce vibration and fatigue due to the lighter weight of the composites compared to traditional concrete

or steel. The bridge had monitoring devices such as data acquisition and processing systems, wireless sensors, and optical fiber sensors. A complete system incorporating all of these elements would take decades to develop. However, some of these concepts are already in use such as optical fiber sensors, and others could become more common in the near future.

Bradberry (2001) determined the structural design of a concrete bridge deck with FRP as the top mat of reinforcement. The 8 in. thick deck is supported on prestressed concrete Type C beams and is designed for self-weight, bridge rails, overlay, HS20 wheel loading, and bridge rail impact loads. AASHTO distribution formulas were used to analyze the continuous beam. Bradberry's design was used to construct the deck of the Sierrita de la Cruz Creek Bridge in Potter County, Texas. The bridge was 45.3 ft wide, allowing for 2 lanes of traffic and 10 ft shoulders on either side. The bridge was 553 ft long. It has seven 79 ft prestressed concrete Texas Type C-beam spans. The north end has 2 spans. The middle has 3 spans with epoxy-coated steel reinforcing bars in the deck, and the south end has 2 spans with a top mat of GFRP reinforcing bars and a bottom mat of epoxy-coated steel reinforcing bars (Bradberry 2001).

Harlan (2004) discussed the live load testing of the Sierrita de la Cruz Creek Bridge. The testing was performed by Bice et al. (2002). Two spans were instrumented, one with all steel bars and one with the GFRP bars as to the top mat of reinforcement. The bridge was live load tested after approximately one year of service. Dump trucks weighing about 54 kips each were provided by the Texas Department of Transportation to load the deck. Testing was performed using one and two truck loadings. Unfortunately, no data was collected from the strain gauges due to vandalism of the gauges. However, it was observed that no new cracks had formed after one year of service, and the old cracks had not propagated when the load was applied. The present cracks were concluded to be shrinkage cracks. It was also observed that there was a longitudinal crack down the center of the GFRP-reinforced span that was not present in the all steel-reinforced span. This may indicate that the GFRP span was more flexible than the steel span. The longitudinal crack did not propagate or widen with the live load tests (Harlan 2004).

2.4 Conclusions and Recommendations

From the research discussed in this review, GFRP is becoming an increasingly attractive alternative to steel for reinforcing concrete bridge decks. GFRP's resistance to corrosion and strength makes it especially good for use in the top mat of reinforcement where the more adverse environmental conditions are present. However, GFRP is still a new material leaving questions about its long-term strength and durability.

Accelerated tests have been performed on the GFRP bar alone and on GFRP bars embedded in concrete. In order to attempt to model 50 years of service in a short period of time, conditioning much more extreme than what a bridge deck experiences was used. Attempting to create the same type of degradation in a short period of time that typically takes years to develop cannot guarantee accurate results. Testing in the lab of concrete beams shows that GFRP is a favorable material and that properly designed concrete members reinforced with GFRP behave similarly to steel-reinforced members. Research in the field needs to be carried out to ensure these results carry over in real-life applications. With the limited long-term monitoring of GFRP-reinforced bridge decks in service, more data needs to be collected to investigate GFRP's behavior over time and to verify the degradation models developed by researchers.

Particularly interesting is the effect temperature has on GFRP bars in concrete. Longitudinally, the GFRP should behave better than steel since it has a similar thermal coefficient to concrete. However, transversely, the stresses from the large difference in coefficients could cause problems. From the long-term testing, temperature was shown to be the main cause of strain in the reinforcing bars in concrete. The effects of temperature on structures must be determined.

This thesis investigates the long-term performance of GFRP-reinforced bridge decks when in service through live load testing and daily monitoring. This research will give a better understanding of the durability of GFRP and its feasibility of use as reinforcement in concrete bridge decks.

Chapter 3 - Methods and Materials

3.1 Introduction

Two structures were tested and monitored to investigate the long-term behavior and durability of GFRP reinforcing bars in concrete decks. The instrumentation and layout of the Gills Creek Bridge and the I-81 weigh station slab and the testing procedures are described in this chapter.

3.2 Route 668 Bridge Over Gills Creek

The Route 668 Bridge is a steel girder bridge comprised of five W27x94 Grade 50 hot-rolled sections supporting each end span. Each girder is spaced center-to-center at 6 ft 6 in. The dimensions of the bridge deck over Gills Creek are shown in Figure 3.1. Span A is at the south end of the bridge. The two end spans are 45 ft in length with the center span measuring 80 ft in length for a total of 170 ft. The bridge's total width is 30 ft 4 in. The construction of the bridge is described by Harlan (2004).

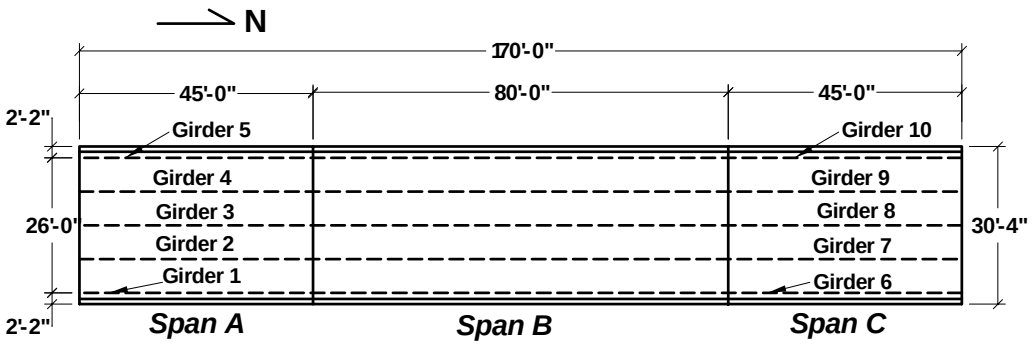

Figure 3.1: Plan View of Gills Creek Road

3.2.1 Bridge Deck Instrumentation and Layout

The bridge deck is reinforced concrete with a minimum thickness of 8 in. between the girders and 9 in. at the overhangs. Spans B and C have a top and bottom mat of epoxy-coated steel reinforcing bars. The longitudinal bars are No. 4 steel bars, and the transverse bars are No. 6 steel bars. Span A has a top mat of GFRP bars and a bottom mat of steel bars. The bottom mat of Span A is the same as the other two spans with No. 4 and No. 6 steel bars. The top mat is comprised of all No. 6 GFRP bars. The design

minimum concrete cover to the center of the bar is 2 ¾ in. for the steel bars and 2 in. for the GFRP bars.

3.2.1.1 Span A

Span A was instrumented with electrical resistance (ER) strain gauges, vibrating wire (VW) gauges, and thermocouples. The layout of the instrumentation can be seen in Figure 3.2. The lead wires of all the gauges and the thermocouple wires run through an access hole in the metal deck form and through a PVC pipe for easy accessibility for testing. All of the gauges and thermocouples were monitored with a permanent datalogger, and the ER strain gauges were used for the live load testing.

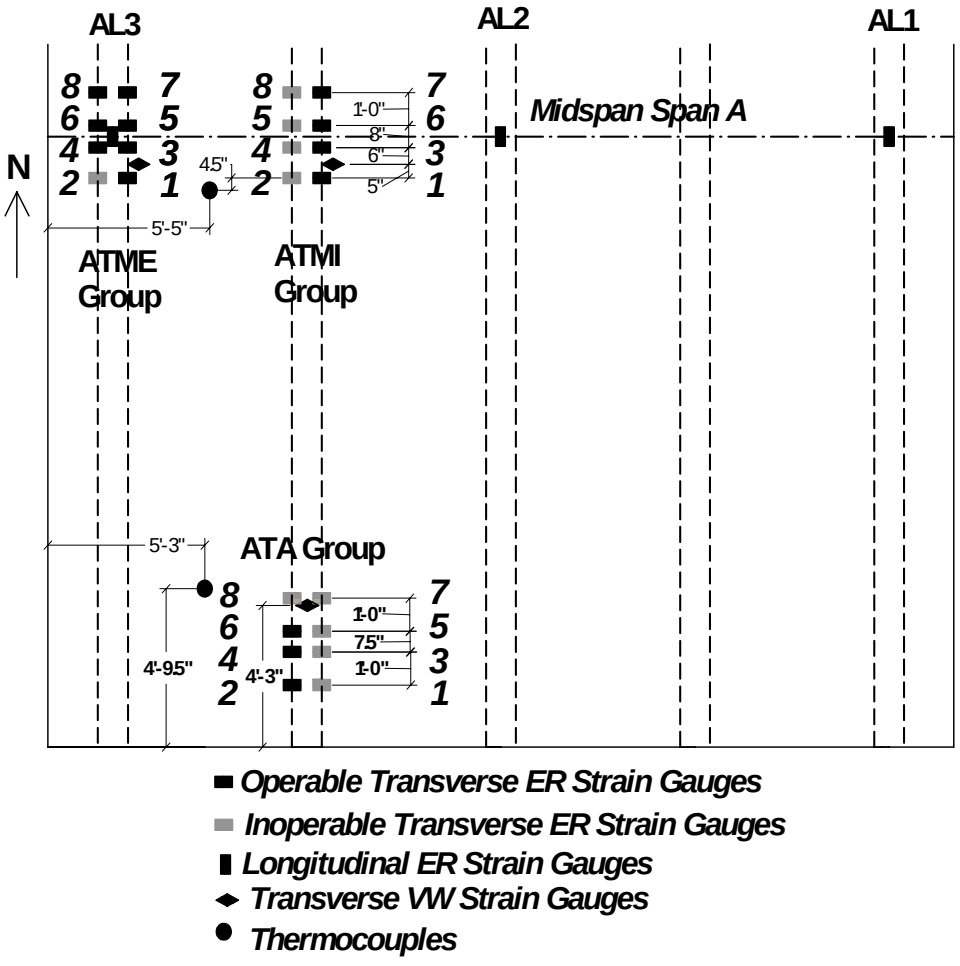

Figure 3.2: Span A Instrumentation Plan

3.2.1.1.1 Electrical Resistance Strain Gauges

Span A was instrumented with four sets of ER strain gauges. All of the gauges were applied to the top mat of GFRP reinforcement.

The first group was located near the south abutment above the first interior girder. Four transverse bars were gauged with two gauges, one at each side of the top flange of the steel girder, for a group total of eight ER strain gauges. These eight gauges were labeled ATA1 through ATA8 representing the location of Span 'A' on the 'T'ransverse bars at the 'A'butment.

The second group was located at the midspan of Span A above the first interior girder. Similar to the first group, four transverse bars were gauged with one gauge at each side of the top flange of the girder, totaling to eight ER strain gauges. These gauges were labeled ATMI1 through ATMI8 representing the location of Span 'A' on the 'T'ransverse bars at the 'M'idspan 'I'nterior girder.

The third group was located over the exterior girder at midspan. The same bars as the second group were gauged at the edges of the exterior girder's top flanges. These gauges were labeled ATME1 through ATME8 representing the location of Span 'A' on the 'T'ransverse bars at the 'M'idspan 'E'xterior girder.

The fourth set was applied to the upper mat longitudinal bars of Span A at midspan. There were three gauges, one located above each exterior girder and one located above the center girder. These gauges were labeled AL1 through AL3 representing the location of Span 'A' on the 'L'ongitudinal bars.

3.2.1.1.2 Vibrating Wire Strain Gauges

Vibrating wire (VW) strain gauges were also installed in the bridge deck. VW gauges are more accurate and last longer than ER strain gauges, however they are also more expensive. Due to the higher expense, only two VW gauges were placed at three critical locations: the first interior girder at the abutment, the first interior girder at the midspan, and the first exterior girder at the midspan of the bridge.

At each location a gauge was installed at the top mat and the bottom mat. The strains measured by the top mat VW strain gauges are compared to the strains measured by the ER strain gauges in the Results section. The strains measured by the bottom mat VW strain gauges are used to determine the location of the neutral axis of the deck to see

if the deck is cracked. The VW gauge at the abutment on the top mat is labeled VAT representing the 'V'ibrating wire gauge located at the "A'butment on the 'T'op mat. Similarly, the gauge at the abutment on the bottom mat is labeled VAB. The gauges at the midspan over the interior girder are labeled VMIT and VMIB, and the gauges at the midspan over the exterior girder are labeled VMET and VMEB with the 'T' and the 'B' indicating the top and bottom mat, respectively.

3.2.1.1.3 Thermocouples

Thermocouples are located over the interior girder at the abutment and at midspan. At each location there is a thermocouple located at the top mat of reinforcement, the bottom mat of reinforcement, and in between the two mats. The thermocouples are used to monitor the temperatures within the bridge deck. The thermocouples are labeled TAT, TAM, TAB, TMT, TMM, and TMB. Each label indicates the instrumentation type ('T'hermocouple), location over the interior girder ('A'butment or 'M'idspan), and the location within the deck ('T'op, 'M'iddle, or 'B'ottom).

3.2.1.2 Span C

Span C was instrumented with only ER strain gauges. The layout of the instrumentation can be seen in Figure 3.3. Just like Span A, the lead wires of the gauges are easily accessible through an access hole in the metal deck form. The strain gauges were used for live load testing. Span C was not monitored by a permanent datalogger.

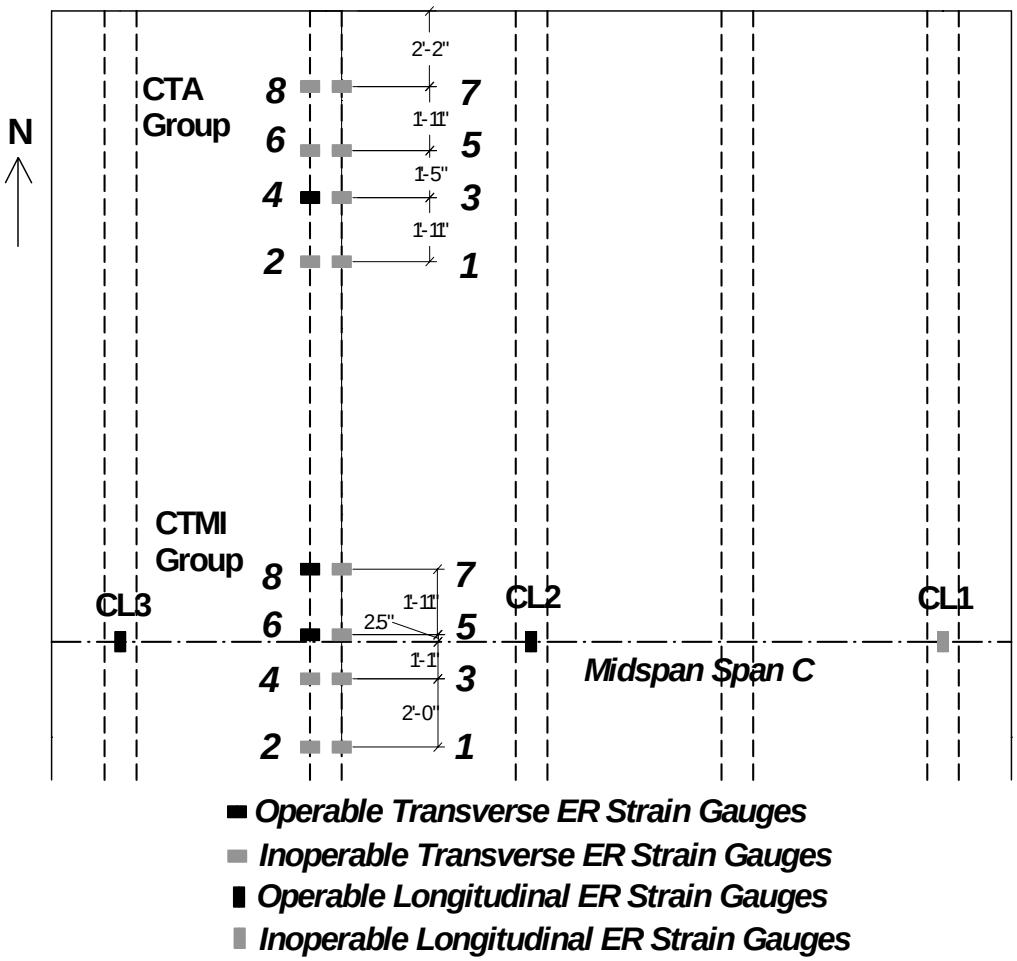

Figure 3.3: Span C Instrumentation Plan

3.2.1.2.1 Electrical Resistance Strain Gauges

Span C was instrumented with three sets of ER strain gauges. All of the gauges were applied to the top mat of steel reinforcement.

The first group was located near the north abutment above the first interior girder. Four transverse bars were gauged with one gauge at each side of the top flange of the steel girder, for a group total of eight ER strain gauges. These eight gauges were labeled CTA1 through CTA8 representing the location of Span 'C' on the 'T'ransverse bars at the 'A'butment.

The second group was located at the midspan of Span C above the first interior girder. Similar to the first group, four transverse bars were gauged with one gauge at each side of the top flange of the girder, totaling to eight ER strain gauges. These gauges

were labeled CTM1 through CTM8 representing the location of Span 'C' on the 'T'ransverse bars at 'M'idspan.

The third set was applied to the upper mat longitudinal bars of Span C at midspan. There were three gauges, one located above each exterior girder and one located above the center girder. These gauges were labeled CL1 through CL3 representing the location of Span 'C' on the 'L'ongitudinal bars.

3.2.2 Test Preparation Procedures

A truck-mounted under-bridge inspection platform, or Moog, was used to provide easy access to the underside of the superstructure. VDOT provided the inspection platform, testing truck, and traffic control for the two days of setting up and live load testing.

On the date of testing, each ER strain gauge in the bridge deck was tested with a voltmeter to see that it still had 350 ohms of resistance, indicating it was working properly. For Span A, the following seventeen strain gauges were in working condition at the time of testing and were connected to the mobile data acquisition system for recording: ATME1, ATME3, ATME4, ATME5, ATME6, ATME7, ATME8, ATMI1, ATMI3, ATMI6, ATMI7, ATA2, ATA4, ATA6, AL1, AL2, and AL3. For Span C, the following five strain gauges were connected to the mobile data acquisition system: CL2, CL3, CTA6, CTA8, and CTM4.

3.2.2.1 Bridge Girder Instrumentation

3.2.2.1.1 Electrical Resistance Gauges

Each steel girder of Span A and C had strain gauges applied to the top of the bottom flange at midspan. An ER gauge is pictured in Figure 3.4. These gauges were the same type of gauge installed in the deck on the epoxy-coated steel reinforcing bars. The strains recorded by the strain gauges were used to calculate the girder distribution factors and the dynamic load allowances. ER strain gauges were not applied on the top flange as in the previous test because the data collected from the top flanges did not provide very useful information.

Figure 3.4: ER Strain Gauge on Steel Girder

For the previous live load test, the researcher had gauged the middle girder and two exterior girders. A voltmeter was used to see if the previous gauges were still operable and could be reused for the live load test. After investigation, it was determined that none of the strain gauges could be used for the test, so they were removed. New gauges were installed using the same procedure as recommended by the manufacturer. Insulated lead wires were soldered to the gauges and were run to the mobile data acquisition system. A minimum amount of weatherproofing was applied since the gauges were only to be used for the live load testing that occurred in one day.

3.2.2.1.2 Deflectometers

Deflectometers were clamped to the bottom flange of each girder at the midspan of Spans A and C. A deflectometer is pictured in Figure 3.5. The deflectometers used were the same as the ones used in prior testing for other projects. They are made of an aluminum plate between two thicker aluminum plates. The cantilevered plate in the middle is gauged with four strain gauges that are weatherproofed. At the end of the cantilevered plate is a metal loop. The metal loop was attached to a weight at ground level with wire, to pre-deflect the deflectometer approximately one inch before the

testing. The pre-deflection caused a strain in the top of the plate. When the truck ran over the bridge causing the girders to deflect, the decrease in strain was measured and converted to a corresponding deflection. The deflectometers are connected to the mobile data acquisition system using shop-installed plugs. During each test, the deflection of the girder was recorded.

Figure 3.5: Deflectometer Clamped to Steel Girder

The deflectometers were calibrated in the Structures Lab at Virginia Polytechnic Institute and State University. The calibration was performed by deflecting the deflectometer at exact amounts measured by an exact length measuring device to determine what factor needed to be input into the mobile data acquisition system to have the correct deflections be recorded in the field. The deflections recorded by the deflectometers were used to calculate the bridge design parameters, girder distribution factors and dynamic load allowance, for both Span A and C.

3.2.2.1.3 Weigh-In-Motion Gauges

Weigh-in-motion (WIM) gauges were also clamped to each steel girder at the midspan of Spans A and C, except girder 6. Figure 3.1 shows the numbering system of the girders. Girder 6 was not instrumented because only nine WIM gauges were

available for use. The WIM gauges were also used to calculate the girder distribution factors and dynamic load allowance for Spans A and C. The results were compared to those of the deflectometers and the ER strain gauges to see if the WIM gauges had similar results. WIM gauges are easier to install than ER strain gauges, so it would be optimal to be able to use only WIM gauges in future testing. The WIM gauges were clamped to the underside of the bottom flange of each girder. Each gauge had a short cable already attached to it. Longer cables were used to connect the short cables to the mobile data acquisition system. The WIM gauges were supplied by VTRC.

3.2.2.2 Data Acquisition

The bridge girder instrumentation and the ER strain gauges located in the bridge deck were connected to a mobile data acquisition system for the live load testing. The system was the Megadac 3108 AC data acquisition system from Optim Electronics. The Megadac was housed in a large cargo van that was located at the approach of the bridge in the northbound lane during testing.

When testing Span A, the cargo van was parked on the south abutment of the bridge. The 17 working ER strain gauges in the bridge deck, 5 ER strain gauges on the steel girders, 5 deflectometers, and 5 WIM gauges were connected to the Megadac. Figure 3.6 shows the Megadac with the gauges and deflectometers wired to it. Before testing, the readings were checked to confirm that the instrumentation was connected correctly and any problems were corrected. Once all of the instrumentation had reasonable readouts, the readings were zeroed and the tests executed.

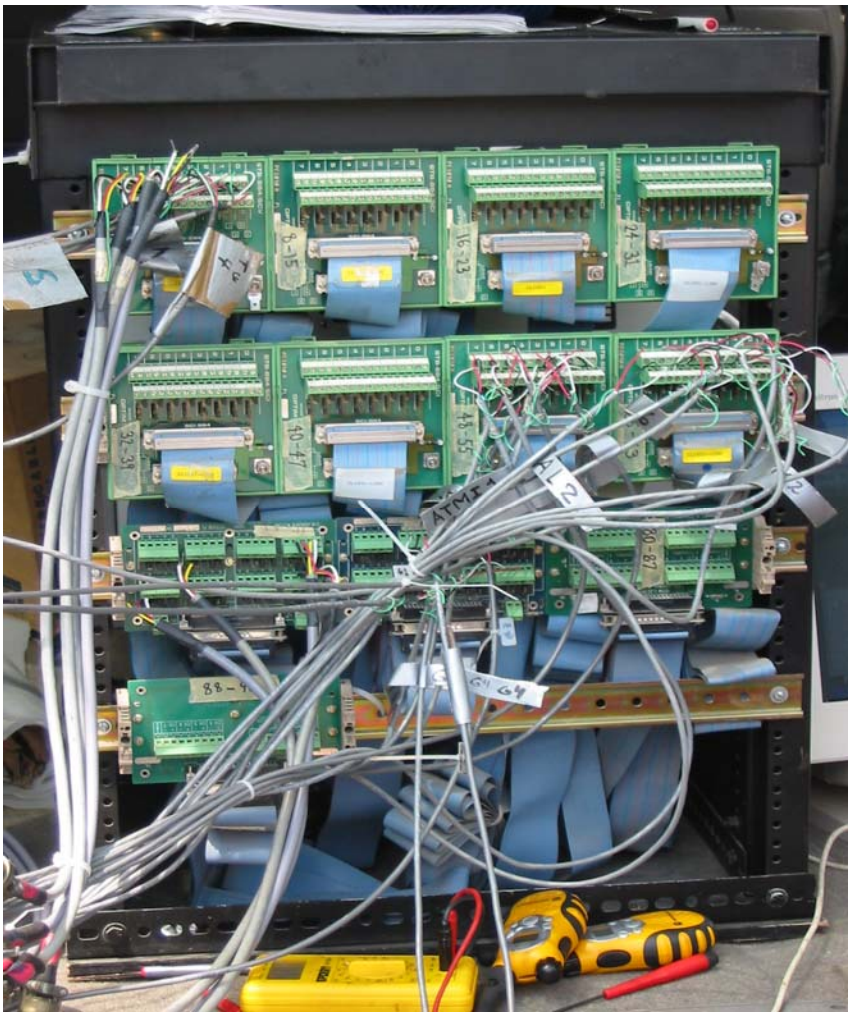

Figure 3.6: Megadac

When testing Span C, the cargo van was parked on the north abutment of the bridge. The 5 working ER strain gauges in the bridge deck, 5 ER strain gauges on the steel girders, 5 deflectometers, and 5 WIM gauges were connected to the Megadac. As with Span A, the readings were checked before testing to ensure proper connections were made. The readings were then zeroed and the tests executed.

3.2.3 Live Load Testing

Live load testing was performed on the Gills Creek Bridge on June 17, 2004, approximately one year after the initial live load testing was performed by Matthew Harlan.

3.2.3.1 Truck Description

A dump truck from VDOT was used for the live load testing of the bridge deck. It was the same truck used for the live load testing of the bridge one year prior. The truck was loaded with stone at a quarry. The front axle of the truck weighed 13.52 kips and the rear axle weighed 36.32 kips. The rear axle consisted of two axles, so the weight was assumed to be split between the two. The front wheels measured 6 ft-9 in. center-to-center and 7 ft-10 in. out-to-out. The rear wheels measured 6 ft center-to-center and 8 ft-4 in. out-to-out. The distance between the first and second axle was 14 ft-10 in. and between the second and third axle was 4 ft-5 in. The dump truck is pictured in Figure 3.7.

Figure 3.7: VDOT Dump Truck used for Live Load Testing

3.2.3.2 Truck Orientations

All testing was performed in the southbound lane of traffic on the bridge. There were two truck orientations. One was with the truck's front axle wheel over the exterior girder. A line was marked one foot from the face of the parapet (25.5 in. from the edge of the deck) to indicate the center of the exterior girder. This orientation was chosen in the initial live load test to load the overhang as much as possible. The truck was positioned as close as it can safely get to the edge. Although this orientation did not

result in the greatest effect on the overhang, it did create the greatest effect on the exterior girder.

The second orientation was with the truck straddling the first interior girder. A line was marked 4 ft from the face of the parapet to indicate the location of the front wheel of the truck. This position created the greatest effect on the first interior girder.

3.2.3.3 Quasi-Static and Dynamic Tests

The quasi-static test had the truck moving just fast enough to prevent any jerky or unsteady movements. This test represented a static loading on the bridge. A test was characterized by the VDOT truck crossing the span of interest as the strains and deflections were recorded by the mobile data acquisition system. After crossing the span, the truck would stop and cross back over the span in reverse to get the readings for the next test.

For the dynamic test, the truck started about 300 ft away from the bridge and built up a speed of approximately 50 mph when it crossed the bridge. This was the fastest safe speed at which the overloaded truck could travel. After crossing the bridge, the truck turned around and crossed the bridge going the opposite direction.

The following information was recorded for each test:

- Data set number
- Direction that the truck was traveling (northbound or southbound)
- The orientation of the truck (exterior or interior)
- The speed of the truck (assumed to be zero for the quasi-static testing)

3.2.3.4 Test Sequence

Span A was tested first. The cargo van with the Megadac located in the back was pulled up to the abutment at Span A in the northbound lane. It was oriented with the back towards the bridge to easily connect the lead wires for the strain gauges, deflectometers, and WIM gauges. After connecting the instruments, the system was balanced. Three sets of tests were run for Span A. The first set was a quasi-static test over the exterior girder. The second set of tests was a quasi-static test over the first interior girder. The final set of tests was a dynamic test over the first interior girder. The dynamic test could only be done on the exterior girder since the girder is located too close

to the parapet to be safely driven on at high speeds. The number of tests run for Span A is the following:

- Quasi-static exterior truck orientation – five tests
- Quasi-static interior truck orientation – six tests
- Dynamic interior truck orientation – six tests

After running the live load tests on Span A, the cargo van was moved to the northern abutment to test Span C. The instruments were connected and the system balanced. Span C was tested in the same order as Span A, resulting in the following number of tests:

- Quasi-static exterior truck orientation – five tests
- Quasi-static interior truck orientation – five tests
- Dynamic interior truck orientation – six tests

Upon completion of the tests, all of the instrumentation was disconnected from the Megadac. The wires for the ER strain gauges in the bridge deck were reconnected to the longterm data acquisition system. The deflectometers and WIM gauges were disconnected from the girders and kept for later use. The ER strain gauges located on the bottom flanges of the girders were left in place.

3.3 I-81 Weigh Station Slab

The weigh station slab is located along Interstate 81 near the Troutsville exit. This site was chosen since the tractor trailers coming to be weighed provide high loads and therefore, high stresses in the deck. The slab was installed in a test pit in the ramp leading to the scales. It is bolted to three steel girders that hold it in place. The slab is the second of a series of concrete slabs designed, constructed, and installed at the weigh station by Ross Amico. The slab is 5 ft in length running along the direction of traffic. It is 15 ft-3 in. wide. The design and construction of the decks are described in the research by Amico (2005).

3.3.1 Slab Instrumentation and Layout

The weigh station slab was designed to match the Gills Creek Bridge, with the same bar sizes and spacing and same girder spacing. The only difference between the two is the slab thickness. The weigh station deck is reinforced concrete with a varying

thickness to make the roadway level. It has a minimum thickness of 6 7/8 in. and a maximum thickness of 7 5/8 in. The design of the weigh station slab matches the Gills Creek bridge with the same bar sizes and spacing and same girder spacing. The only difference is the slab thickness. The top mat of reinforcing bars is GFRP and the bottom mat is steel. The top mat is comprised of No. 6 GFRP bars both transversely and longitudinally, and the bottom mat is comprised of No. 6 steel bars transversely and No. 4 steel bars longitudinally. The minimum concrete cover for the GFRP bar is 2 in. to the center of the bar.

The deck was instrumented with ER strain gauges and thermocouples. The layout of the instrumentation can be seen in Figure 3.8. All of the gauges were applied to transverse bars. The lead wires of all the gauges and the thermocouple wires run through a pipe into a hole that is easily accessible for testing. All of the gauges and thermocouples were monitored with a permanent datalogger, and the ER strain gauges were used for the live load testing.

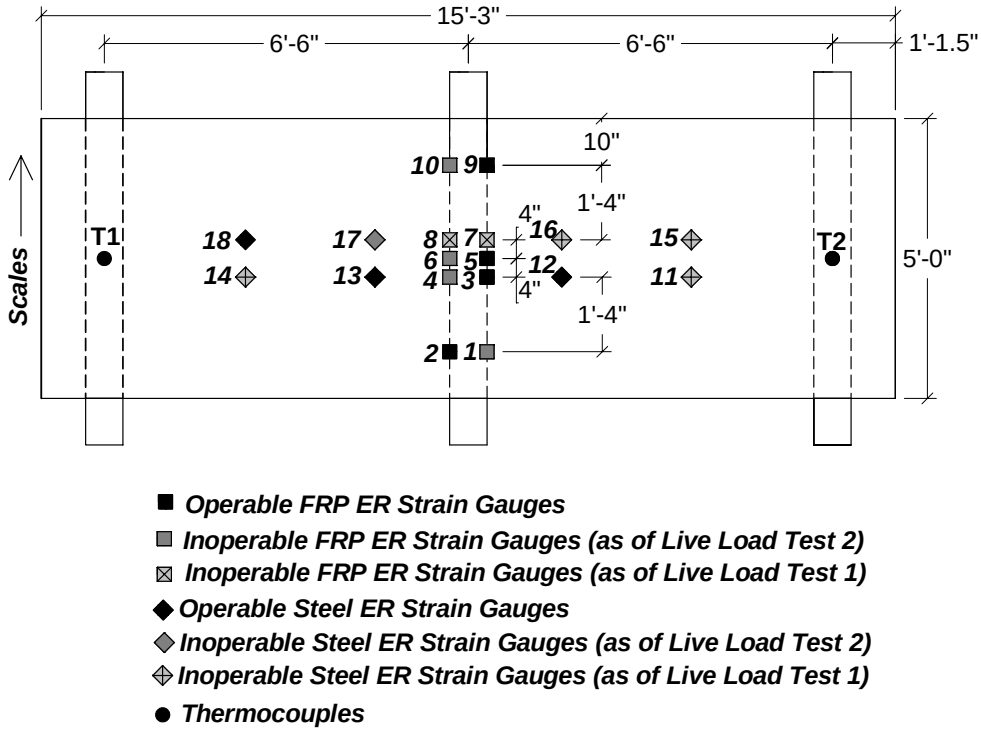

Figure 3.8: Weigh Station Slab Instrumentation Plan

3.3.1.1 Electrical Resistance Strain Gauges

The weigh station deck was instrumented with two sets of ER strain gauges. The location of the instrumentation can be seen in Figure 3.8. The duration of the use of each gauge is indicated by its symbol's shading.

The first group was located in the center of the deck on the transverse GFRP reinforcing bars. Five bars were gauged with two gauges each approximately 4 in. from the centerline of the deck, for a total of ten ER strain gauges. These gauges were used to record maximum strains within the GFRP reinforcing bars caused by the truck traffic during the live load testing. These eight gauges were labeled 1 through 10.

The second group was located on the transverse steel reinforcing bars. Two bars were gauged with four gauges each approximately 4 in. and 3 ft 3 in. on either side of the centerline of the deck, for a total of eight ER strain gauges. These gauges were labeled 11 through 18.

3.3.1.2 Thermocouples

A set of thermocouples are located approximately 6 ft 6 in. on either side of the centerline of the deck. Each set is comprised of three thermocouples: one at the top reinforcement mat, one at the bottom reinforcement mat, and one in between the mats. The thermocouples are used to monitor the temperatures within the deck. The thermocouples are labeled T1T, T1M, T1B, T2T, T2M, and T2B with the last letter indicating its location.

3.3.2 Test Preparation Procedures

3.3.2.1 Data Acquisition

Two live load testing sessions were executed. The first was performed with the Megadac 3108 AC data acquisition system from Optim Electronics. The weigh station deck ER strain gauges were connected to a Megadac which was housed in a large cargo van. During testing, the cargo van was parked next to the lane of traffic with the rear of the van facing the access hole so the lead wires of the gauges could be reached.

Before testing, each strain gauge was tested with a voltmeter to see if it was still working properly. Of the 18 gauges, 12 gauges were working. The gauges that were used can be seen in Figure 3.8. The lead wires for the gauges that were not working were

cut back to keep them separate from the operable gauges. The operable gauges were connected to the Megadac. Before testing, the readings were checked to confirm that the instrumentation was connected correctly and any problems were corrected. Once all of the instrumentation appeared to have reasonable readouts, the readings were zeroed and the tests executed.

The CR9000 datalogger made by Campbell Scientific, Inc. was used for the second live load testing session. This system is easier to transport and to work with than the Megadac. The same procedure as the first testing was followed. For this test, 7 of the original 18 gauges were working. Figure 3.8 indicates which gauges were used in the second session.

3.3.3 Live Load Testing

The first live load testing was performed on the slab located at the weigh station on May 13, 2004, approximately two months after the slab was installed. The second session of testing was performed on October 20, 2004, approximately five months after the first test. Since the slab is located at a place of heavy load traffic, the typical traffic could be used for the testing as opposed to the traditional overloaded testing truck. The same procedure was followed for both tests.

3.3.3.1 Truck Orientation

Marks were made on the slab with chalk at one foot increments to define where the truck's right wheel was located when crossing the slab. This indicated where the load was being applied by the wheels. A line was drawn at center line, at 1 ft to the right of center line, at 2 ft from center line, and at 3 ft.

3.3.3.2 Dynamic Tests

Only dynamic tests were performed so the weigh station could retain its normal operating procedures. The speed limit at the slab's location is 40 mph, so that was the speed used for analysis. For each truck, the strains were recorded as it crossed and the location of its front right tire was noted. Only the records for the trucks that were pulled over to be weighed were kept since the weight of the truck was needed for analysis. The following information was recorded for each test:

- Data set number
- Truck description
- The location of the truck (marking color)
- The weight of the truck

The truck description was used to communicate with an observer in the weigh station tower who was recording the weights of the trucks. This process was continued until the desired number of trucks had been pulled over and weighed and the data recorded. Nine data sets from the first testing session and eight data sets from the second testing session were used for analysis.

3.4 Long Term Data Acquisition

3.4.1 Campbell Programming and Setup

To collect the long term data, a CR23X Micrologger made by Campbell Scientific, Inc. was used. This device runs off of a user-provided program that specifies which channels are being used and at what frequency the readings are to be taken. The programs for both the bridge and the weigh station slab are presented in Appendix C, and the wiring diagram for the Campbell installed at the bridge is presented in Appendix D. Readings were taken every hour at the two locations. The program also included the day and time that the readings were taken. Testing was done in the lab to ensure that the strain output from the Campbell was accurate by comparing its readings to that of a strain indicator box. The Campbell takes a panel temperature that is within the system so temperatures could be monitored using the Campbell itself, the thermocouples, and the thermisters in the VW gauges (in the bridge only).

3.4.2 Gills Creek Bridge

The Campbell was used to monitor the instrumentation of Span A of the Gills Creek Bridge. Since there were not enough ports to connect all of the instrumentation on the datalogger itself, additional boards had to be used. Two multiplexers were used, one for the ER strain gauges and one of the VW gauges. The thermocouples were connected directly to the Campbell. All of the components were screwed to a plate that was then secured in an environmentally resistant box. Figure 3.9 is a picture of the datalogger. After programming the datalogger in the lab, it was taken to the field location and the

lead wires of the instrumentation were run through the access hole in the box and connected to the datalogger. Weatherproofing putty provided by the box manufacturer was placed in the access hole to fully seal the box, and desecant packs were placed in the box to control the internal humidity. The box was locked and placed on the south abutment wall on the underside of the bridge. A solar panel was mounted on the parapet of the bridge to ensure that the datalogger had a constant power source.

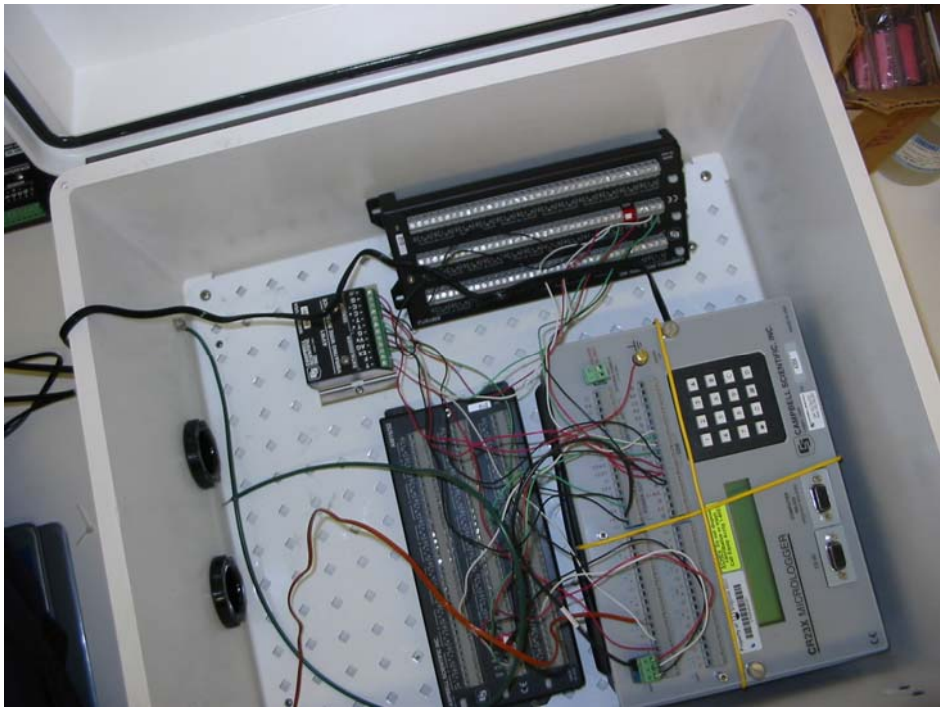

Figure 3.9: CR23X Micrologger and Instrumentation Components

The data acquisition system was installed on November 20, 2004. Each strain gauge was tested with a voltmeter to make sure that it had the correct resistance of 350 ohms across it, indicating whether it was still working properly. The working strain gauges were then connected to the Campbell. Figure 3.2 indicates which strain gauges were operable at the time of installation. The vibrating wire gauges and thermocouples were connected as well. The readings were monitored for approximately one year.

3.4.3 Weigh Station Slab

At the I-81 weigh station, the CR23X micrologger was installed to collect long term information about the strains and temperatures within the slab. One multiplexer was used for the ER strain gauges, and the thermocouples were connected directly to the datalogger. An environmentally resistant box was already located in the field. It was

secured to a 4x4 post with a PVC pipe that runs up from the access hole to channel the lead wires. After programming the datalogger in the lab, it was taken to the field location, and the lead wires of the instrumentation were run through the PVC pipe and into the box and were connected to the datalogger. Weatherproofing putty was placed in the access hole to fully seal the box, and desecant packs were placed in the box to control the internal humidity. The box was locked to secure the equipment. A solar panel was mounted on the 4 x 4 post to ensure that the datalogger had a constant power source.

The data acquisition system was installed at the weigh station after the second live load testing session on October 20, 2004. The strain gauges that were used for the live load test were connected to the Campbell. The thermocouples were also attached. The readings taken by the Campbell at the weigh station are not analyzed in this report. However, the program used for the Campbell is presented in Appendix C.

Chapter 4 - Results and Discussion

4.1 Gills Creek Bridge

A live load test was performed on the bridge on June 17, 2004, approximately one year after the initial testing. The data was collected at a rate of 400 readings per second. This was a huge amount of data points to analyze, especially for the quasi-static tests that lasted for around thirty seconds. For all the quasi-static tests, a program was applied to keep only one out of every 10 data points. For all the tests on Span A, both quasi-static and dynamic, a three-point running average was applied to the remaining points. The dynamic tests on Span C were not reduced or averaged. All of the analyses of the live load tests were performed using the final data. This section investigates the behavior of the bridge during testing and how the bridge's performance compares to one year prior.

4.1.1 Transverse Deck Strains

During the live load testing of the Gills Creek Bridge, the strains in the GFRP bars were recorded using the ER strain gauges in the bridge deck. As stated in Chapter 3, there were four sets of gauges in Span A with three of those sets used for measuring transverse strains. The locations of the three sets were at the abutment over the interior girder, at the midspan over the exterior girder, and at the midspan over the interior girder. All of the gauges from the initial live load test were still working. There were enough gauges in each section to determine a transverse stress profile for each location. However, Span C only had five gauges working, so the strains could not be used to determine a profile. Figure 3.2 and Figure 3.3 show the operable gauges.

To find the transverse stress profile at each location in Span A, several steps were taken. With each truck crossing, the strain in each gauge was recorded. Each group of gauges was analyzed separately. For each gauge, the maximum strain was determined along with the time that the maximum strain occurred. The time when the highest maximum strain in the group occurred was identified. The strains that were measured at that time were recorded for all the gauges in the group. These strains were converted to stresses using the assumed modulus of elasticity of the GFRP bars, 6,300 ksi. A stress profile was plotted for each group using the stresses at the time of maximum strain. Essentially, it is like taking a snapshot in time and recording the stresses in each bar at

that moment. This process was performed for each of the three groups of ER strain gauges. Table 4.1 is an example of the calculations performed to determine the stresses and includes the times those stresses were measured for the first quasi-static test performed on the exterior girder.

Table 4.1: Calculation of Stresses in Transverse GFRP Bars

	ATA2	ATA4	ATA6	ATMI1	ATMI3	ATMI6	ATMI7	ATME1	ATME3	ATME4	ATME5	ATME6	ATME7	ATME8
(1) Initial με	-91.6	-49.9	-2.8	-5.5	-11.0		-9.4	-33.4	-9.4	-4.3	-3.5	-6.3	-18.9	-7.9
(2) Max με	-88.8	-49.1	-1.2	-4.7	-8.6		-7.9	-32.4	-7.9	-2.0	-3.1	-5.1	-17.3	-5.9
(3) '2 -1	**2.8**	**0.8**	**1.6**	**0.8**	**2.4**		**1.6**	**1.0**	**1.6**	**2.4**	**0.4**	**1.2**	**1.6**	**2.0**
(4) Min με	-102.2	-66.8	-9.8	-18.9	-25.2		-22.4	-46.0	-14.9	-7.9	-9.8	-10.6	-28.3	-13.0
(5) '4-1	**-10.6**	**-16.9**	**-7.1**	**-13.4**	**-14.1**		**-13.0**	**-12.6**	**-5.5**	**-3.5**	**-6.3**	**-4.3**	**-9.4**	**-5.1**
(6) Abs Max με	**10.6**	**16.9**	**7.1**	**13.4**	**14.1**		**13.0**	**12.6**	**5.5**	**3.5**	**6.3**	**4.3**	**9.4**	**5.1**
(7) Time	36.02	15.65	21.00	23.15	23.62		27.27	26.25	25.10	25.10	28.30	30.15	26.97	22.90
	ATA			ATMI				ATME						
(8) Abs Max btw middle gages	16.9			14.1				12.6						
(9) Time	**15.65**			**23.62**				**26.25**						
(10) Corr Strain	-98.6	-66.8	-6.3	-16.5	-25.2		-18.9	-46.0	-13.4	-5.9	-6.3	-7.9	-26.7	-10.2
(11) Adj Strain	**-7.1**	**-16.9**	**-3.5**	**-11.0**	**-14.1**		**-9.4**	**-12.6**	**-3.9**	**-1.6**	**-2.8**	**-1.6**	**-7.9**	**-2.4**
(12) Stress (ksi)	-0.045	-0.106	-0.022	-0.069	-0.089		-0.059	-0.079	-0.025	-0.010	-0.017	-0.010	-0.050	-0.015
(13) Stress per bar (ksi)	**-0.045**	**-0.106**	**-0.022**	**-0.069**	**-0.089**		**-0.059**	**-0.079**	**-0.017**		**-0.014**		**-0.032**	

The process of calculating the stresses in each bar is as follows. Row (1) is the average baseline strain before the truck is on the span and was found by averaging the first three strain readings. Row (2) is the maximum strain of each gauge. Row (3) is the relative maximum strain determined by subtracting row (1) from row (2). Row (4) is the minimum strain of each gauge. Row (5) is the relative minimum strain determined by subtracting row (1) from row (4). The absolute maximum is found in row (6) by taking the maximum of the absolute values of rows (3) and (5). Row (7) is the time that each absolute maximum value occurred. Row (8) displays the absolute maximum in each group, and row (9) is the corresponding time to that maximum value. Row (10) is the strain at each gauge at the specified time from row (9). The adjusted strains in row (11) are found by subtracting the initial in row (1) from row (10). Row (12) is the stress found by multiplying the adjusted strain by the modulus of elasticity of 6,300 ksi. Finally, row (13) determines the stress in each bar by averaging the stresses recorded by the gauges on the same bar.

The strains recorded from gauge ATMI6 were not used since the values were clearly inaccurate. The stresses calculated for each bar were plotted against the gauge location to generate a transverse stress profile for the three gauging locations. For

comparison, the allowable tensile stress was calculated. Harlan (2004) tested a sample of the GFRP bars in the laboratory and found the average ultimate tensile strength to be 109 ksi with a standard deviation of 3.23 ksi. According to the *ACI Guide for Design and Construction of Concrete Reinforced with FRP Bars* reported by ACI Committee 440 (2003), the design tensile strength should be calculated using the following equation:

$$f_{fu} = C_E f^*_{fu} \qquad \textbf{Equation 4-1}$$

where f_{fu} is the design strength of FRP taking into consider reductions for the service environment, C_E is the environmental reduction factor which for GFRP in concrete exposed to earth and weather is 0.7 or 70%, and f^*_{fu} is the guaranteed tensile strength of an FRP bar. The guaranteed tensile strength is found by taking the average tensile strength of samples, $f_{u,ave}$, minus three times the standard deviation, σ. Applying this equation, f^*_{fu} = 109-3(3.23) = 99.3 ksi. Then plugging the results into Equation 4-1, f_{fu} = 0.7(99.3) = 69.5 ksi. ACI 440 specifies in Table 8.2 that for GFRP the creep rupture stress limit, $F_{f,s}$ is equal to 0.20f_{fu}. Applying this equation, the allowable tensile stress for the GFRP bars is 0.2(69.5) or 13.9 ksi. ACI 440 does not specify an allowable compressive strength for FRP.

The allowable compressive strength of the GFRP can also be calculated using the guaranteed tensile strength used in design which is not as high as the actual strength measured in the lab. The GFRP bars in the deck are Grade F70 which corresponds to a guaranteed tensile strength of 70 ksi. Applying Equation 4-1 to an f^*_{fu} value of 70 ksi, f_{fu} = 0.7(70) = 49 ksi. That would make the design allowable tensile stress 0.2(49) or 9.8 ksi.

Figure 4.1 is the stress profile of the ATA gauges from the quasi-static tests. The ATA gauges are located over the first interior girder at the abutment of Span A. The stresses ranged from -124 psi to 50 psi. The maximum tensile stress of 50 psi was well below the allowable tensile stress of 13.9 ksi. Test 11 was the only test showing the bars going into tension. Besides test 11, the stresses were all compressive ranging from -124 to -2.5 psi.

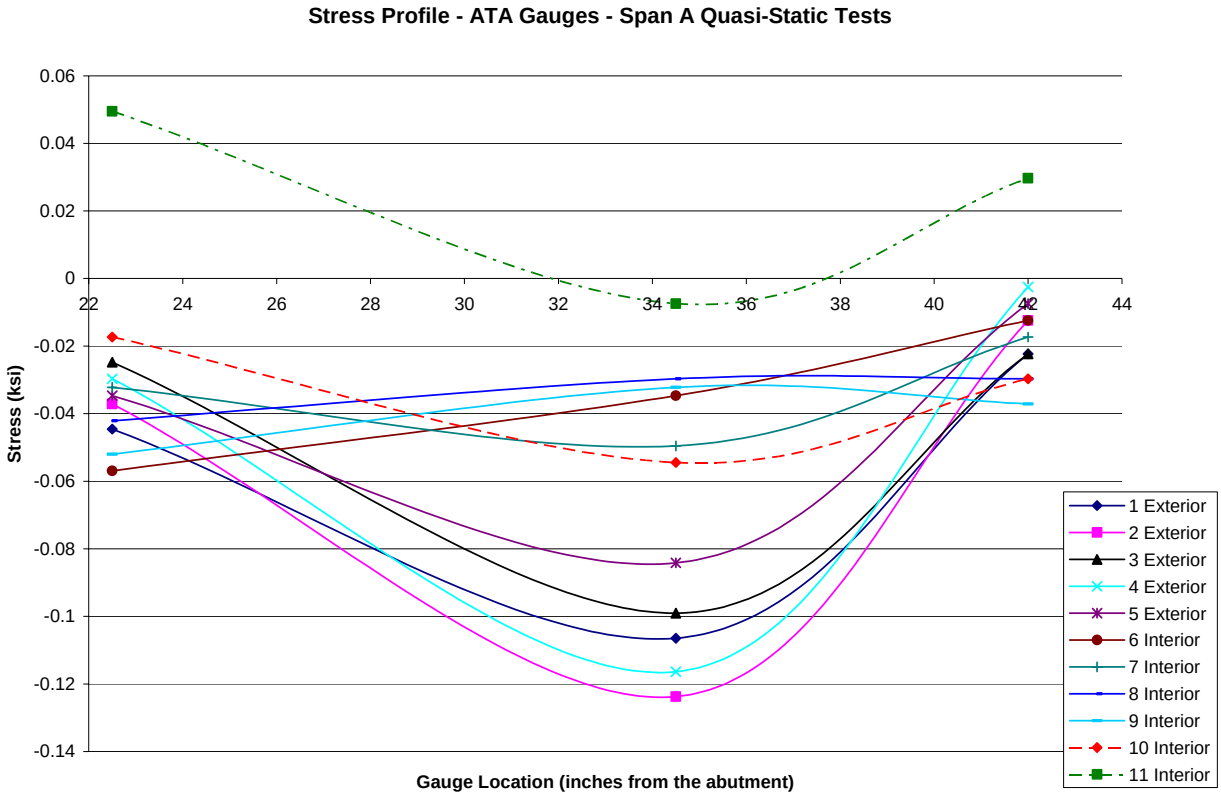

Figure 4.1: Stress Profile for ATA Gauges Under Quasi-static Loading

Figure 4.2 shows a comparison of the ATA stress profile measured in 2004 and the stress profile from 2003. The stresses in the ATA gauges for the quasi-static tests in 2004 ranged from about -125 psi to 50 psi. The same test performed one year prior had stresses between 0 psi and 80 psi. Both years had tensile stresses under the allowable tensile stress of GFRP of 13.9 ksi.

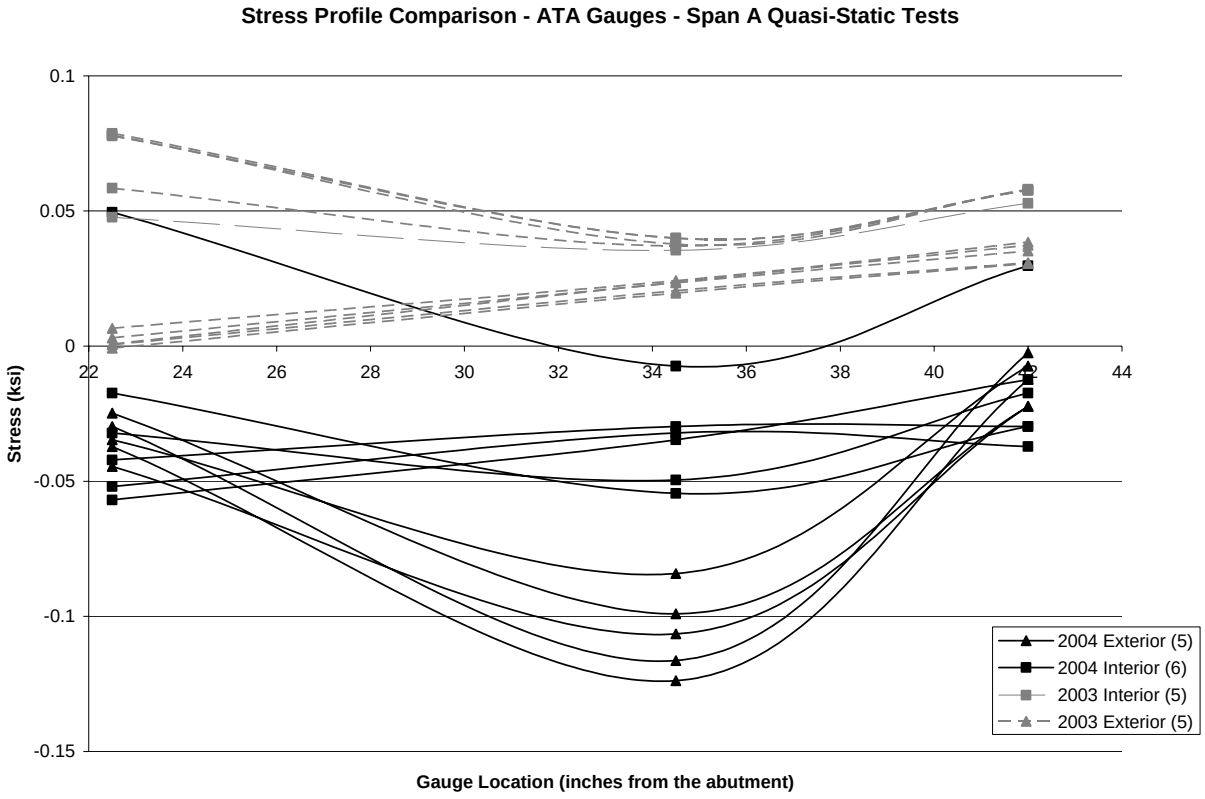

Figure 4.2: Comparison of Stress Profiles for ATA Gauges Under Quasi-static Loading

Aside from a few exceptions, the stresses recorded in 2004 were compressive, and the stresses from 2003 were tensile. One explanation for the shift to compression could be the marking of the tire location. For the live load test in 2003, the location of the side of the wheel was marked at both the exterior girder testing and the interior girder testing. The driver of the test truck followed the line with the edge of the wheel along the line. For the live load test in 2004, the path was marked for the centerline of the wheel. However, during the quasi-static testing, the outside edge of the wheel was following the line instead of the center of the tire. This would mean the wheel load was further away from the parapet and offset from girder 4. The new location would result in the wheel load being more central over the slab than at the girder creating a more positive moment and compression in the FRP bars. When the wheel is closer to being over girder 4, there is more of a tendency to produce negative moment in that region causing tension in the top of the slab.

With a difference of a few inches, the exact location of the tires may not have influenced the results to such a great extent. The reason that the gauges were in tension during the 2003 live load tests was attributed to the stiffness of the supporting member at the abutment causing the deck to be more influenced by local bending effects. For the interior orientation, the truck straddles the first interior girder causing a negative moment over the girder. Therefore, the stresses in the GFRP bars located in the top of the deck over the girder would be in tension. If the connection at the abutment had lost stiffness, the slab would be free to behave more like a plate. A lost of stiffness could be due to settlement of the abutment or cracking. Cracking of the abutment was observed at each approach. This behavior would cause more of a response to global bending effects which put the entire top of the plate in compression when loaded. This is the response seen from the live load tests in 2004.

In the 2003 results, the tests run over the exterior girder had a linear relationship while tests run over the interior girder were more parabolic with the central gauge (ATA4) having the lowest stress. The 2004 live load results over the exterior girder were parabolic similar to the 2003 tests over the interior girder. Note that the ATA6 gauge was not producing readings when connected to the Campbell both before and after the live load testing. The ATA gauge stresses resulting from the interior orientation recorded in 2004 did not have a distinct trend.

The stress profiles for the ATMI and ATME gauges from the quasi-static tests are shown in Figure 4.3 and Figure 4.5, respectively. The ATMI gauges are over girder 4 at midspan, and the ATME gauges are over girder 5 at midspan. The comparison between the quasi-static stress profiles of a few months after the deck was poured and one year later for the ATMI and ATME gauges are shown in Figure 4.4 and Figure 4.6, respectively.

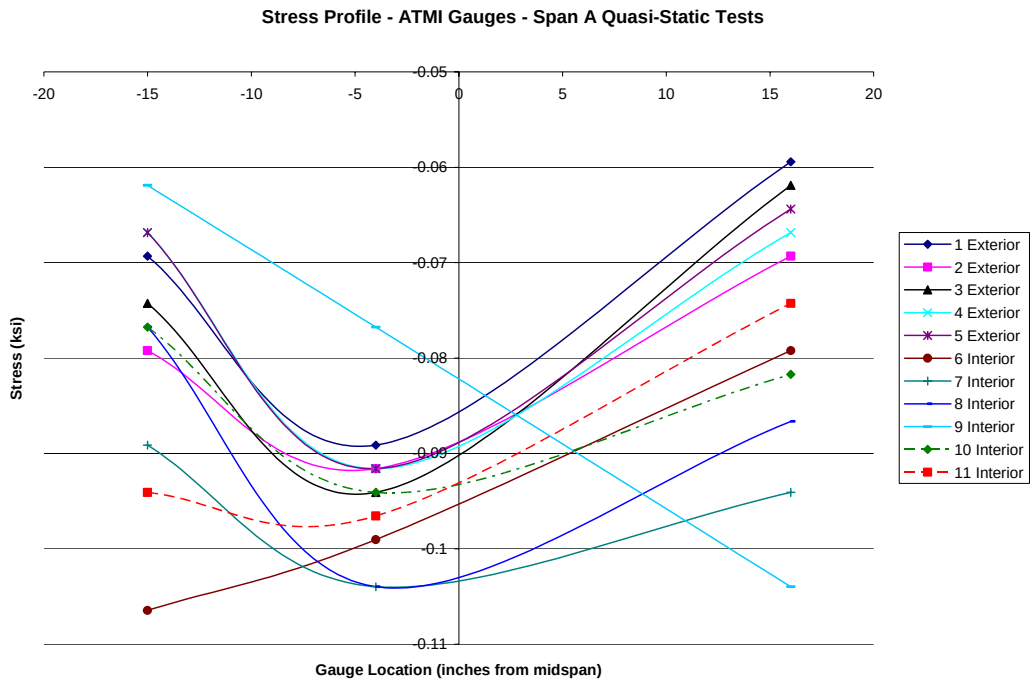

Figure 4.3: Stress Profile for ATMI Gauges Under Quasi-static Loading

In the 2004 live load testing, the ATMI gauges had very similar responses to the interior and exterior orientations. The stresses ranged from -106 psi to -62 psi for the interior orientation, and -95 psi to -60 psi for the exterior orientation. In general, the interior orientation created larger stresses in the GFRP bars. This makes sense because the ATMI gauges are located over the first interior girder. Essentially, when the truck load is closer the stresses are higher. It is interesting that for both orientations, the stress profile has a parabolic trend, with the higher stresses at the edge bars.

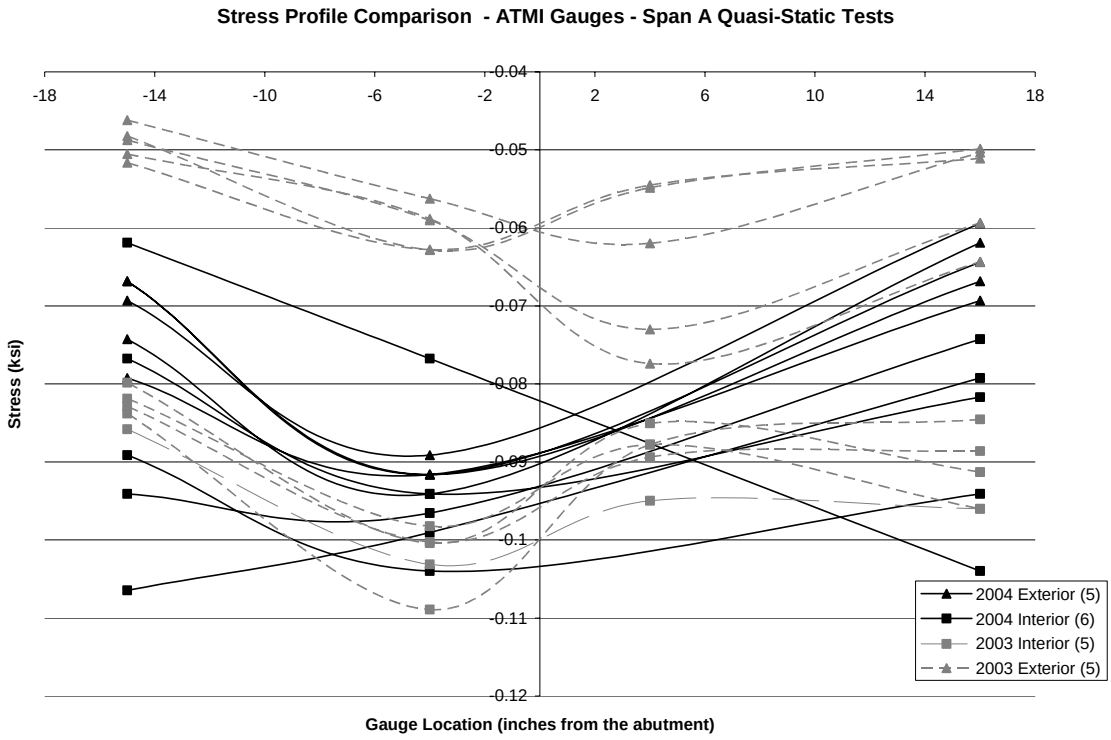

Figure 4.4: Comparison of Stress Profiles for ATMI Gauges Under Quasi-static Loading

The ATMI gauge readings from the 2003 live load test varied less. This is most likely due to the durability of the ER gauges themselves. As the gauges age, they become less reliable, and the standard deviation of their readings increase. The stresses ranged from -109 psi to -80 psi for the interior orientation, and -77 psi to -46 psi for the exterior orientation. In general, the ATMI gauges showed higher compressive stresses in 2004 than in 2003. Although no cracking in the deck was evident upon visual inspection, the deck may be becoming more flexible. Increased flexibility can cause higher deflections and higher stresses in the GFRP reinforcing bars. Also, the supports may have become more flexible allowing increased deflection.

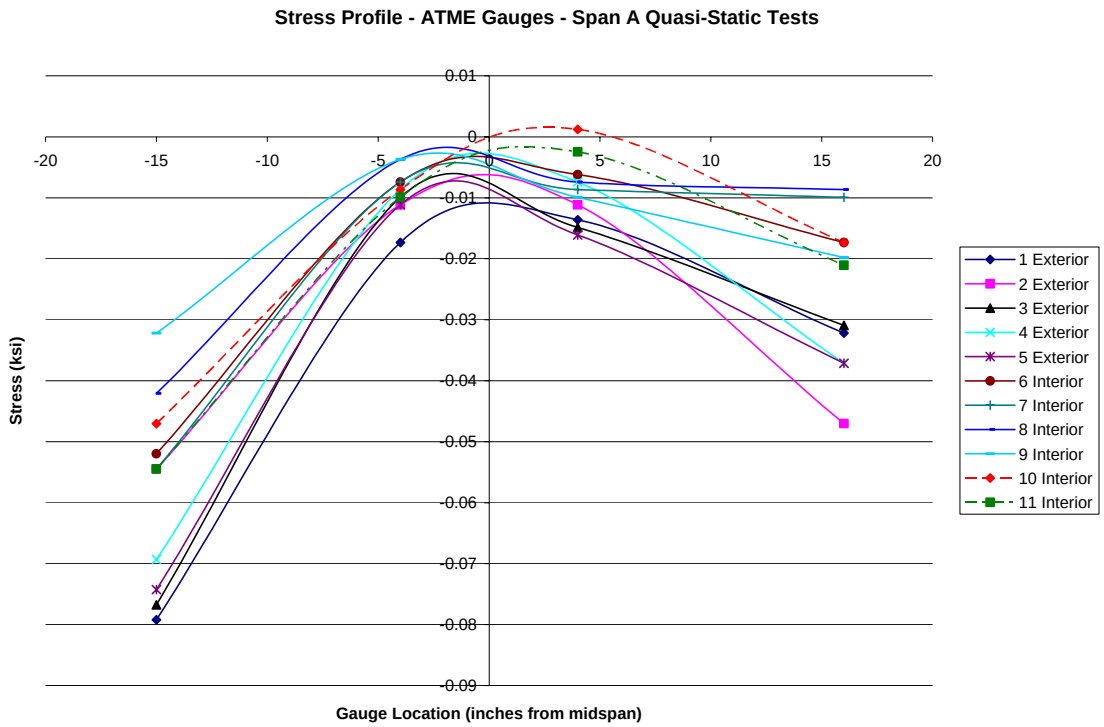

Figure 4.5: Stress Profile for ATME Gauges Under Quasi-static Loading

The ATME gauges had very similar responses to the interior and exterior orientations in the 2004 live load tests. The stresses ranged from -54 psi to 12 psi for the interior orientation, and -80 psi to -7 psi for the exterior orientation. In general, the exterior orientation created larger stresses in the GFRP bars since the load was closer. Note that the ATME gauges had lower stresses than the ATMI gauges. This is because for the exterior orientation the truck did not straddle girder 5, but rode on top. Smaller stresses in the top transverse bars would result from the truck riding on top of the girder. Following the trends of the other gauges, the ATME gauges had higher compressive stresses in 2004 than in 2003.

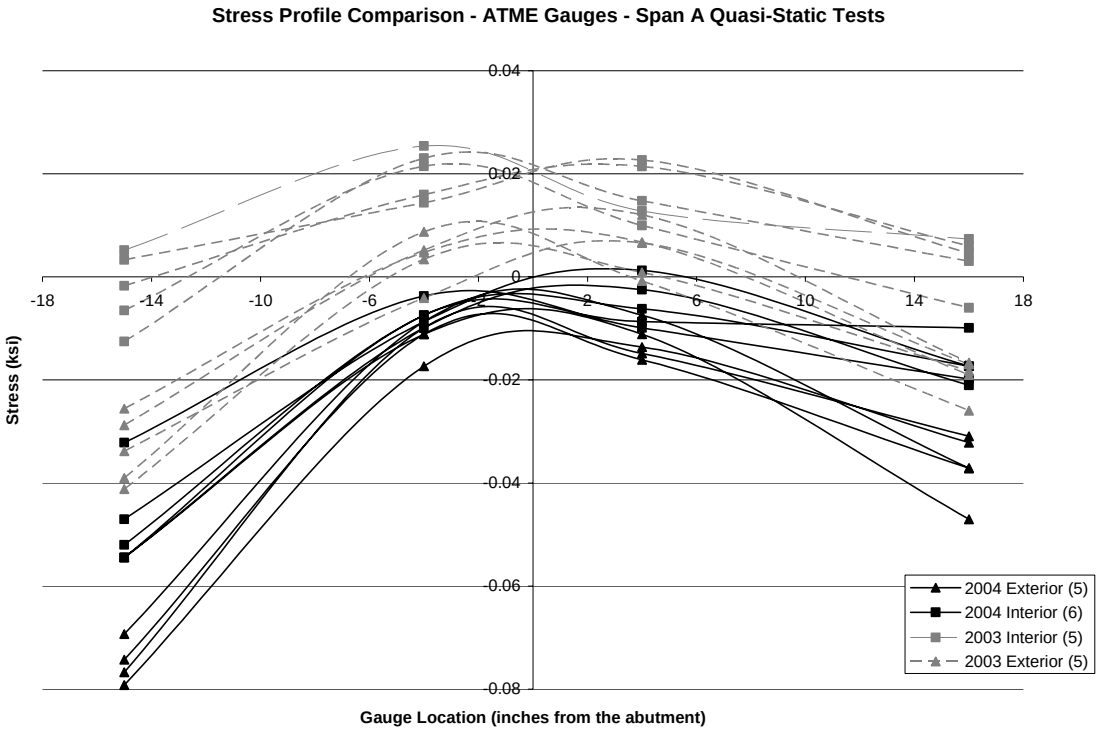

Figure 4.6: Comparison of Stress Profiles for ATME Gauges Under Quasi-static Loading

Figure 4.7, Figure 4.9, and Figure 4.11 show the stress profiles for the ATA, ATMI, and ATME gauges. The comparison between the dymanic stress profiles of a few months after the deck was poured and one year later for the ATA, ATMI, and ATME gauges are shown in Figure 4.8, Figure 4.10 and Figure 4.12, respectively. All of the gauges had higher compressive stress in 2004 than in 2003. In 2004, the ATA gauges were mostly in tension for the dynamic loading. When the truck is traveling at fast speed, the bearings must provide more resistance causing a more local response. The 2004 ATMI gauges were all in compression. In 2003, some of the ATME gauges were in tension and some in compression. The 2004 dynamic live load tests resulted in all of the ATME gauges in compression.

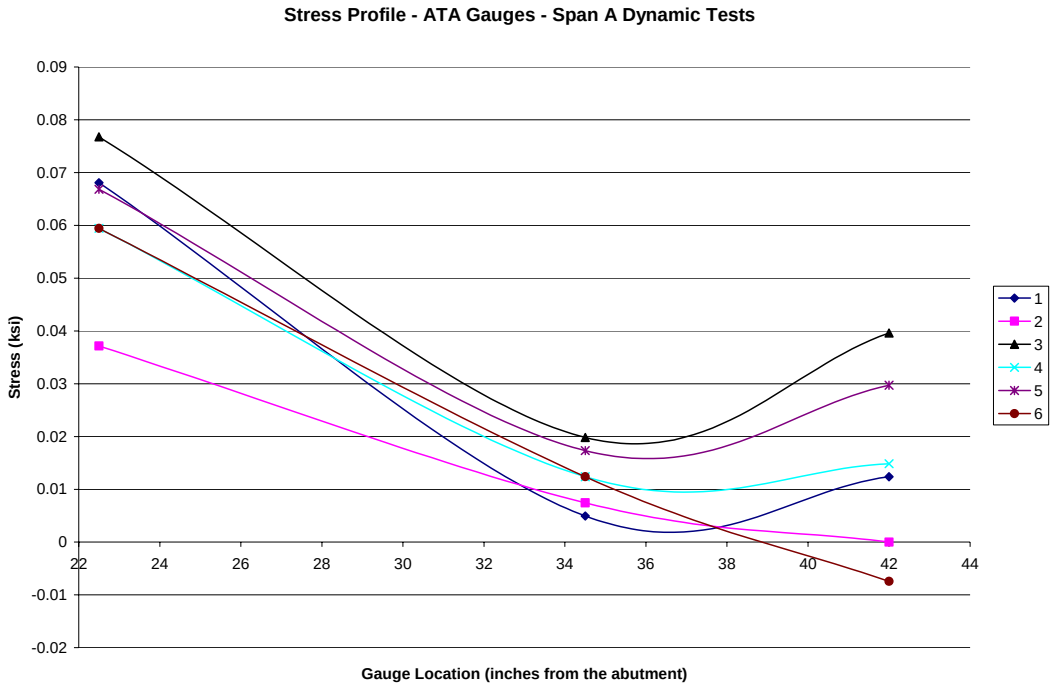

Figure 4.7: Stress Profile for ATA Gauges Under Dynamic Loading

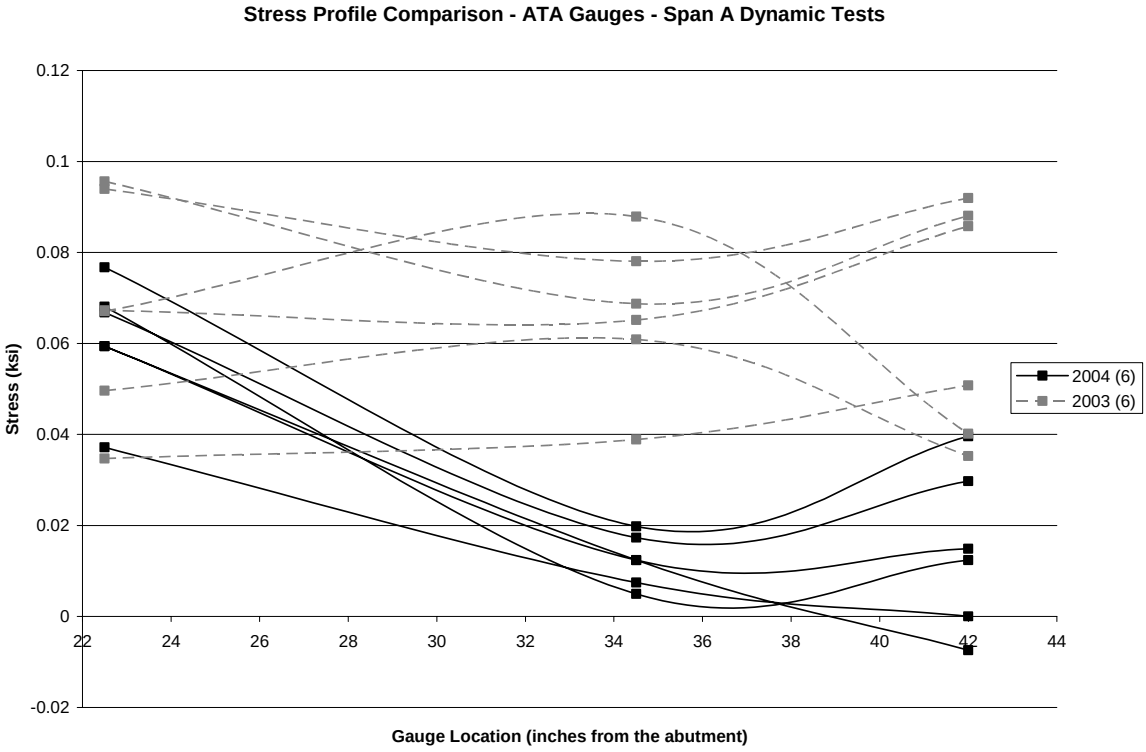

Figure 4.8: Comparison of Stress Profiles for ATA Gauges Under Dynamic Loading

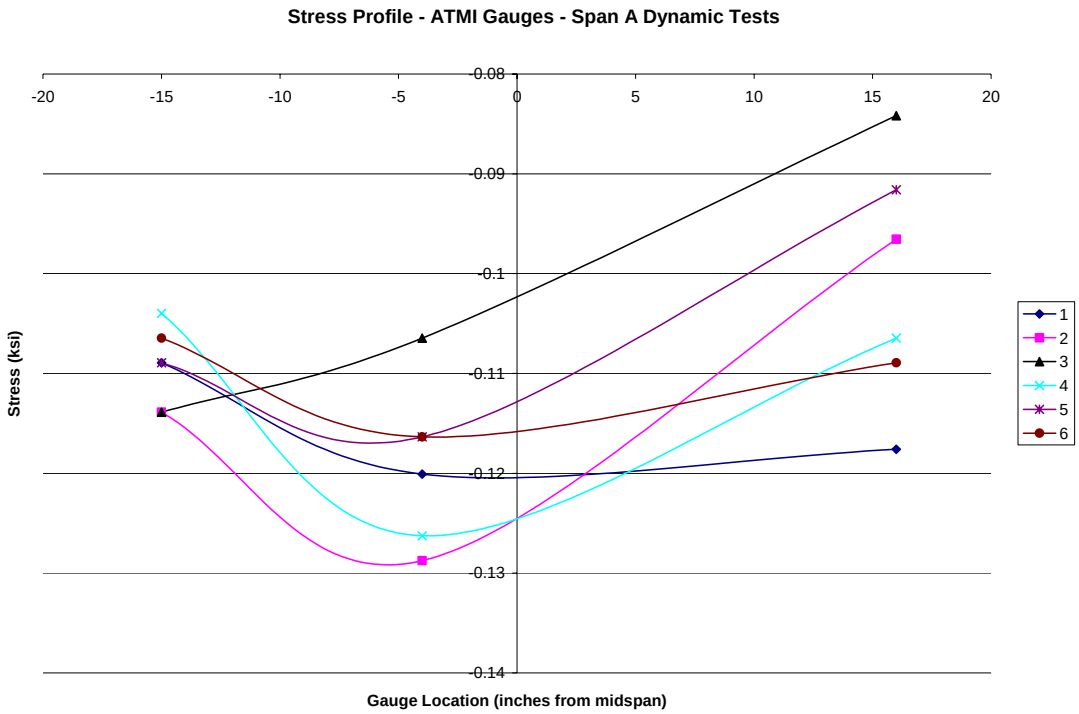

Figure 4.9: Stress Profile for ATMI Gauges Under Dynamic Loading

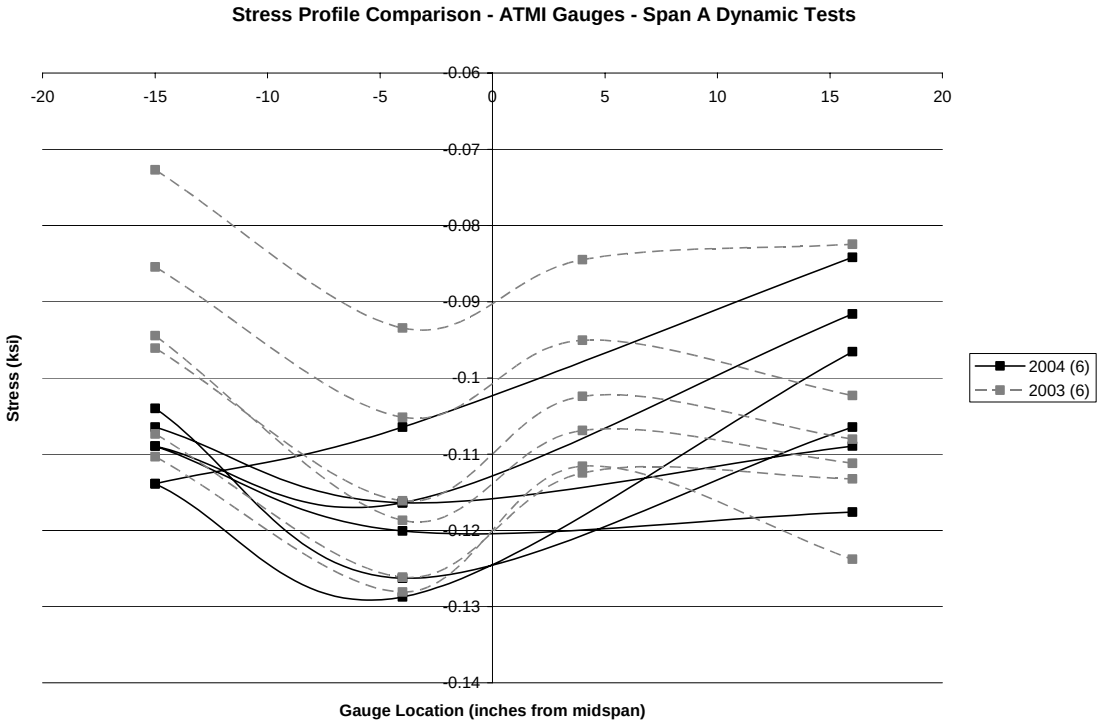

Figure 4.10: Comparison of Stress Profiles for ATMI Gauges Under Dynamic Loading

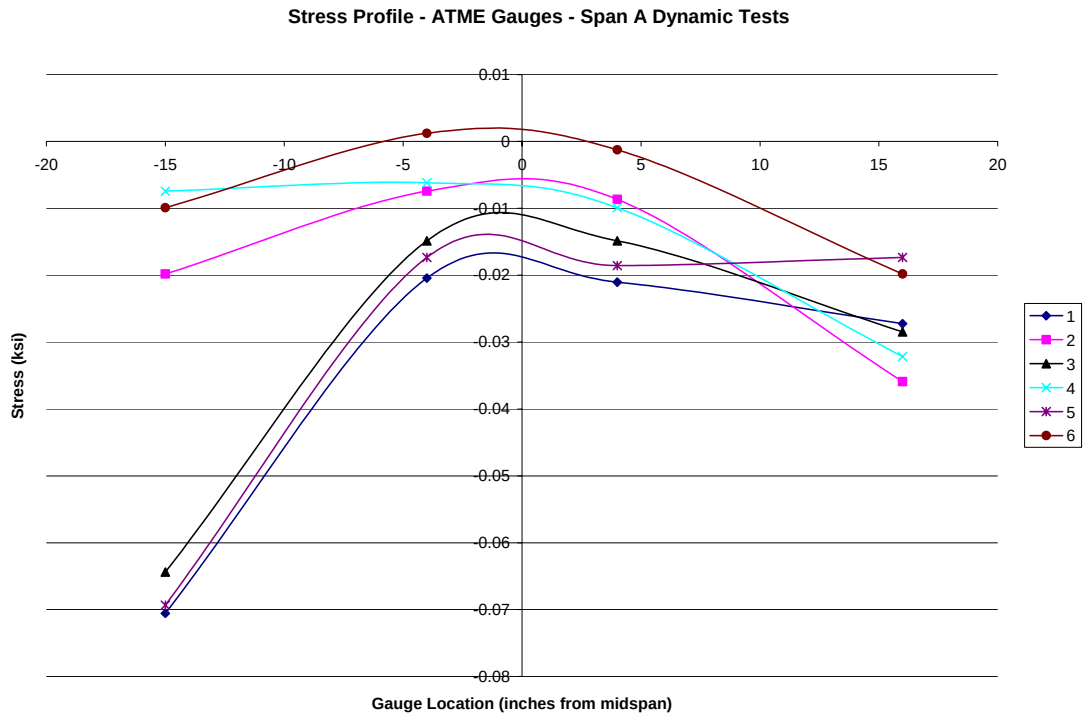

Figure 4.11: Stress Profile for ATME Gauges Under Dynamic Loading

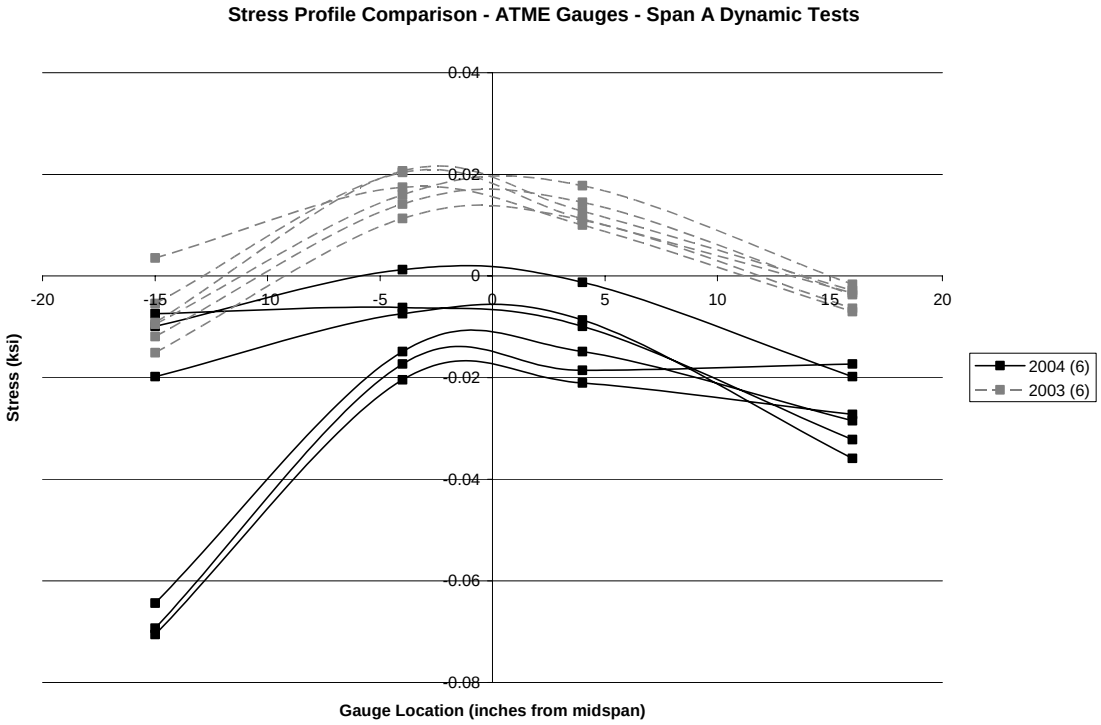

Figure 4.12: Comparison of Stress Profiles for ATMI Gauges Under Dynamic Loading

The general trend of the transverse stresses in the GFRP was that the stresses became more compressive a year after the initial live load testing. The truck used for the initial testing had a total front axle weight of 16.04 kips and a rear axle weight of 33.56 kips. For the second test, the truck weighed 13.52 kips in the front and 36.52 kips in the rear. Such a small difference in weights would not have a very big influence over the strains produced. The increase in compression may be due to an increase in flexibility of the supports or the deck itself. Please note there were no cracks detected at the time of either live load testing session. All of the tensile stresses measured in the bars were very low compared to the calculated allowable tensile stress of 13.9 ksi. Unfortunately, there was no limit to compare the compressive stresses.

4.1.2 Girder Distribution Factors

4.1.2.1 Introduction and AASHTO Equations

The girder distribution factor (GDF) is used in design to determine what fraction of the total load is being carried by a single girder. The GDF is then applied to the design loads when designing the bridge. Two documents produced by the American Association of State Highway and Transportation Officials (AASHTO) outline how to determine the required GDF.

The AASHTO Standard Specification (2002) defines the GDF to be used dependent on the bridge's type of superstructure. The GDF for a wheel load for an interior girder is defined with the following equation:

$$g = S/D \qquad \textbf{Equation 4-2}$$

where g = GDF for a wheel line

S = center-to-center spacing of the interior girders

D = denominator dependent on type of deck and girders

Table 3.23.1 of the AASHTO Standard Specification tabulates the GDF values to be used. For a concrete bridge deck with steel I-beam stringers, the distribution factor is S/7.0 for bridges designed for one traffic lane and S/5.5 for bridges designed for two traffic lanes. For the exterior girder distribution factors, the AASHTO Standard Specification states to use the assumption that the deck acts as simple spans between the

girders to determine the bending moment reaction at the girder from the live load. This process is known as the lever rule.

The AASHTO LRFD Specifications (1998) provides equations in Table 4.5.2.2.2b-1 to calculate the distribution of live loads per lane for moment in interior beams. For a concrete bridge deck on steel beams with one design lane loaded, the following equation applies:

$$g = 0.06 + \left(\frac{S}{14}\right)^{0.4}\left(\frac{S}{L}\right)^{0.3}\left(\frac{K_g}{12.0Lt_s^3}\right)^{0.1} \qquad \textbf{Equation 4-3}$$

where g = GDF for interior beams (fraction of truck or lane load)

S = center-to-center spacing of interior girders (ft)

L = span length (ft)

t_s = thickness of deck slab (in.)

K_g = longitudinal stiffness parameter.

K_g is defined in Equation 4.6.2.2.1-1 of the AASHTO LRFD Specifications which is the following:

$$K_g = n\left(I + Ae_g^2\right) \qquad \textbf{Equation 4-4}$$

where n = modulus of elasticity of beam material (ksi) divided by the modulus of elasticity of deck material (ksi)

I = moment of intertia of beam (in^4)

e_g = distance between centers of gravity of basic beam and deck (in.)

The distribution factor equation changes slightly when designing for moment with two or more design lanes loaded.

$$g = 0.075 + \left(\frac{S}{9.5}\right)^{0.6}\left(\frac{S}{L}\right)^{0.2}\left(\frac{K_g}{12.0Lt_s^3}\right)^{0.1} \qquad \textbf{Equation 4-5}$$

The restrictions to the use of Equations 4-3 and 4-5 are that the girder spacing must be between 3.5 ft and 16 ft, the deck slab thickness must be between 4.5 in. and 12 in., the span length must be between 20 ft and 240 ft, and there must be more than three girders.

The AASHTO LRFD Specifications specifies the use of the lever rule for the exterior girder when one design lane is loaded. When more than one design lane is loaded, Table 4.6.2.2.2d-1 specifies the distribution factor be found with the equation:

$$g = e g_{interior} \qquad \textbf{Equation 4-6}$$

where, $g_{interior}$ is the distribution factor for the interior girder and e is defined by:

$$e = 0.77 + d_e / 9.1 \qquad \textbf{Equation 4-7}$$

with d_e being the width of the overhang, between -1.0 ft and 5.5 ft. A negative value of d_e indicates that the web is outboard of the curb or traffic barrier. For the live load tests performed on the Gills Creek Bridge, only one lane was loaded.

4.1.2.2 Girder Responses from Live Load Tests

In order to determine the girder distribution factors, the girder responses must first be determined. To get an idea of the accuracy of the instrumentation, example plots of the readings from the deflectometers, ER strain gauges, and WIM gauges on Span A are shown in Figure 4.13 through Figure 4.15. In Span A, the accuracy of the deflectometers was approximately ±0.001 in. The ER strain gauges had an accuracy of approximately ±8 με, and the WIM gauges had an accuracy of approximately ±3 με. For Span C, the deflectometers had an accuracy of approximately ±0.001 in. The ER strain gauges had an accuracy of approximately ±3 με, and the WIM gauges had an accuracy of approximately ±0.5 με. Note that the ER strain gauge on girder 1 did not work during the live load testing. Also, the WIM gauge on girder 2 was not reading accurate results, and a WIM gauge was not installed on girder 6.

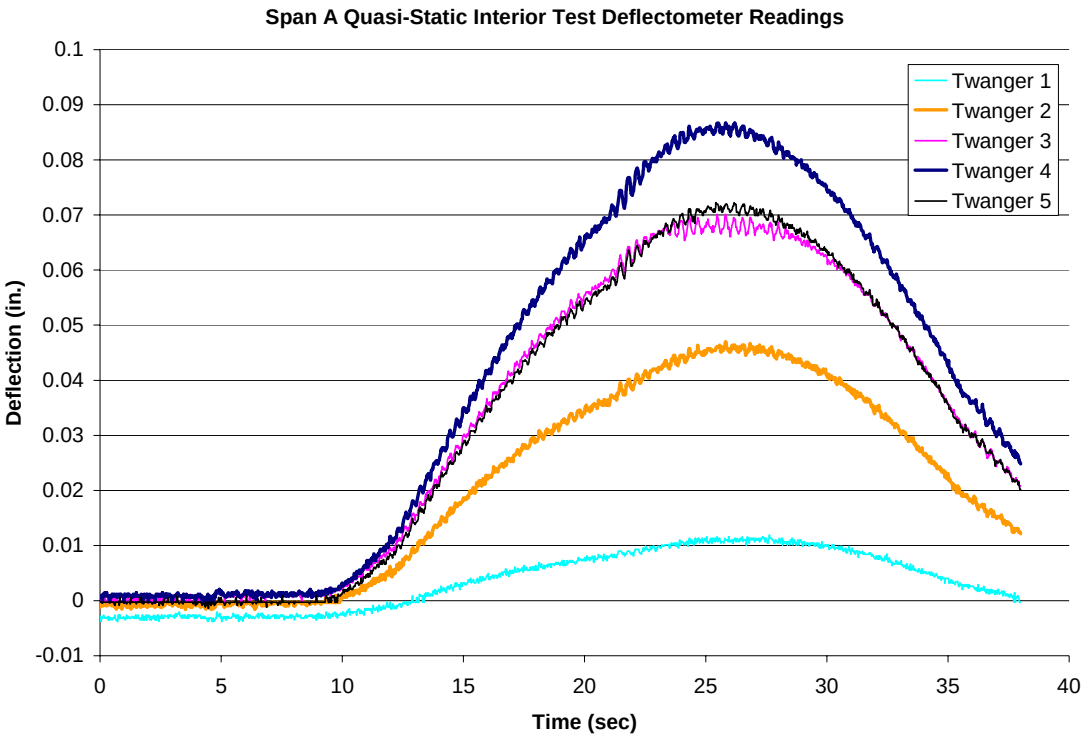

Figure 4.13: Example of Deflectometer Results for Span A

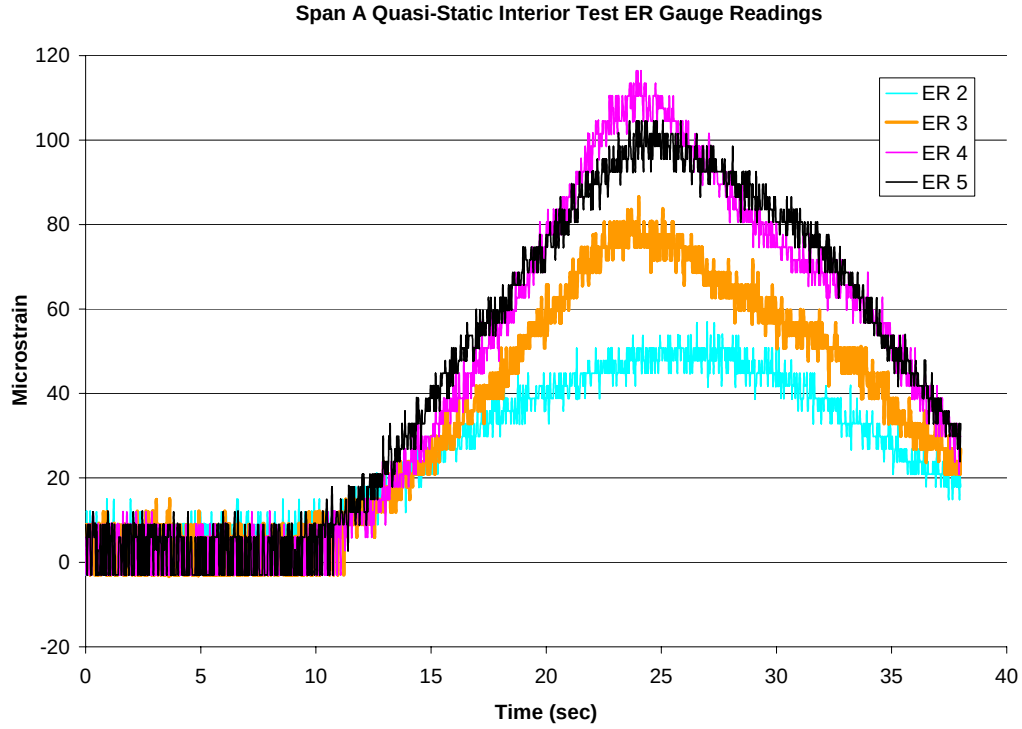

Figure 4.14: Example of ER Gauge Results for Span A

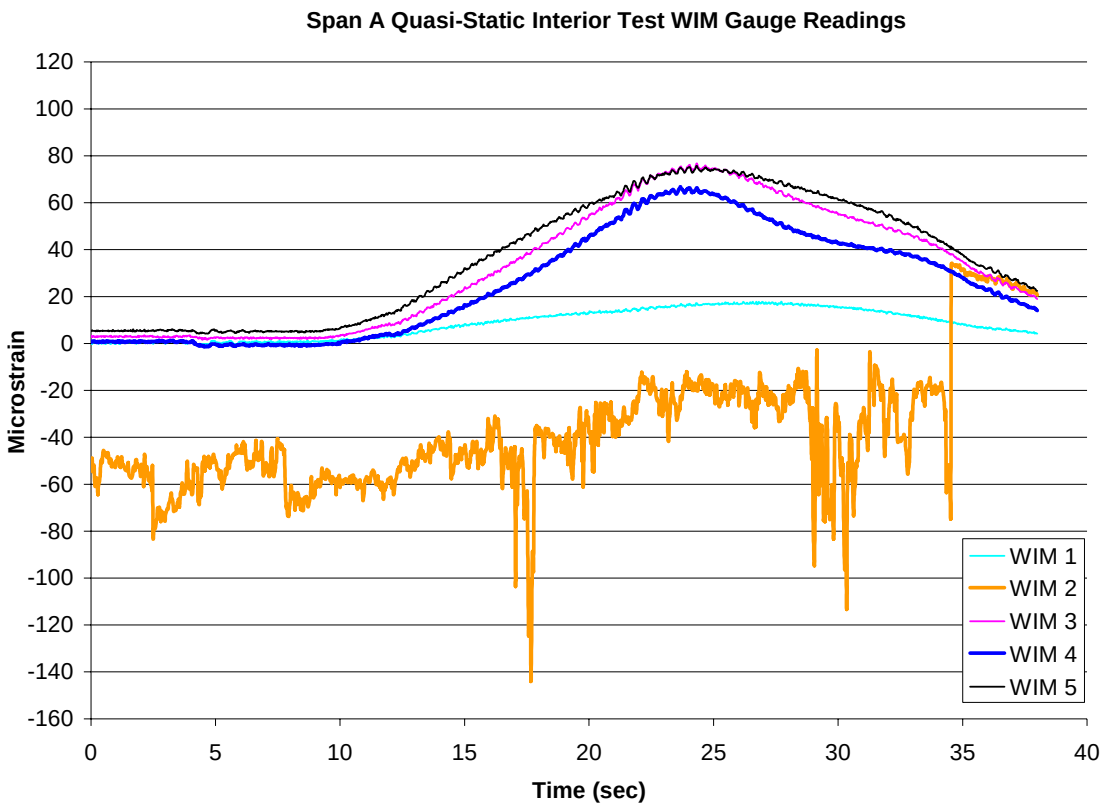

Figure 4.15: Example of WIM Gauge Results for Span A

The average maximum deflections for Span A and Span C were compared for each truck orientation in Figure 4.16 through Figure 4.18. The girder deflections of Span A were higher than of Span C for all the truck orientations. The biggest deflection difference was from the dynamic live load tests. Span A and Span C also followed different trends. When the truck is traveling over the first interior girder (girders 4 and 9), it was expected that the girder with the highest deflection would be the girder under the truck. This was true for the interior orientation tests for Span A but not for Span C in both the dynamic and quasi-static tests. For the exterior orientation, both Spans A and C had the largest maximum deflection at the exterior girder under the truck location (girders 5 and 10).

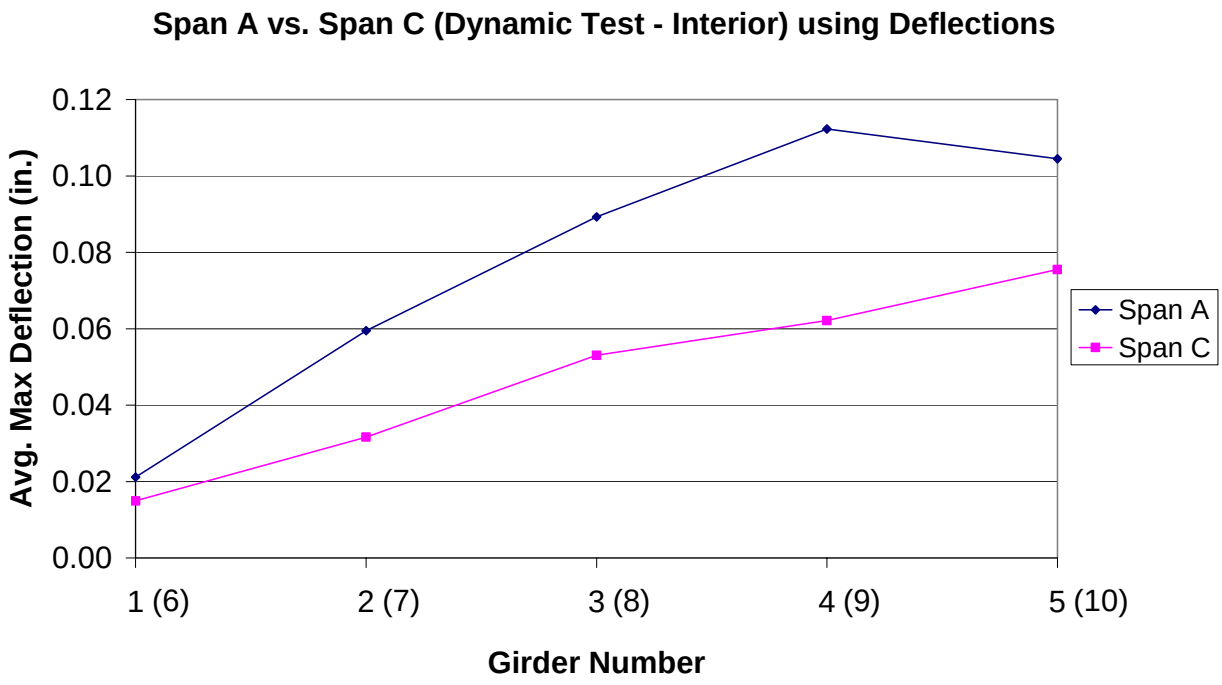

Figure 4.16: Comparison of Maximum Girder Deflections for Span A and Span C Under Dynamic Loads

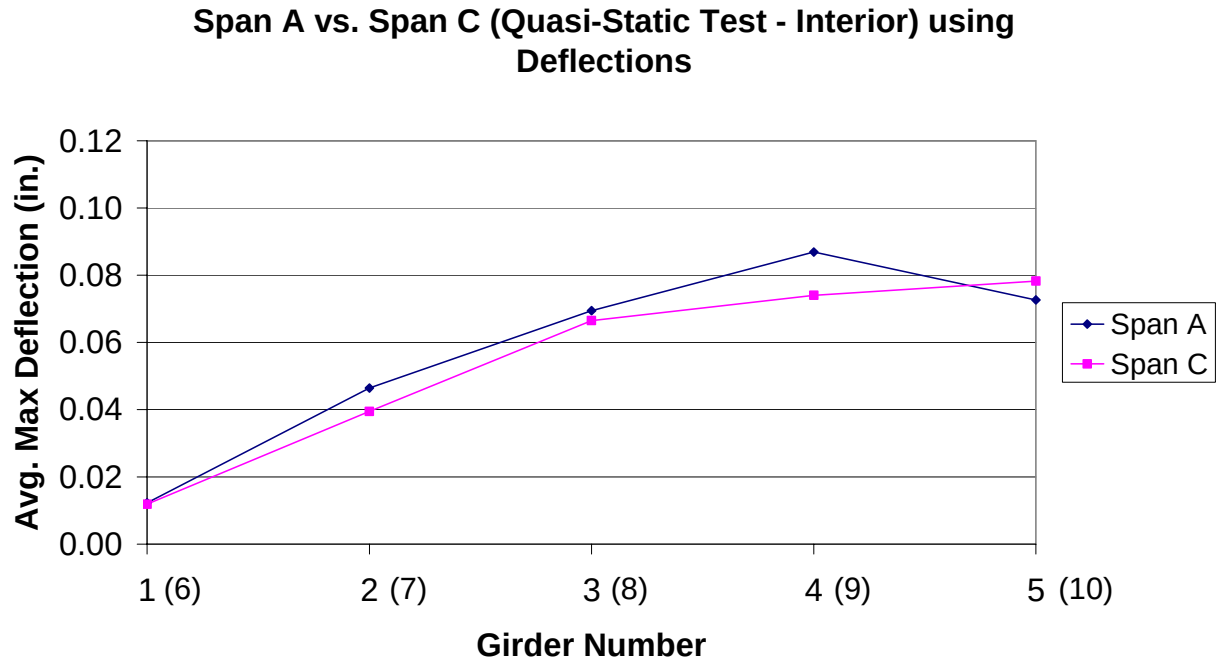

Figure 4.17: Comparison of Maximum Girder Deflections for Span A and Span C Under Quasi-static Loads with Interior Truck Orientation

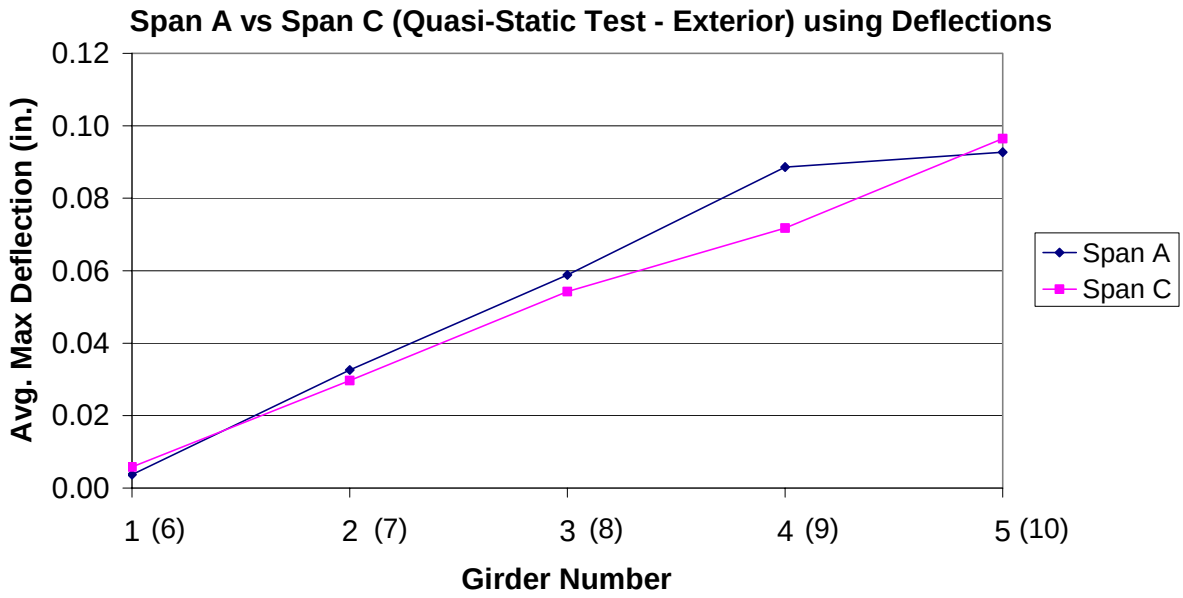

Figure 4.18: Comparison of Maximum Girder Deflections for Span A and Span C Under Quasi-static Loads with Exterior Truck Orientation

Figure 4.19 through Figure 4.21 compare the average maximum strains recorded by the ER strain gauges for Span A and Span C for each truck orientation. Similar to the deflection results, Span A experienced greater strains than Span C with the largest difference from the dynamic tests. For the ER gauges, the dynamic test showed the maximum strain to be highest at the exterior girder near the truck (girders 5 and 10). However, for the quasi-static interior orientation test, the maximum strain was at the first interior girder under the truck (girders 4 and 9). This could indicate the bridge deck works more as a plate when a dynamic load is applied causing the girders to respond in a linear fashion, making the highest strain in the exterior girder nearest the passing truck for both spans. When the truck is traveling slower, there is a more local influence, creating the greatest strain to be in the girder directly under the truck. Therefore, for the interior orientation, the highest strains were in girder 4 and 9 and for the exterior orientation, the highest strains were in girder 5 and 10. Note that the ER strain gauge installed on girder 1 was not operating at the time of the live load test so its maximum strain value was determined using a linear function between girders 2 and 3.

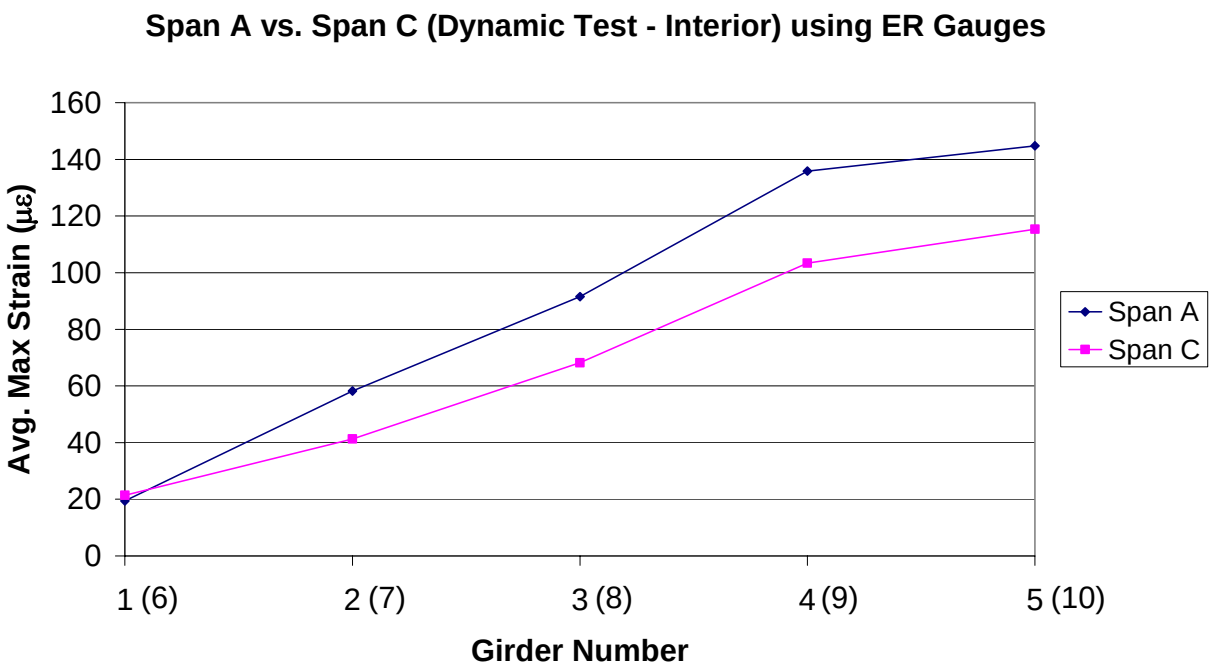

Figure 4.19: Comparison of Maximum Girder ER Strains for Span A and Span C Under Dynamic Loads

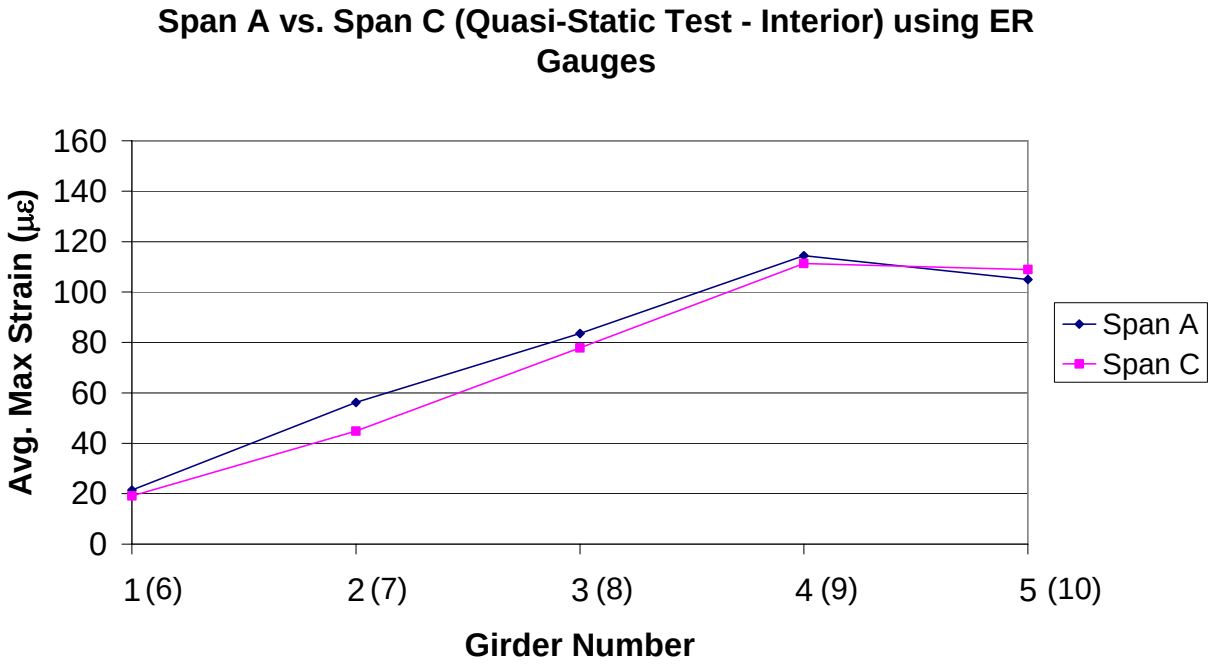

Figure 4.20: Comparison of Maximum Girder ER Strains for Span A and Span C Under Quasi-static Loads with Interior Truck Orientation

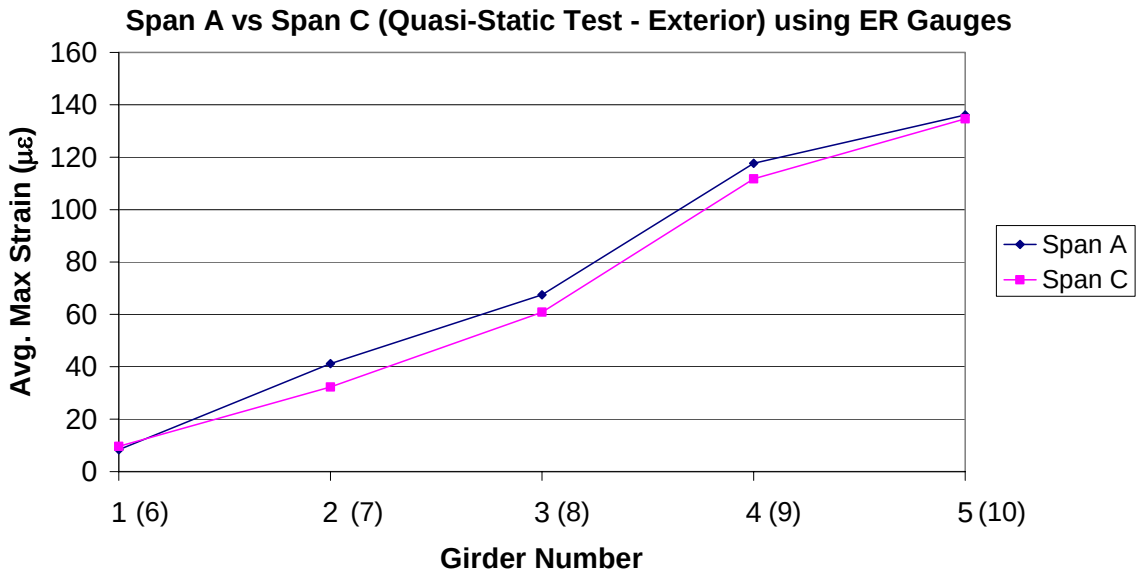

Figure 4.21: Comparison of Maximum Girder ER Strains for Span A and Span C Under Quasi-static Loads with Exterior Truck Orientation

The maximum WIM strains for Span A and Span C were compared for each truck orientation in Figure 4.22 through Figure 4.24. For the dynamic test, Span A had greater strains than Span C. The quasi-static tests had higher strains in Span A for girders 1 through 3 and in Span C for girders 9 and 10, the girders closest to the passing truck. Note that the WIM gauges on girders 2 and 6 were determined with linear interpolation. The WIM gauge on girder 2 was not reading accurate results (See Figure 4.15), and a WIM gauge was not installed on girder 6. Span C had a very different trend than Span A. Span C had more of a linear trend. In Span A, girder 4 seemed lower than expected for all three types of live load tests. This may be due to an error in installation or in the WIM gauge itself. All of the truck orientations produced the highest strain at the exterior girder near the truck path, except for in Span A for the quasi-static test with the interior truck orientation. In Span A for the quasi-static test with the interior truck orientation, the highest strains were at girders 3 and 5. The truck was straddling the first interior girder (girder 4) for this test. The high strains could be caused by the local response to the wheels that are near those two girders or, as noted earlier, there could be an error in the WIM gauge on girder 4. The average maximum strains measured by the WIM gauges are lower than the strains measured by the ER gauges. This is true for both the dynamic and the quasi-static tests.

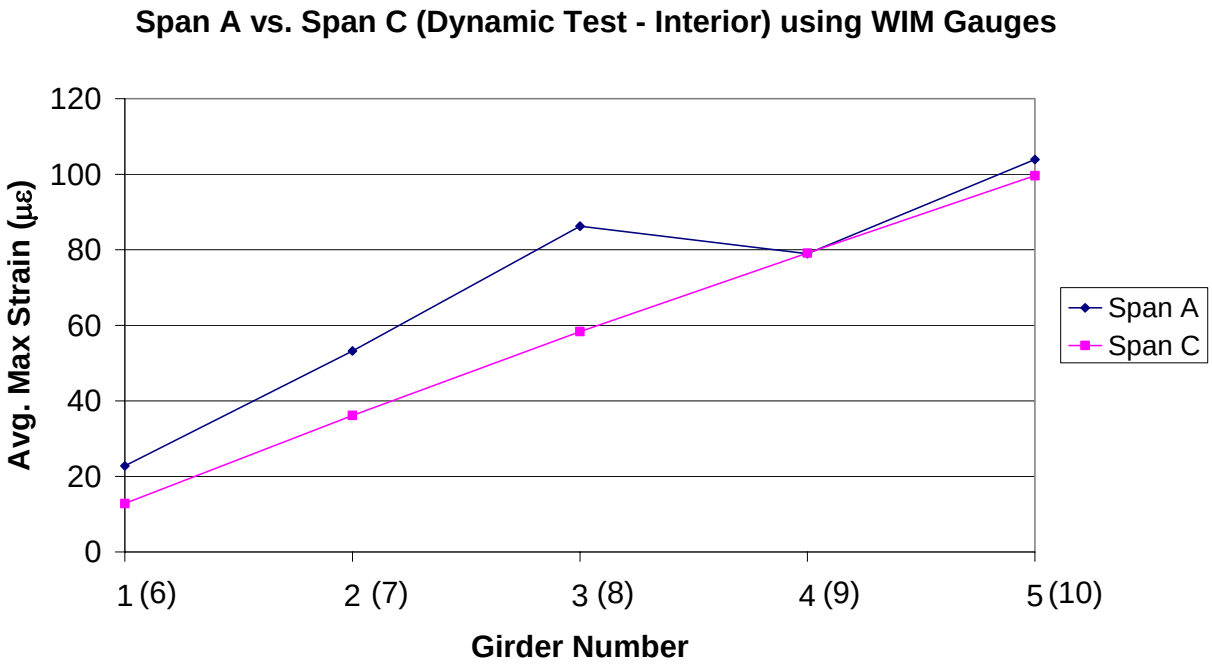

Figure 4.22: Comparison of Maximum Girder WIM Strains for Span A and Span C Under Dynamic Loads

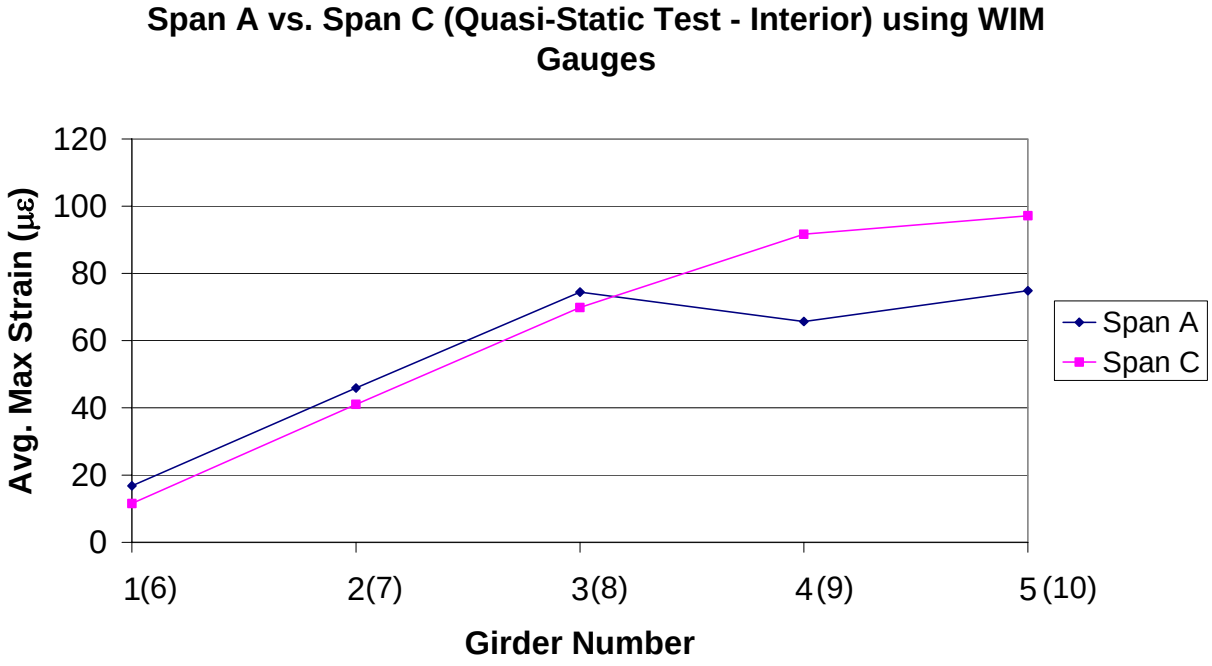

Figure 4.23: Comparison of Maximum Girder WIM Strains for Span A and Span C Under Quasi-static Loads with Interior Truck Orientation

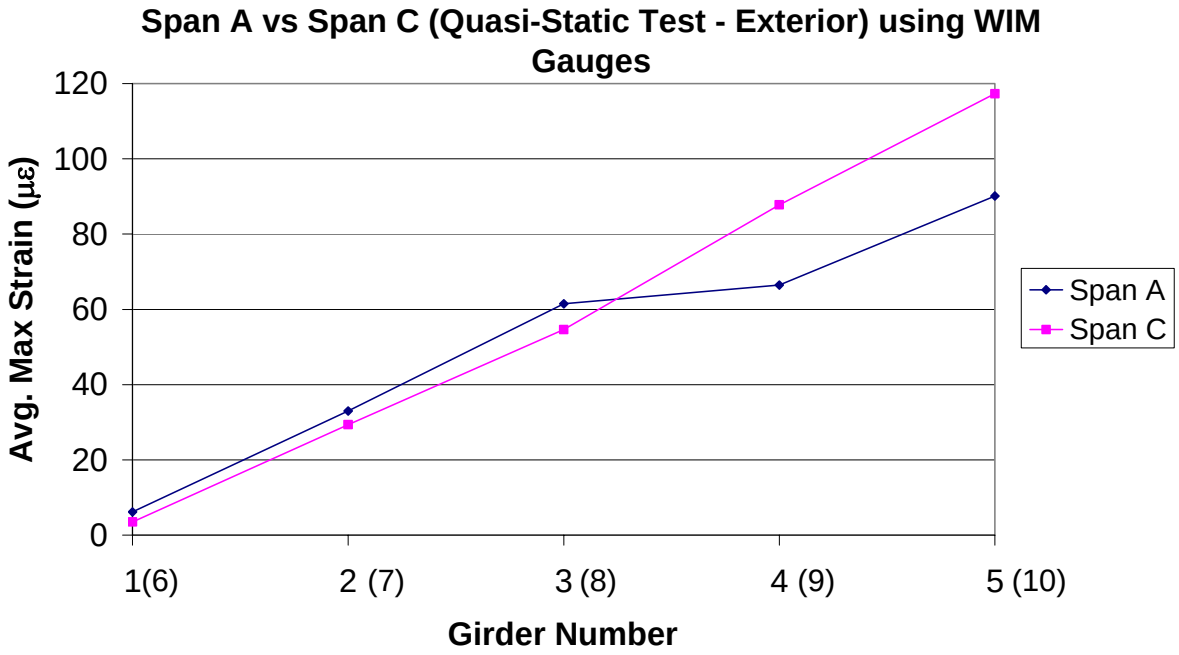

Figure 4.24: Comparison of Maximum Girder WIM Strains for Span A and Span C Under Quasi-static Loads with Exterior Truck Orientation

4.1.2.3 Determination of Girder Distribution Factors for Live Load Tests

The girder distribution factors were calculated using the data collected from the live load testing. Since the deck dimensions and girder locations along the length of the bridge remain constant, three sets of the data can be used to determine the distribution factors: the strain in the girders measured by the ER strain gauges, the strain in the girders measured by the WIM gauges, and the deflection of the girders measured by the deflectometers. All three of these methods could be used since each girder was instrumented. All of the live load tests were used for calculating the girder distribution factors. For the calculations, the reduced quasi-static data was used but none of the running-average data was used.

The procedure used to calculate the distribution factors was the same for each method and was carried out for each live load test. The procedure followed using the girder deflections is as follows. First, the maximum deflection of each girder was determined ($\Delta_{i,max}$). Secondly, the time of the highest $\Delta_{i,max}$ was recorded. Just like with the analysis of the transverse strains in Section 4.1.1, the calculation is like taking a

snapshot at the time of the maximum deflection. The deflection of each girder at the time of the highest $\Delta_{i,max}$ was recorded which is denoted as $\Delta_{corresp}$. Each girder's corresponding deflection was divided by the sum of all of the corresponding girder deflections to determine what fraction of the total deflection the girder is experiencing at the given time. This fraction is the girder distribution factor, referred to in AASHTO LRFD as g. For ease of comparison, the distribution factors were normalized by converting them into the denominator, D. To find D, the distribution factors were multiplied by two since there were two wheel lines and g is only for one wheel line. A sample of the calculation of D can be seen in Table 4.2. The maximum deflections were recorded. In this case, the maximum deflection of all the girders was the deflection at girder 4 at a time of 22.8 seconds, identified in bold print. The corresponding deflections at that time were recorded. Each corresponding deflection was divided by the sum of the corresponding deflections to get the girder distribution factor for each girder. Then to get the D value, the girder center-to-center spacing of 6.5 ft was divided by the GDF times two.

Table 4.2: Span A Quasi-Static Interior Configuration GDF Data

	Deflections				
	$\Delta_{i,max}$ (in.)	Time (sec)	$\Delta_{corresp.}$ (in.)	GDF	"D"
G1	0.0136	22.8	0.0113	0.039	82.4
G2	0.0479	22.8	0.0454	0.159	20.5
G3	0.0701	22.8	0.0689	0.241	13.5
G4	**0.0876**	22.8	0.0876	0.306	10.6
G5	0.0734	22.8	0.0734	0.256	12.7

The girder distribution factors were calculated for each type of test using all three sources (deflectometers, ER strain gauges, and WIM gauges). To determine the GDF's, the deflections and strains of each girder need to be known. Some of the data needed to be interpolated to calculate the GDF's. For Span A, the ER strain gauge on girder 1 was inoperable so a linear relationship was used between the strains of girder 2 and 3 to find the strain in girder 1. The linear relationship was determined to be reasonable when examining the results of the deflectometers. A linear interpolation was also used to determine the WIM strain for girder 6. Girder 6 could not be instrumented since only nine WIM gauges were available. Interpolation was used for the WIM gauge on girder 2

since it did not have reasonable readings (See Figure 4.15). Fortunately, only one interpolation or less had to be used per GDF calculation. Table 4.3 through Table 4.6 show the GDF values that were calculated using the deflections of the girders only. The GDF value in bold print is the controlling girder distribution factor for the respective test. The GDF_{avg} values for all five girders should sum to 1.0 when added together since they are fractions of the total load carried by the girder.

Table 4.3: GDF Results for Span A Interior Configuration Tests

Span A - Interior Truck Configuration								
	Quasi-Static Data				Dynamic Data			
Girder #	Δ_{avg} (in.)	GDF_{max}	GDF_{min}	GDF_{avg}	Δ_{avg} (in.)	GDF_{max}	GDF_{min}	GDF_{avg}
G1	0.012	0.045	0.039	0.041	0.021	0.056	0.037	0.049
G2	0.046	0.165	0.159	0.161	0.059	0.161	0.140	0.153
G3	0.069	0.245	0.239	0.241	0.089	0.237	0.227	0.232
G4	0.087	0.306	0.302	**0.304**	0.112	0.304	0.287	**0.294**
G5	0.073	0.256	0.249	0.253	0.105	0.291	0.261	0.273
				Σ = 1.000				Σ = 1.000

Table 4.4: GDF Results for Span C Interior Configuration Tests

Span C - Interior Truck Configuration								
	Quasi-Static Data				Dynamic Data			
Girder #	Δ_{avg} (in.)	GDF_{max}	GDF_{min}	GDF_{avg}	Δ_{avg} (in.)	GDF_{max}	GDF_{min}	GDF_{avg}
G6	0.012	0.045	0.039	0.042	0.015	0.069	0.057	0.062
G7	0.039	0.150	0.138	0.144	0.032	0.146	0.117	0.130
G8	0.066	0.252	0.241	0.246	0.053	0.231	0.217	0.226
G9	0.074	0.279	0.272	0.275	0.062	0.264	0.248	0.255
G10	0.078	0.304	0.281	**0.293**	0.075	0.353	0.307	**0.326**
				Σ = 1.000				Σ = 1.000

Table 4.5: GDF Results for Span A Exterior Configuration Tests

Span A - Exterior Truck Configuration				
	Quasi-Static Data			
Girder #	Δ_{avg} (in.)	GDF_{max}	GDF_{min}	GDF_{avg}
G1	0.004	0.015	0.008	0.012
G2	0.033	0.120	0.116	0.117
G3	0.059	0.215	0.210	0.213
G4	0.089	0.322	0.319	0.321
G5	0.093	0.340	0.336	**0.338**
			Σ =	1.000

Table 4.6: GDF Results for Span C Exterior Configuration Tests

Span C - Exterior Truck Configuration				
	Quasi-Static Data			
Girder #	Δ_{avg} (in.)	GDF_{max}	GDF_{min}	GDF_{avg}
G6	0.006	0.026	0.015	0.019
G7	0.030	0.116	0.112	0.114
G8	0.054	0.212	0.209	0.211
G9	0.072	0.282	0.275	0.279
G10	0.096	0.380	0.374	**0.377**
			Σ =	1.000

The GDF and D values for Span A calculated from the deflections of the girders are presented in Table 4.7. Table 4.8 shows the same calculations for Span C. The D value is the denominator of equation 4-2, g = S/D. The minimum GDF corresponds to the maximum D value. Similarly, the maximum GDF corresponds to the minimum D value.

Table 4.7: GDF's and D-values for Span A from Deflection Data

			Span A						
			GDF's (per axle)			Denominator "D" (per wheel)			
Truck Config.	Type	# Passes	Min	Max	Avg.	Min	Max	Avg.	Comb. Avg.
Interior	Quasi-Static	5	0.302	0.306	0.304	10.8	10.6	10.7	10.9
	Dynamic	6	0.287	0.304	0.294	11.3	10.7	11.1	
Exterior	Quasi-Static	5	0.336	0.340	0.338	9.7	9.6	9.6	9.6

Table 4.8: GDF's and D-values for Span C from Deflection Data

			Span C						
			GDF's (per axle)			Denominator "D" (per wheel)			
Truck Config.	Type	# Passes	Min	Max	Avg.	Min	Max	Avg.	Comb. Avg.
Interior	Quasi-Static	5	0.272	0.279	0.275	11.9	11.7	11.8	12.3
	Dynamic	6	0.248	0.264	0.255	13.1	12.3	12.7	
Exterior	Quasi-Static	5	0.374	0.380	0.377	8.7	8.5	8.6	8.6

The process of determining the GDF's and the "D" factors was also carried out using the strains recorded by the ER gauges and the WIM gauges. Figure 4.25 shows a graphical representation of the "D" factor for both the 2003 and 2004 live load testing. For the interior configuration, the quasi-static and dynamic "D" values were averaged together to get a combined average as shown in Table 4.7 and Table 4.8. The AASHTO Standard Specification Interior distribution factor of S/7.0, AASHTO LRFD Interior factor of S/7.4, and AASHTO Exterior distribution factor of S/6.5 for one lane loaded are also included in Figure 4.25 for comparison to the recorded results. For ease of comparison, the AASHTO LRFD distribution factor was converted from a fraction of a lane load to a wheel line. The calculations of the AASHTO LRFD distribution factors and the intermediate results for the ER strain gauges and WIM gauges are in Appendix A. Please note that a larger D value corresponds to a smaller GDF.

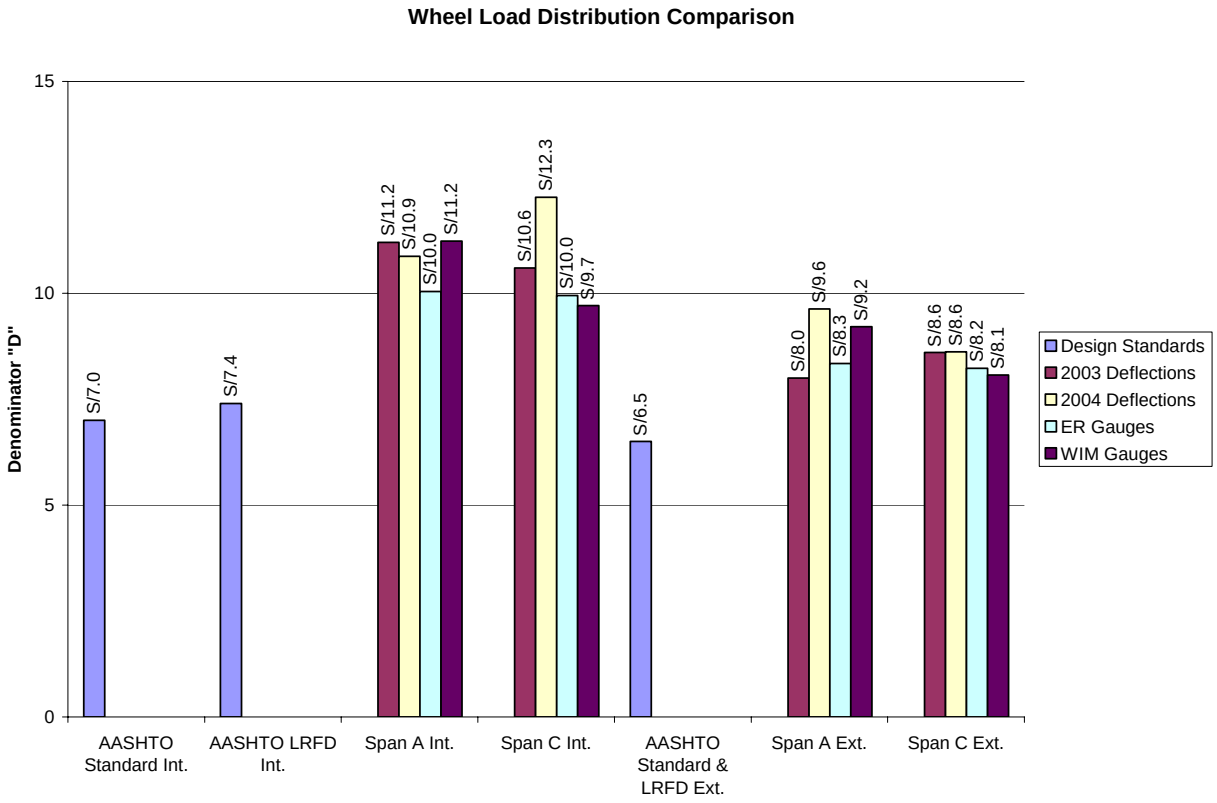

Figure 4.25: Distribution Factor Comparison

For the interior girder, the distribution factors determined for Span A and Span C do not vary significantly. Using the deflections, the GDF determined for Span A was greater than for Span C, S/10.9 versus S/12.3. The GDF's determined for Span A and C using the ER strains were the same at S/10.0. Finally, the GDF values from the WIM strains are smaller for Span A than Span C, S/11.2 versus S/9.7. With the GDF values determined from the three methods, it is unclear if Span A has a higher or lower distribution factor than Span C for the interior girder orientation. However, all the GDF's for both Span A and C were less than the design values of S/7.0 from the AASHTO Standard and S/7.4 from the AASHTO LRFD, indicating that the interior girders are taking a smaller fraction of the load than designed for.

For the exterior girder, the calculated GDF's for Span A are slightly less than for Span C using all three methods, with S/9.6 versus S/8.6 using deflections, S/8.3 versus S/8.2 using ER strains, and S/9.2 versus S/8.1 using WIM strains. All of these values were less than the design limit of S/6.5 calculated using the lever rule.

When comparing the distribution factors from the live load tests performed in 2004 to those from 2003, there is no clear trend in the changes. For the interior girder orientation, the GDF of 2003 for Span A is slightly lower than for Span C. However, the values of S/11.2 for Span A and S/10.6 for Span C are very similar to the values recorded in 2004. This indicates that there was no significant change in the distribution factors over the year between live load tests. The 2003 GDF values for the exterior girder orientation show a trend contrary to the 2004 results. In 2003, Span A had a higher GDF than Span C, S/8.0 versus S/8.6. The 2004 GDF values for Span A were lower than Span C. Like the interior orientation values, the GDF from 2003 was very close to the GDF's from 2004 for the exterior orientation.

Figure 4.26 is a comparison of the average distribution factors for the two truck orientations of Spans A and C calculated using the deflections. It includes results from the quasi-static and the dynamic live load tests of 2003 and 2004. The distribution factors should be the same for the quasi-static and dynamic tests of a given span during the same year since GDF's are independent of the type of loading. The biggest difference is from the 2004 tests of S/11.8 and S/12.7. Using the girder spacing of 6.5 feet, the actual distribution factors were calculated to 0.551 and 0.512. That is a difference of

0.390, or 3.9% of the total load per wheel line. With such a small difference, the distribution factors for the quasi-static and dynamic tests are essentially equivalent.

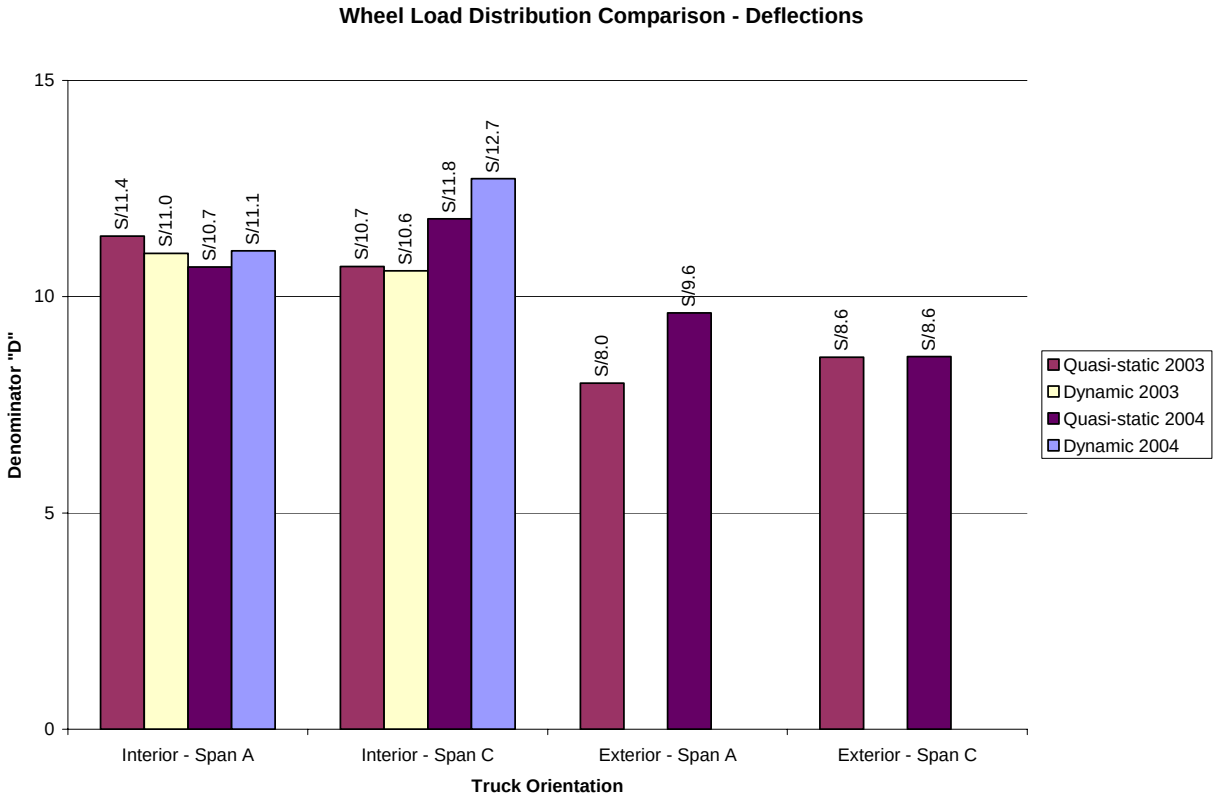

Figure 4.26: Distribution Factors Under Quasi-static and Dynamic Loads Using Deflections

The quasi-static and dynamic GDF's were averaged for each span to compare the spans. In the year 2004, the average GDF for the interior configuration of Span A was S/10.9 and for Span C was S/12.25. That equates to GDF's of 0.596 for Span A and 0.531 for Span C, a difference of 6.6% of the total load per wheel line. The GDF difference for 2003 was 3.0%. Although, the 2004 difference is more than twice that calculated for 2003, 6.6% is still a small difference. The deck should be monitored in later years to see if the difference continues to increase but for now the GDF's are within the design limits and do not vary enough to be alarming. It can be concluded from the comparison of Span A and C that the distribution factors calculated from the girder deflections for the deck reinforced with GFRP and epoxy-coated steel are the same as the

deck reinforced with all epoxy-coated steel. This is only true since the girder spacing, girder properties, and deck properties are constant.

Comparisons between the distribution factors of the two spans were also made using the information obtained from the ER strain gauges and the WIM gauges. Only data from the live load testing in 2004 was used since only three girders were equipped with ER strain gauges and WIM gauges in 2003. The average distribution factors are displayed in Figure 4.27 and Figure 4.28. The average distribution factors for the interior orientation determined using the ER strains for quasi-static and dynamic loading are similar with S/10.3 and S/9.8 for Span A and S/10.4 and S/9.5 for Span C. The exterior orientation resulted in nearly identical average GDF's for Span A and Span C with S/8.3 and S/8.2, respectively.

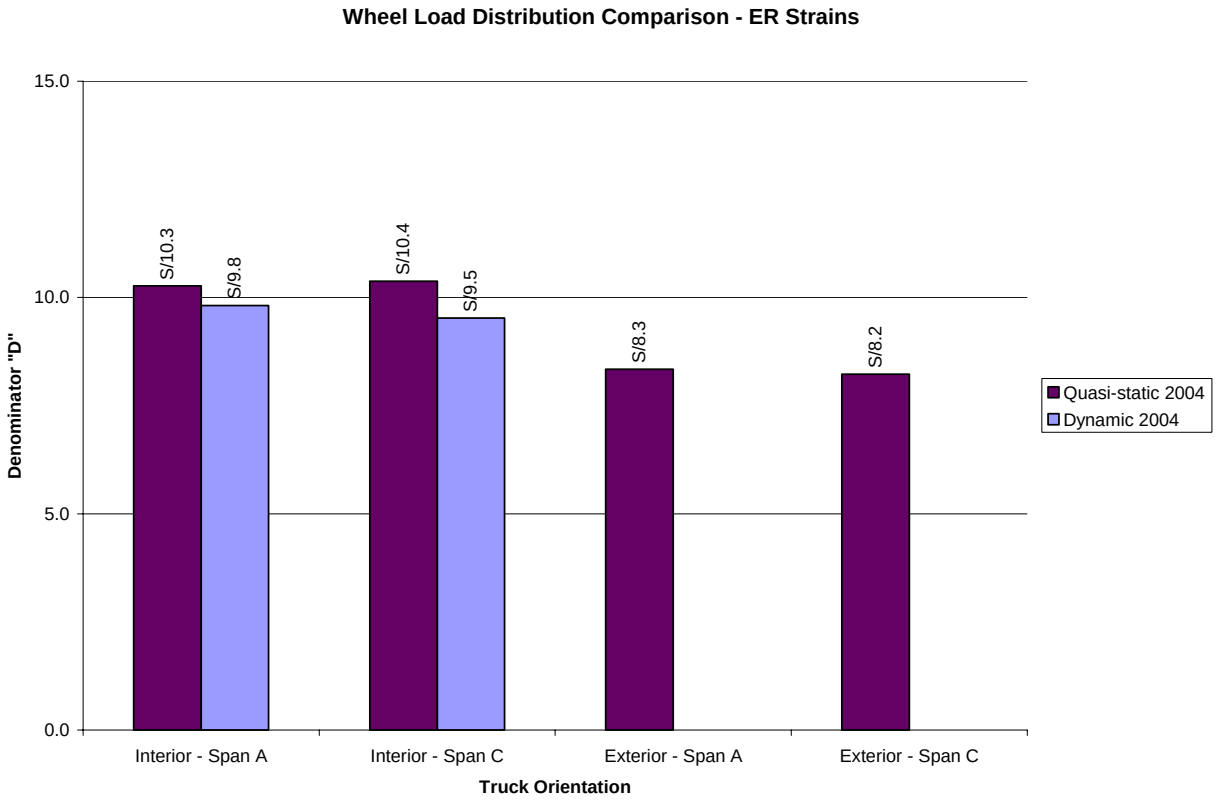

Figure 4.27: Distribution Factors Under Quasi-static and Dynamic Loads Using ER Strains

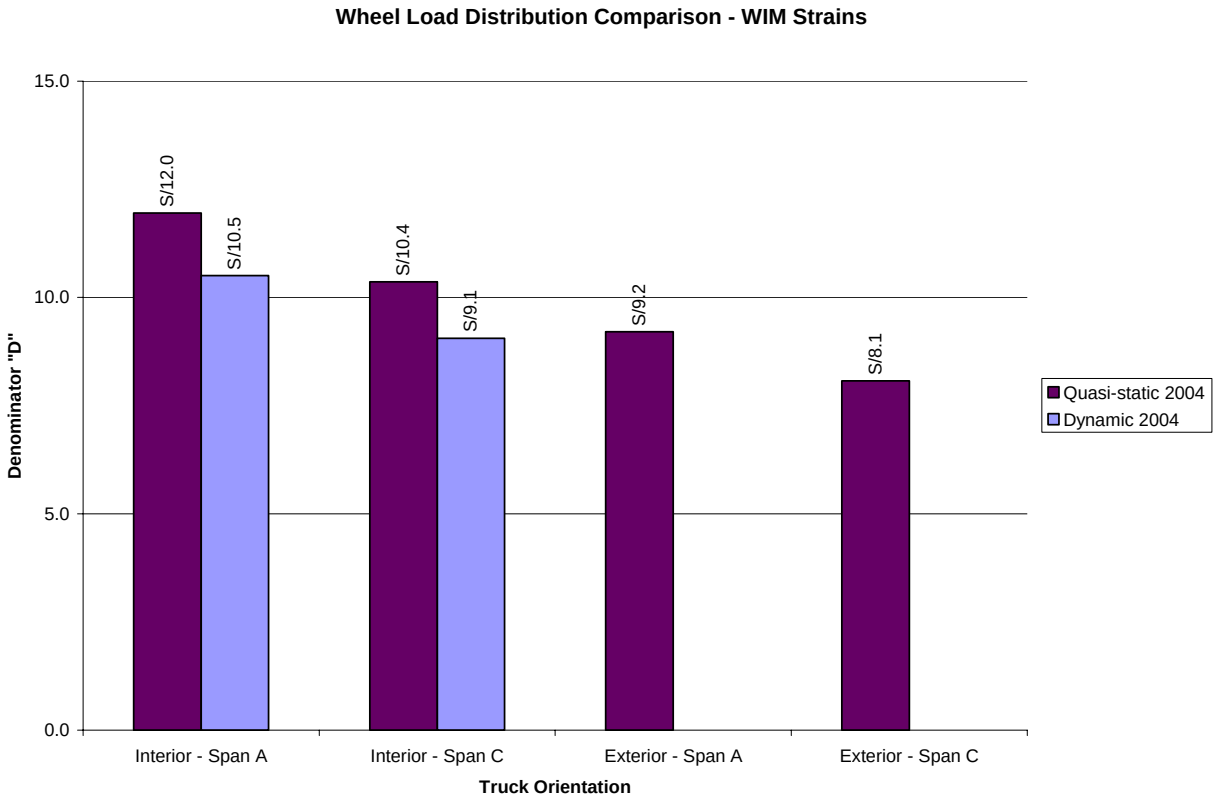

Figure 4.28: Distribution Factors Under Quasi-static and Dynamic Loads Using WIM Strains

The average distribution factors determined with the WIM strains had the most variation. For the interior orientation of Span A, the quasi-static was S/12.0 and the dynamic was S/10.5. That is equivalent to 0.542 and 0.619, a difference of 7.7%. This difference is the highest seen with all the methods used in determining the distribution factors. The difference between the two spans is the difference between the average of Span A, S/11.25, and the average of Span C, S/9.75. That is equivalent to 0.578 and 0.667, a difference of 8.9%. The difference indicates that the first interior girder in Span C is carrying 8.9% more of the total load per wheel line than in Span A. The difference is significant; however, the values are well within the distribution design requirements from the AASHTO Standards of S/7.0 (0.929) and from the AASHTO LRFD of S/7.4 (0.878). The difference may be due to an inaccuracy in the WIM gauges. Also, the questionable WIM gauge readings for girder 4 in Span A could influence the results. For all the methods, the average distribution factors calculated for the exterior orientation were very similar between Span A and C.

4.1.3 Dynamic Load Allowances

4.1.3.1 Introduction and AASHTO Definitions

Another design factor that needs to be considered is the dynamic load allowance, or impact factor (IM). The load imposed on a bridge structure is influenced by the speed at which the vehicle is traveling. With increased speed, the load being applied increases as well. The dynamic load allowance quantifies this phenomenon. The dynamic load allowance is influenced by how level and smooth the roadway is. This means that any imperfections in the deck surface, bumps in the roadway, or settlement of the joints or abutments change the dynamic load allowance value.

The AASHTO Standard Specification defines the IM in equation 3-1 as:

$$I = 50/(L+125) \qquad \textbf{Equation 4-8}$$

where I = impact factor (cannot exceed 30%)

L = length of portion of slab that is loaded to produce the maximum stress in member (ft).

The Gills Creek bridge has a span of 45 ft, so the IM would be $I = 50/(45+125) = 29\%$. AASHTO LRFD Specifications specifies in Table 3.6.2.1-1 that for all bridge components other than deck joints, and for all limit states other than fatigue and fracture, the IM is 33%.

4.1.3.2 Determination of Dynamic Load Allowances from Live Load Tests

Similar to the GDFs, dynamic load allowances were calculated using the strain in the girders measured by the ER strain gauges, the strain in the girders measured by the WIM gauges, and the deflection of the girders measured by the deflectometers. Only the live load tests done over the interior girder were used since no dynamic tests were performed over the exterior girder due to safety reasons.

The procedure used to calculate IM was the same for each method and was as follows. The baseline quasi-static and dynamic girder response (deflection or strain) of each test was determined by averaging the first five readings recorded. These readings are representative of the deflection or strain in the girder before the truck is on the span. Then, for each quasi-static and dynamic test, the maximum girder response was recorded. The base line response was subtracted from the maximum to get the calculated response

from each test. Table 4.9 presents the calculation of IM for Span A. Row (1) is the average of the quasi-static calculated responses for each girder. Rows (2) through (7) are the calculated responses for each dynamic test. The (N) indicates the truck was traveling northbound, and the (S) indicates the truck was traveling southbound. To find the IM, the dynamic calculated responses were divided by the average quasi-static response in row (1) and then subtracted by 1 to get the percentage increase. The IM values are in rows (8) through (13). Rows (14) through (19) show the maximum, minimum, and average IM values for the southbound and northbound tests.

Table 4.9 and Table 4.10 show the calculation of IM for Span A and C, respectively. The highlighted values are the maximum responses for each test using each of the three methods. The values in bold print are the IM values corresponding to the maximum responses. Note that the maximum responses all occurred at the exterior girder closest to the truck, which are girder 5 of Span A and girder 10 of Span C. The only exception is the deflection responses in Span A where the maximum deflection was at girder 4, the first interior girder directly under the truck.

Table 4.9: Calculation of IM for Span A

		Span A													
		Deflection Responses (in.)					ER Strain Responses (με)				WIM Strain Responses (με)				
Row #		G1	G2	G3	G4	G5	G2	G3	G4	G5	G1	G2	G3	G4	G5
1	**Quasi-static$_{Avg}$**	0.015	0.048	0.070	0.087	0.073	53.3	81.0	111.9	103.5	17.5		73.4	65.6	69.8
2	**Dynamic 1 (N)**	0.019	0.062	0.095	0.123	0.112	63.3	104.5	155.2	159.4	22.4		98.9	93.2	113.6
3	**Dynamic 2 (S)**	0.024	0.063	0.093	0.114	0.103	61.5	90.2	128.4	137.3	29.2		87.1	74.3	96.2
4	**Dynamic 3 (N)**	0.016	0.057	0.089	0.118	0.111	56.7	96.1	149.3	158.2	19.3		92.3	89.2	112.2
5	**Dynamic 4 (S)**	0.025	0.064	0.092	0.111	0.099	64.5	90.7	125.4	134.3	30.0		84.8	71.8	92.0
6	**Dynamic 5 (N)**	0.018	0.059	0.091	0.120	0.112	60.9	95.5	146.9	158.2	20.8		94.0	89.4	112.8
7	**Dynamic 6 (S)**	0.025	0.065	0.094	0.113	0.100	65.7	94.3	126.6	135.5	29.0		88.2	73.9	93.3
8	**IM 1**	0.268	0.298	0.353	0.417	0.530	0.187	0.290	0.387	0.540	0.274		0.346	0.420	0.628
9	**IM 2**	0.622	0.326	0.324	0.316	0.404	0.153	0.113	0.147	0.327	0.664		0.186	0.132	0.379
10	**IM 3**	0.072	0.188	0.273	0.369	0.512	0.063	0.187	0.333	0.529	0.102		0.257	0.360	0.608
11	**IM 4**	0.653	0.344	0.310	0.278	0.351	0.209	0.120	0.120	0.298	0.708		0.155	0.094	0.319
12	**IM 5**	0.172	0.242	0.300	0.381	0.525	0.142	0.179	0.312	0.529	0.187		0.280	0.362	0.616
13	**IM 6**	0.649	0.370	0.344	0.303	0.367	0.231	0.165	0.131	0.310	0.654		0.202	0.126	0.337
14	**IM$_{min}$ (N)**	0.07	0.19	0.27	0.37	0.51	0.06	0.18	0.31	0.53	0.10		0.26	0.36	0.61
15	**IM$_{max}$ (N)**	0.27	0.30	0.35	0.42	0.53	0.19	0.29	0.39	0.54	0.27		0.35	0.42	0.63
16	**IM$_{avg}$ (N)**	0.17	0.24	0.31	0.39	**0.52**	0.13	0.22	0.34	**0.53**	0.19		0.29	0.38	**0.62**
17	**IM$_{min}$ (S)**	0.62	0.33	0.31	0.28	0.35	0.15	0.11	0.12	0.30	0.65		0.15	0.09	0.32
18	**IM$_{max}$ (S)**	0.65	0.37	0.34	0.32	0.40	0.23	0.16	0.15	0.33	0.71		0.20	0.13	0.38
19	**IM$_{avg}$ (S)**	0.64	0.35	0.33	0.30	**0.37**	0.20	0.13	0.13	**0.31**	0.68		0.18	0.12	**0.34**

Table 4.10: Calculation of IM for Span C

		Span C													
		Deflection Responses (in.)					ER Strain Responses (με)					WIM Strain Responses (με)			
Row #		G6	G7	G8	G9	G10	G6	G7	G8	G9	G10	G7	G8	G9	G10
1	**Quasi-static$_{Avg}$**	0.016	0.040	0.065	0.069	0.077	20.0	42.7	72.1	108.2	103.9	37.0	62.7	84.1	90.3
2	**Dynamic 1 (S)**	0.024	0.052	0.079	0.086	0.100	25.9	53.1	80.2	120.3	125.9	47.3	72.1	94.9	109.4
3	**Dynamic 2 (N)**	0.019	0.045	0.072	0.079	0.090	22.6	48.6	75.7	107.3	116.7	43.0	65.5	84.8	102.7
4	**Dynamic 3 (S)**	0.022	0.052	0.080	0.088	0.102	23.6	52.3	80.9	122.1	126.6	46.6	73.7	95.5	110.7
5	**Dynamic 4 (N)**	0.017	0.042	0.070	0.078	0.090	20.3	46.2	73.3	107.0	117.9	40.9	64.1	83.7	103.6
6	**Dynamic 5 (S)**	0.019	0.045	0.072	0.085	0.102	20.0	48.3	74.3	119.1	128.0	41.5	65.2	90.3	112.1
7	**Dynamic 6 (N)**	0.018	0.043	0.068	0.077	0.088	22.4	45.0	69.6	103.7	114.8	40.6	62.6	80.7	100.7
8	**IM 1**	0.476	0.289	0.225	0.260	0.296	0.294	0.243	0.113	0.112	0.211	0.276	0.150	0.129	0.212
9	**IM 2**	0.171	0.124	0.115	0.153	0.170	0.129	0.138	0.050	-0.008	0.123	0.161	0.045	0.009	0.138
10	**IM 3**	0.356	0.300	0.237	0.286	0.318	0.176	0.227	0.122	0.129	0.218	0.259	0.176	0.136	0.226
11	**IM 4**	0.076	0.059	0.077	0.134	0.173	0.012	0.083	0.018	-0.010	0.134	0.104	0.023	-0.005	0.148
12	**IM 5**	0.193	0.127	0.110	0.241	0.322	0.000	0.133	0.031	0.101	0.232	0.120	0.041	0.074	0.242
13	**IM 6**	0.142	0.065	0.056	0.118	0.147	0.118	0.055	-0.035	-0.041	0.105	0.097	-0.001	-0.041	0.116
14	**IM$_{min}$ (N)**	0.08	0.06	0.06	0.12	0.15	0.01	0.06	-0.03	-0.04	0.10	0.10	0.00	-0.04	0.12
15	**IM$_{max}$ (N)**	0.17	0.12	0.12	0.15	0.17	0.13	0.14	0.05	-0.01	0.13	0.16	0.05	0.01	0.15
16	**IM$_{avg}$ (N)**	0.13	0.08	0.08	0.14	**0.16**	0.09	0.09	0.01	-0.02	**0.12**	0.12	0.02	-0.01	**0.13**
17	**IM$_{min}$ (S)**	0.19	0.13	0.11	0.24	0.30	0.00	0.13	0.03	0.10	0.21	0.12	0.04	0.07	0.21
18	**IM$_{max}$ (S)**	0.48	0.30	0.24	0.29	0.32	0.29	0.24	0.12	0.13	0.23	0.28	0.18	0.14	0.24
19	**IM$_{avg}$ (S)**	0.34	0.24	0.19	0.26	**0.31**	0.16	0.20	0.09	0.11	**0.22**	0.22	0.12	0.11	**0.23**

Looking at the average IM values, there are some cases where the IM values are higher at locations that are not experiencing the maximum response. In Span A, when the truck is traveling southbound, the average IM values calculated from the deflections and WIM strains are higher at girder 1 than at girder 5. Similarly in Span C with the truck traveling southbound, the average IM value calculated from the deflections is higher at girder 6 than girder 10. This would mean that the exterior girder on the opposite side of the truck crossing is most influenced by the speed of the truck. The responses at this location are very small so even small amounts of noise in the system or errors in the measuring device can create large variations between the Quasi-static$_{Avg}$ and the dynamic readings. Also, variations between the readings from the quasi-static tests influenced the Quasi-static$_{Avg}$ value. For example, the deflections of girder 1 during the quasi-static tests ranged from 0.0138 to 0.0161. If another test was performed or a test was eliminated, the Quasi-static$_{Avg}$ value would change and influence the IM value.

For all the cases, the IM values for girder 5 and girder 10 will be examined. The average of the maximum deflection of girder 5 under the quasi-static live load was 0.073 in. The maximum deflections caused by the dynamic live load ranged from 0.099 in. to 0.112 in. Figure 4.29 shows a comparison of a quasi-static and dynamic response versus

time for girder 5 of Span A. The plot illustrates how the girders deflect more when a truck is going faster than when it is going slower, demonstrating the concept of dynamic load allowance.

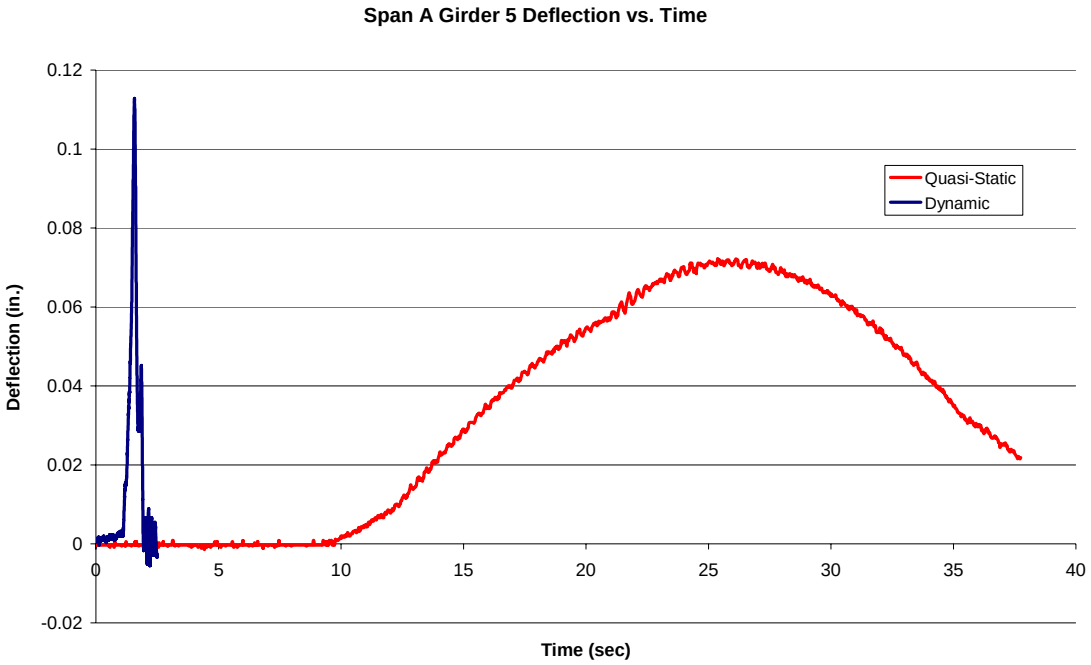

Figure 4.29: Span A Deflections Under Quasi-static and Dynamic Loading

The IM_{avg} values in Table 4.9 and Table 4.10 were calculated by dividing the average of the maximum dynamic deflections for the given truck direction by Quasi-$static_{Avg}$ and then subtracting 1 to get the percentage increase. From Table 4.9, IM_{avg} for girder 5 using deflections was 0.52 for northbound and 0.37 for southbound. The design IM value from the AASHTO Standard was 0.29 and from the AASHTO LRFD was 0.33. Neither of the measured IM values were within the AASHTO requirements.

Figure 4.30 shows a comparison of a quasi-static and dynamic response versus time for girder 10 of Span C. The IM_{avg} calculated for girder 10 was 0.16 for northbound and 0.31 for southbound. These values were within the AASHTO LRFD, however the southbound value was slightly higher than the AASHTO Standard limit of 0.29. The IM values calculated from the girder deflections for both Span A and Span C are shown in Figure 4.31.

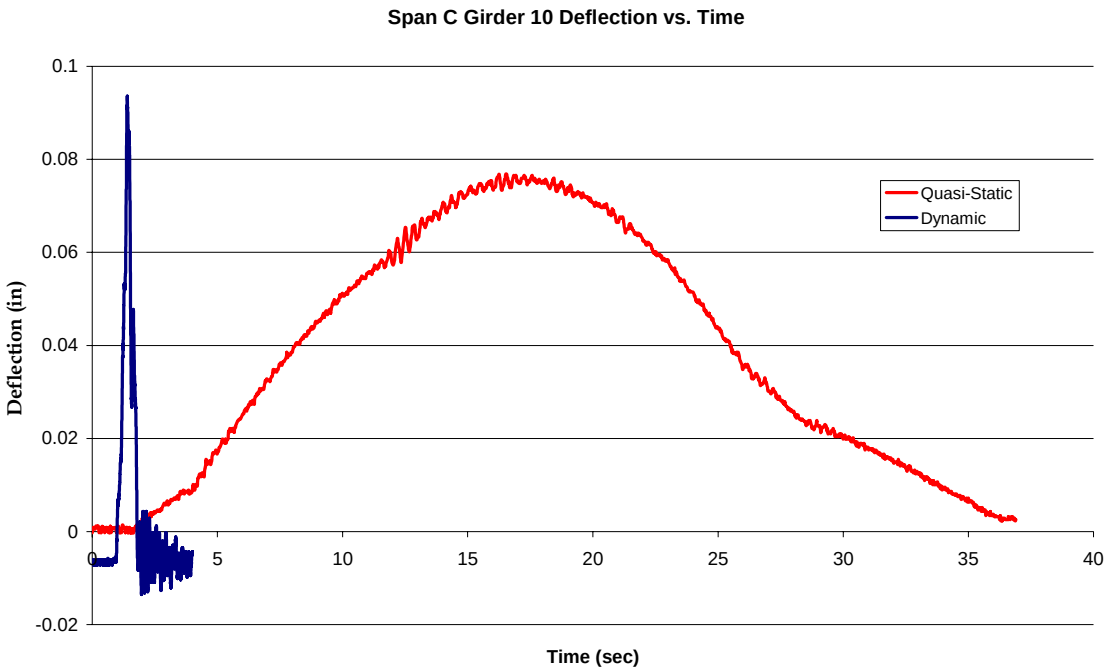

Figure 4.30: Span C Deflections Under Quasi-static and Dynamic Loading

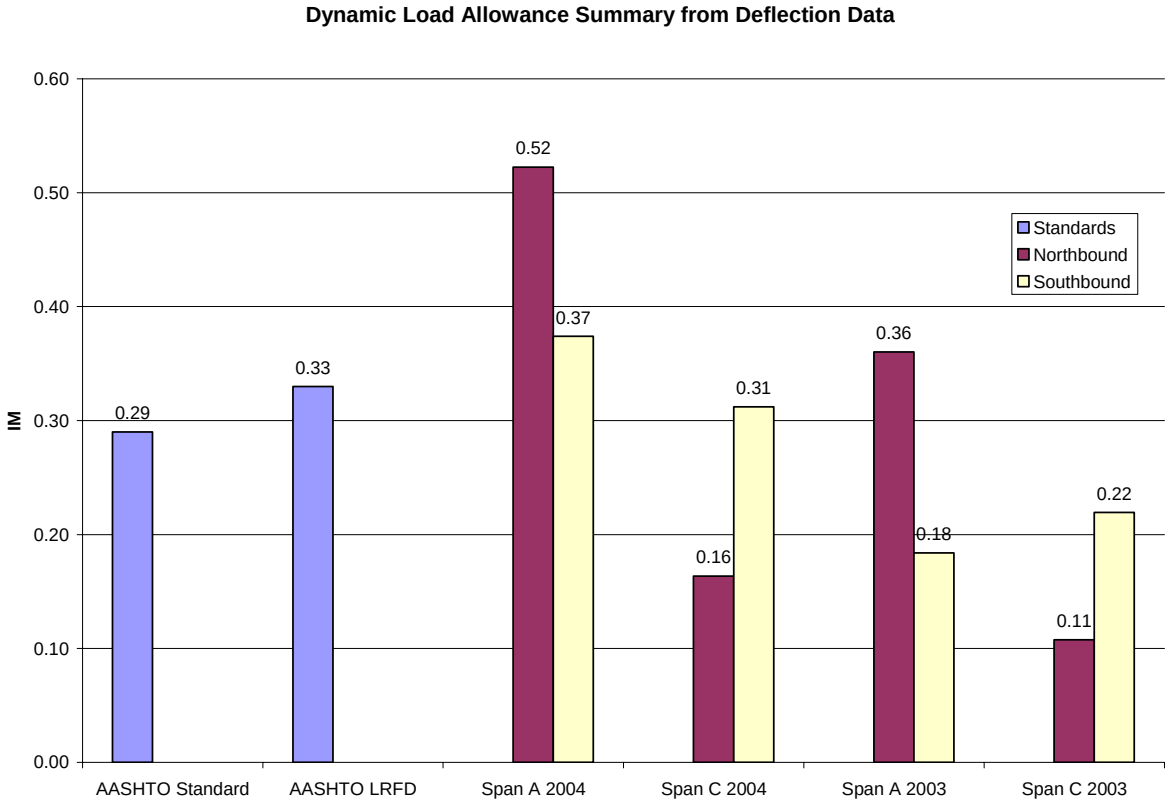

Figure 4.31: Dynamic Load Allowance Summary for Deflection Data

In all cases, the IM values calculated in 2004 were higher than in 2003. The 2004 values in Span A, both southbound and northbound, exceed the limits of the AASHTO Standard and LRFD. Even in 2003 the northbound tests of Span A had IM values that exceeded the limits. One explanation of the increase in IMs is increased flexibility of the bridge deck. With more flexibility, higher loads can create greater responses in the girders. As stated earlier, no visible cracking of the bridge deck was detected. In Span A, the northbound IM values were higher than the southbound. When the truck was traveling northbound onto Span A, it was going over the abutment onto the first span of the bridge. In Span C, the trend was opposite with the southbound IM values being higher. When the truck was traveling southbound onto Span C, it was going over the abutment onto the first span of the bridge. The abutments may cause the IM values to be higher by influencing how the truck load is distributed when traveling at a high speed. Cracking was observed at the approach but no settling.

For comparison, Figure 4.32 shows the IM values calculated from the ER strain gauges on girders 5 and 10. The extremely low strains under the dynamic loads for Span A were concluded to be erroneous in Harlan (2004). The IM values calculated from the WIM strain gauges on girders 5 and 10 are shown in Figure 4.33. There is no WIM strain data from the 2003 live load test to compare to. For both the ER and WIM gauges, the results from 2004 indicate that Span A has IM values that are above the design impact factors of AASHTO. All three methods used to determine the IM values for girders 5 and 10 indicate that Span A has a higher dynamic load allowance than the value used in design. The results for Span C are within the design values.

It is important to note that although the impact factors were above the design values, there was no cracking or compromising of the structure seen during testing. The girders are Grade 50, so they have a minimum tensile strength of 50 ksi. Looking in Table 4.9, the highest strain recorded in the girders of Span A was 159.4 με. The strain is converted to stress using $\sigma=E_s\varepsilon$, where E_s is the modulus of elasticity of the steel, 29,000 ksi. The maximum stress in the girders of Span A was calculated to be 29,000* ($159.4*10^{-6}$) or 4.62 ksi. The stresses in the steel girders were less than 10% of the tensile strength of the girder. For Span C, the stresses in the girders were even smaller.

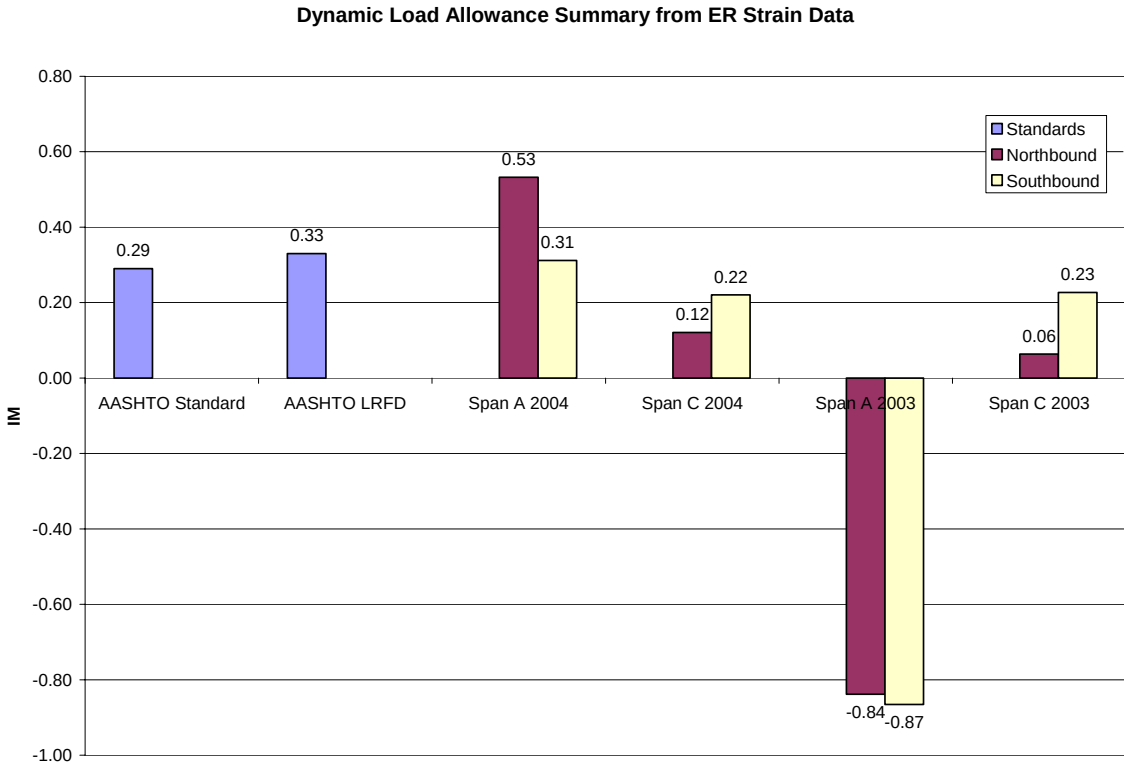

Figure 4.32: Dynamic Load Allowance Summary for ER Strain Data

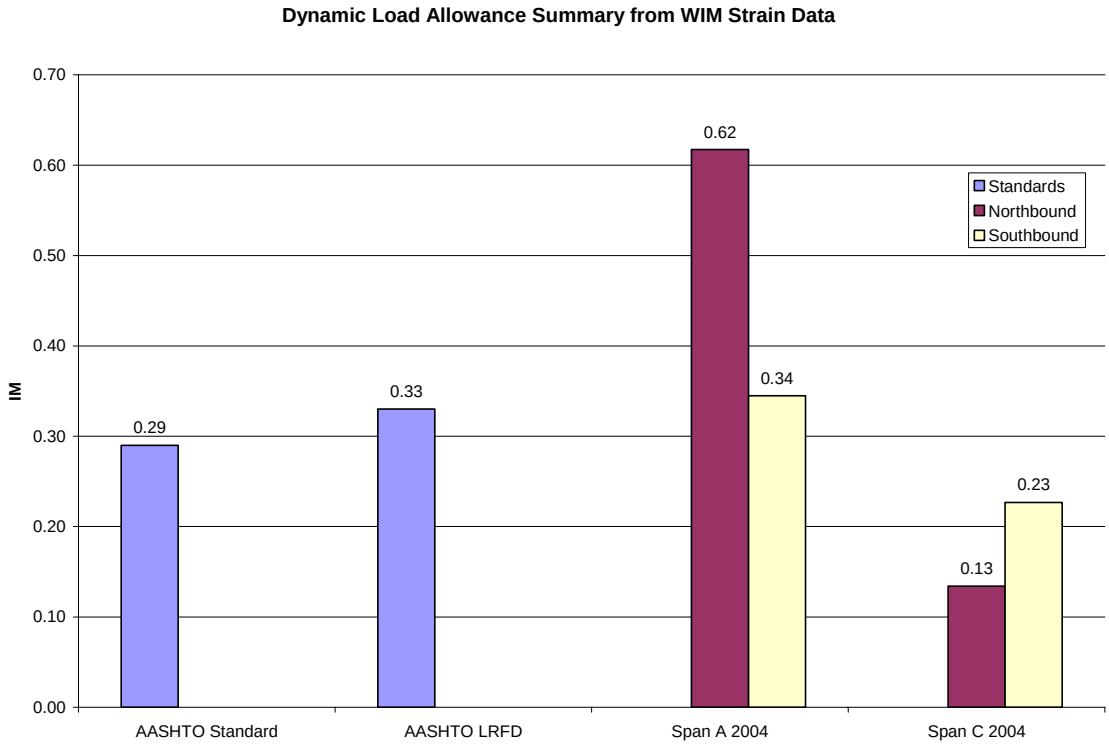

Figure 4.33: Dynamic Load Allowance Summary from WIM Strain Data

4.2 Weigh Station Slab

A live load test was performed on the I-81 weigh station slab on May 13, 2004 and approximately five months later on October 20, 2004 to investigate the change in behavior over time of the GFRP bars in the top mat of reinforcement.

4.2.1 Peak Strains in Reinforcing Bars

The peak strains in the GFRP reinforcing bars were used to see the changes between the two live load testing sessions. For the first live load session, eight of the ten GFRP strain gauges were operable: gauges 1, 2, 3, 4, 5, 6, 9, and 10. At the second live load session, only gauges 2, 3, 5, and 9 were still operable. The even gauges are located approximately 4 in. to the left of the centerline of the slab, and the odd gauges are approximately 4 in. to the right of the centerline. For each test the peak strain was determined. The baseline strain was found by taking an average of the first 20 readings. Then, the baseline strain was subtracted from the recorded maximum strain to calculate the actual peak strain. The noise in the system in May was ±2 με and in October, ±5 με.

For comparison, the loads of a design truck were applied to the slab at specified locations. A structural analysis program called MASTAN2 (Ziemian and McGuire 2000) was used to model and analyze the slab. According to AASHTO, the design truck axle weighs 32 kips. The load was divided evenly to each wheel for a wheel load of 16 kips. The two wheel loads spaced at six feet were applied to the slab at the four truck positions used in the live load tests: the right wheel positioned at centerline and then at 1, 2, and 3 feet from centerline. The moments at the gauge locations were recorded. Figure 4.34 shows an example of how the moments were determined.

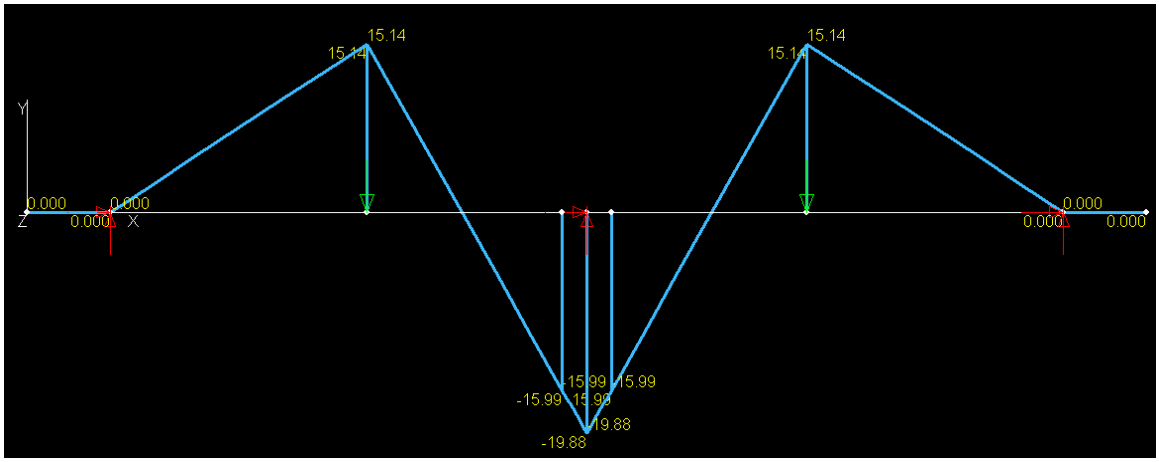

Figure 4.34: Example Moment Diagram from Truck Loading

To find the strains at the gauge locations, the moment at each location was first converted to a stress using $\sigma=Mc/I$, where M is the applied moment, c is the distance from the neutral axis to the center of the GFRP bar, and I is the moment of inertia of the deck. Stresses were found for both an uncracked and cracked section by using the respective I. Only cracking at the top was considered since the location of interest has a negative moment. These stresses were then converted to strains using $\varepsilon=\sigma/E_f$, where E_f is the modulus of elasticity of FRP, 6,300 ksi.

Table 4.11 is an example of how the moments and strains were computed for a given truck load. The same process as with the design truck was applied, but instead of applying the 16 kip loads the actual weights of the trucks were used. For each live load test, the axle of the truck with the highest weight was used. In this example, the greatest axle weight recorded was the trailer at 34,260 lbs. The weight was divided equally between the two wheels and an axle width of 6 ft was assumed. At the time of testing, the right wheel of the truck was recorded to be approximately 2 ft from the centerline of the slab. Using the location of the tires, the moment at the odd gauge was found to be -14.23 k-ft and -15.98 k-ft at the even gauge. The moments were converted to stresses using the cracked and uncracked sections. These stresses then were converted to strains to be compared to the maximum recorded strains of each gauge. Notice that the maximum strain of gauge 1 is higher than the rest. This could be due to a crack developing near the gauge or that the gauge is not working properly and is reporting incorrect strains.

Table 4.11: Comparison of Design Truck and Actual Truck Moments and Strains

			Design Truck		Actual Truck (calculated)		Actual Truck (measured)
Design Criteria		Gauge #	Uncracked	Cracked	Uncracked	Cracked	
Moment (k-ft)	Odd Gauges	1 3 5 9	-13.29		-14.23		N/A
	Even Gauges	2 4 6 10	-14.93		-15.98		N/A
Strain (με)	Odd Gauges	1 3 5 9	21.7	610.6	23.2	653.8	234.79 34.19 28.77 26.35
	Even Gauges	2 4 6 10	24.3	685.9	26.0	734.2	41.32 68.56 51.17 24.93

To compare the two live load sessions, the moments were plotted versus strain for each test along with the predicted strains for the applied moment. The plot for gauge 9 is shown in Figure 4.35. Strains increased over time, ranging from 20 to 26 με in May and then 19 to 41 με in October. However, they were closer to the predicted strains of an uncracked section indicating that minimal to no cracking was experienced at the gauge's location.

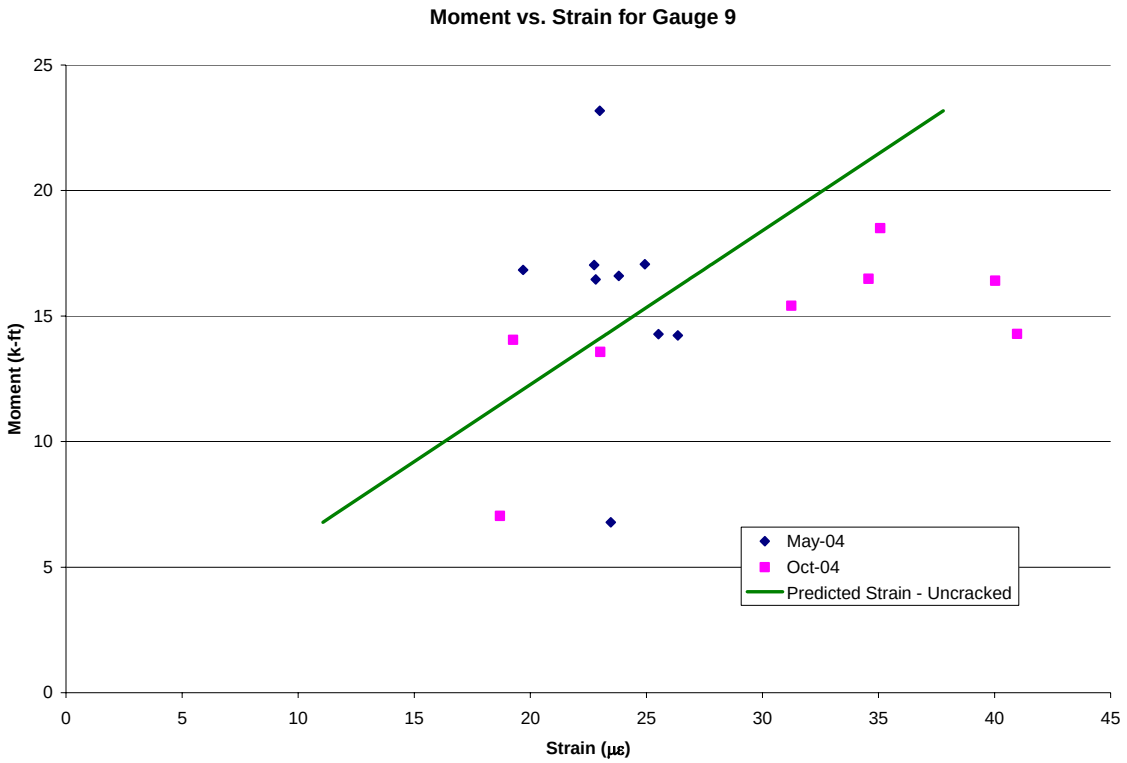

Figure 4.35: Moment vs. Maximum Strain for Gauge 9

The values plotted from the live load tests should lay along the predicted line or at least follow a linear pattern of increased moment causing increased strain. The results from both test dates did not follow that pattern. The noise in the system could have caused the strains to vary slightly. Also, the lines used for determining the truck wheel locations were at one-foot increments, so the wheel load could have been 6 in. to the left or right of the line marked. Even with these variances applied, the points would not have lined up. One explanation could be the vibration in the deck. The left corner of the deck was not securely connected to the support girder underneath, allowing that corner to deflect downward a small amount before making contact with the girder as the load was applied. This caused a substantial amount of vibration in that region of the deck that could have affected the readings of the strain gauges. Another cause could be due to the small size of the slab itself. With only a five foot length in the direction of traffic, each axle crossed the slab separately. As the truck first moved onto the slab, there was a huge load at the approach but nothing to counteract it at the other end. The same was true

when the truck was almost off the slab, causing an uneven loading and a wave of vibrations.

An example of a gauge that had larger strains close to the predicted cracked strains is in Figure 4.36. Gauge 2 had the largest strains for the second live load session. All of the other gauges showed an increase in strain, but not near the predicted strain for a cracked section. Gauge 1 had large magnitudes in May compared to the rest of the gauges. This could mean that it was starting to work improperly, especially because it was not operable in October. That could also be the reason that gauge 2 was showing such high strains in October. It seems unlikely that the location just around gauge 2 was cracked and not around any other gauges.

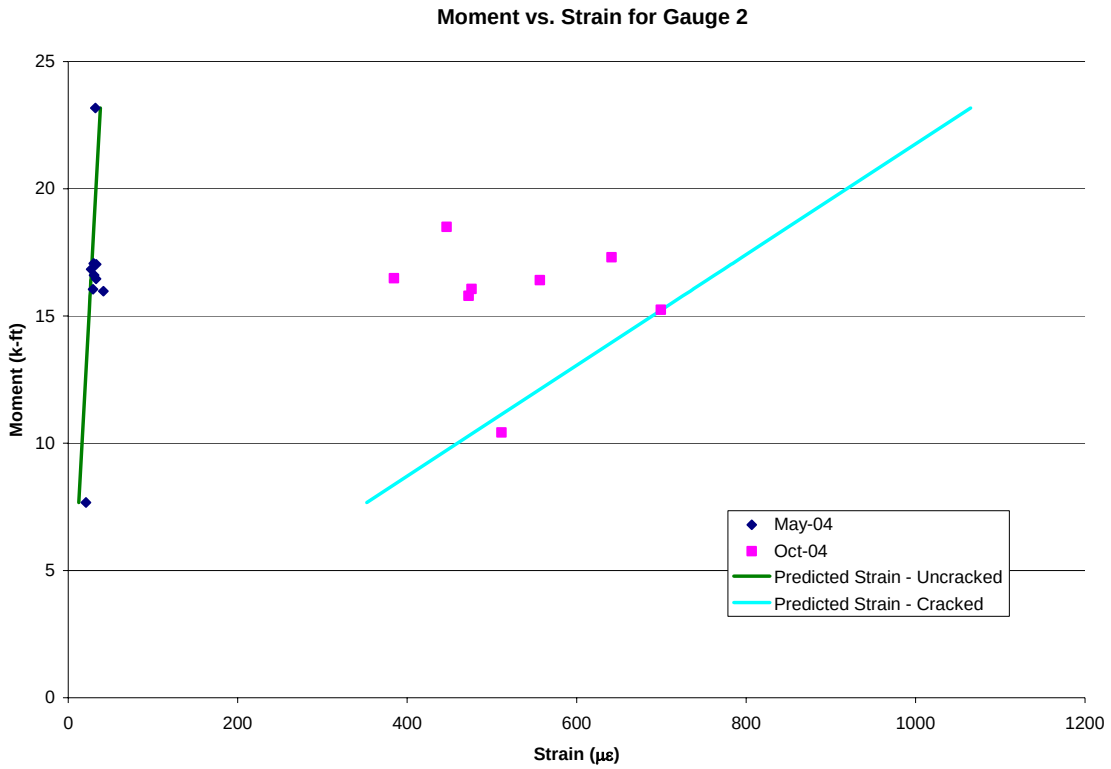

Figure 4.36: Moment vs. Maximum Strain for Gauge 2

To better understand the behavior of the slab over time, the relative flexural flexibility for each gauge was calculated and plotted in Figure 4.37. For the purposes of this thesis, flexural flexibility is defined as the maximum measured strain divided by the applied moment. The higher the value, the more flexible the member is. By plotting the flexibility against the location of each gauge, the change in flexibility along the gauge

lines can be seen. For the gauge line left of the centerline, October was not plotted since it was only one point. Gauge 2 located at 10 in. had a stiffness of 34 με/k-ft in October, considerably higher than in May. All of the values increased between the two test dates, indicating the section was becoming more flexible over time. This could indicate that there was an increase in crack depth or a loss of support under the exterior beam.

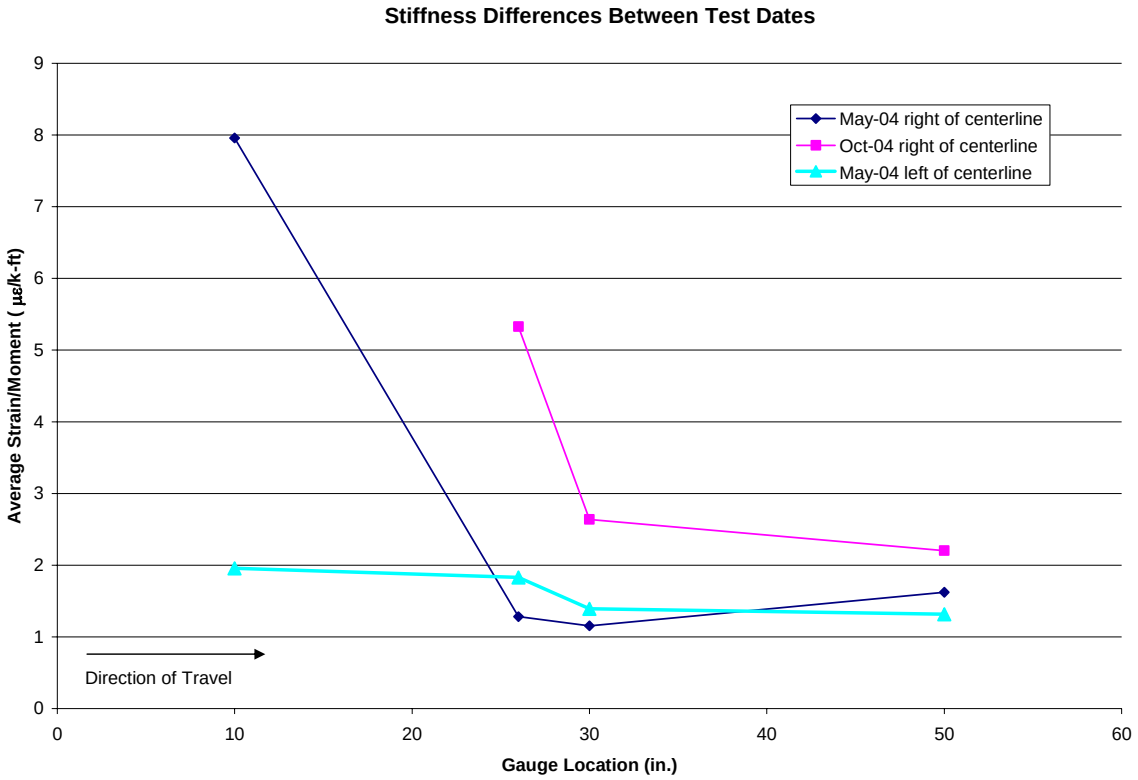

Figure 4.37: Flexural Flexibility Differences Between Test Dates

From the flexibility calculations, the steel reinforcement appears to be performing better than the GFRP. Gauges 12 and 13 on the steel reinforcement bars were compared to the GFRP gauges. Table 4.12 shows the flexibilities of the all the gauges that were operating at both live load test dates. The steel gauges had lower changes in flexibility than the GFRP gauges. This could be due to the location of the bars. The GFRP bars are at the top mat of reinforcement, subjecting them to higher tensile forces in that region. These results would have to be compared to an all-steel reinforced concrete slab to determine if the GFRP is deteriorating faster than steel would.

Table 4.12: Flexural Flexibility Comparison Between GFRP and Steel

	Average Strain/Moment (με/k-ft)					
	Gauge 2	Gauge 3	Gauge 5	Gauge 9	Gauge 12	Gauge 13
May-04	1.96	1.28	1.16	1.62	1.18	1.24
Oct-04	34.13	5.33	2.64	2.20	1.50	1.34

4.2.2 Peak Stresses in Reinforcing Bars

The stresses in the reinforcing bars were examined to see how GFRP and steel compared and if they were within the design limits. Using the maximum strains, the maximum stresses were calculated. For each gauge, the stresses were averaged to find the average maximum stress occurring at each location for the May 2004 test and the October 2004 test. It was found that the GFRP bars experienced less stress than the steel even though the GFRP was subjected to higher strains. This was because steel's modulus of elasticity of 29,000 ksi is much greater than GFRP's modulus of 6,300 ksi. Table 4.13 compares the stresses of the two types of bars.

Table 4.13: Stress Comparison Between GFRP and Steel

	Average Maximum Stress (ksi)					
	Gauge 2	Gauge 3	Gauge 5	Gauge 9	Gauge 12	Gauge 13
May-04	0.194	0.119	0.103	0.149	0.462	0.519
Oct-04	3.299	0.479	0.233	0.191	0.632	0.591

The ACI 440 allowable tensile stress of the GFRP bars was determined in Section 4.1.1 as 13.9 ksi. The calculated maximum stresses in the GFRP bars are well below the allowable, indicating that the GFRP bars are performing adequately.

4.3 Long-term Observations

Span A of the Gills Creek Bridge was monitored from November 20, 2003 to November 1, 2004, approximately one year (347 days). The instrumentation in the bridge deck was connected to a long-term data acquisition system, and readings were taken every hour. The 24 readings from each day were averaged to get the daily average to illustrate the trends more easily. At the time of installation, there were 17 ER strain gauges, 6 VW gauges, and 6 thermocouples still working properly.

4.3.1 Temperatures

Temperatures were recorded by two types of instrumentation: thermocouples and thermisters. The thermocouples are at two locations, half way between girders 4 and 5

near the abutment and near midspan. At each location, there is a thermocouple at the top, middle, and bottom of the deck. The thermisters are in the VW gauges which are in three locations, at the abutment over girder 4, at midspan over girder 4, and at midspan over girder 5. A thermister is at the top and bottom of the deck at each location. The exact locations can be seen in Figure 3.2. All of the temperature instrumentation operated correctly throughout the year except for the middle thermocouple at the midspan (TMM). TMM began not taking readings every hour on day 59, and then stopped working completely on day 127. Figure 4.38 shows a plot of the temperature recorded by the thermocouple at the abutment of Span A in the top of the deck (TAT).

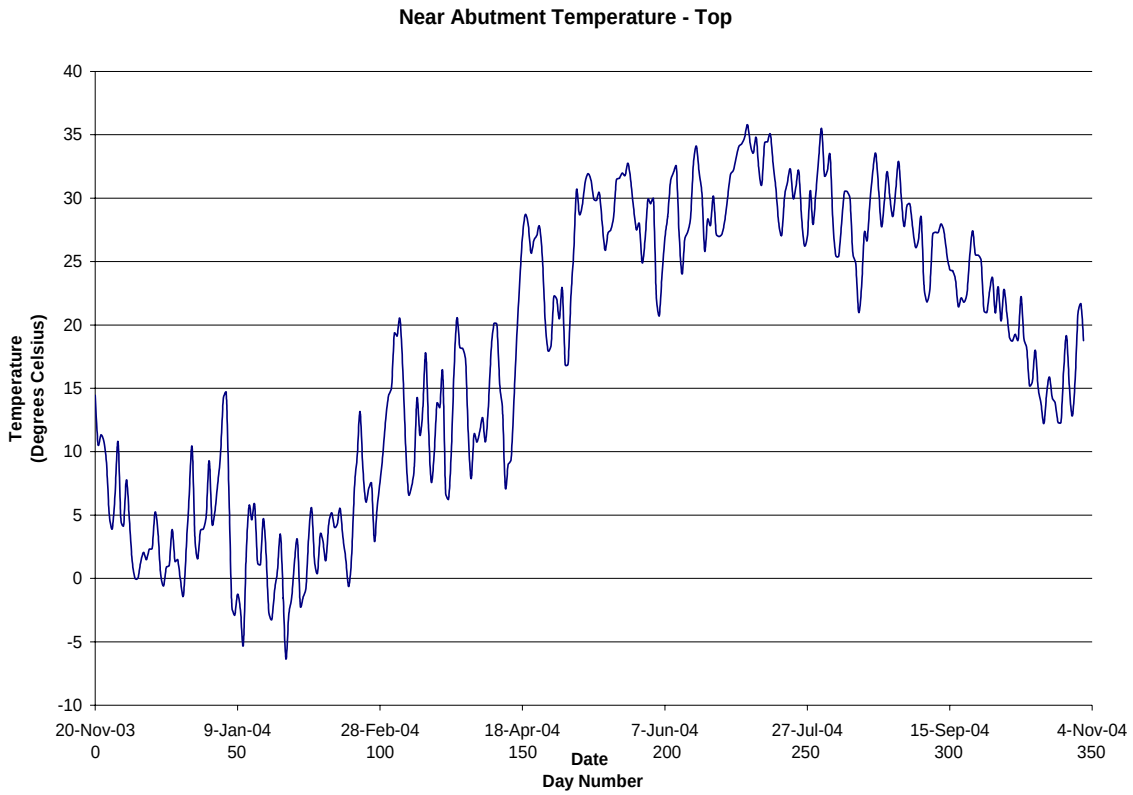

Figure 4.38: TAT Long-term Readings

All of the thermocouples had similar readings. There was very little difference between the top deck temperature at the abutment and at the midspan, no more than one degree Celsius. The bottom of the deck at midspan was always slightly warmer than at the abutment; never more than one degree Celsius. At a given location, the top of the deck was usually the warmest. The middle thermocouple read a temperature somewhere

in between the top and bottom thermocouples. Figure 4.39 shows what the temperature was through the depth of the deck at the abutment throughout the year. To see the differences, the bottom temperature was subtracted from the top temperature and from the middle temperature. In Figure 4.39, the bottom temperature is represented by x = 0 since it was used as the baseline for comparison. The middle temperature was always between the top and bottom temperatures.

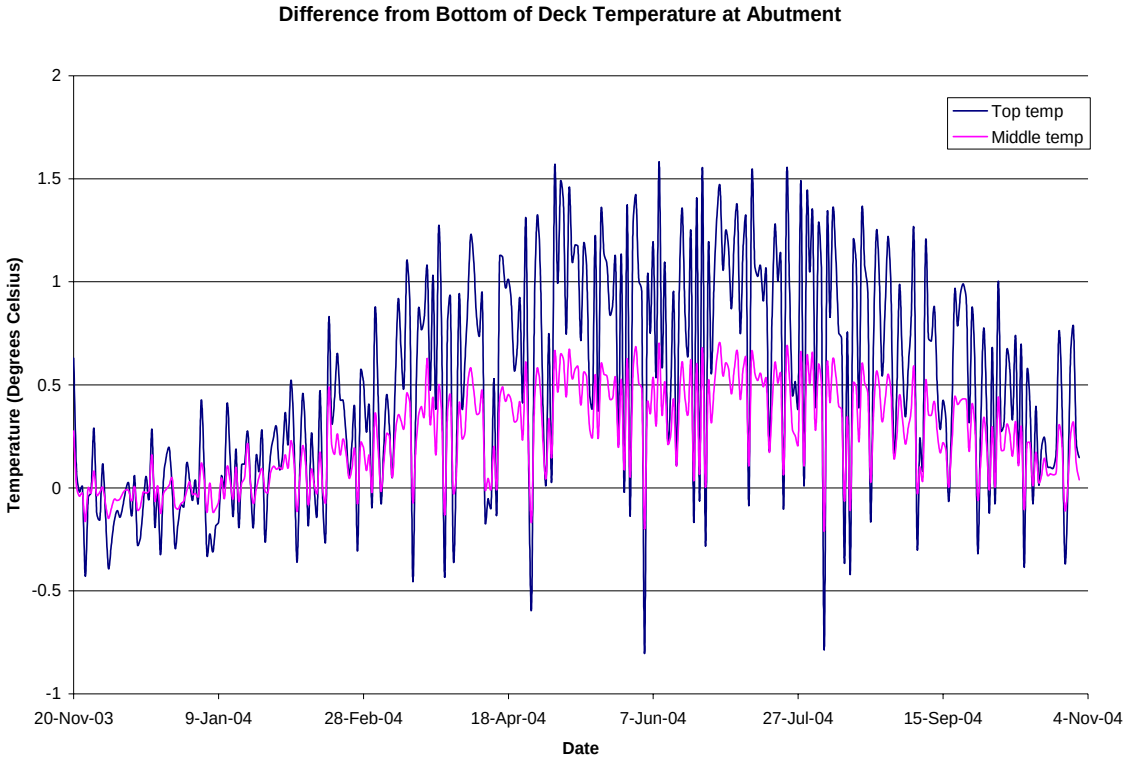

Figure 4.39: Comparison of Deck Temperatures at Abutment

Comparing the temperatures recorded at the abutment by the thermocouples and by the thermisters, the thermocouples read a little higher than the thermisters at both the top and the bottom of the deck. This could be due to the positioning of the thermocouple, with the thermocouple located half way between girders 4 and 5 and the thermister over girder 4. The two temperatures are plotted in Figure 4.40 and Figure 4.41.

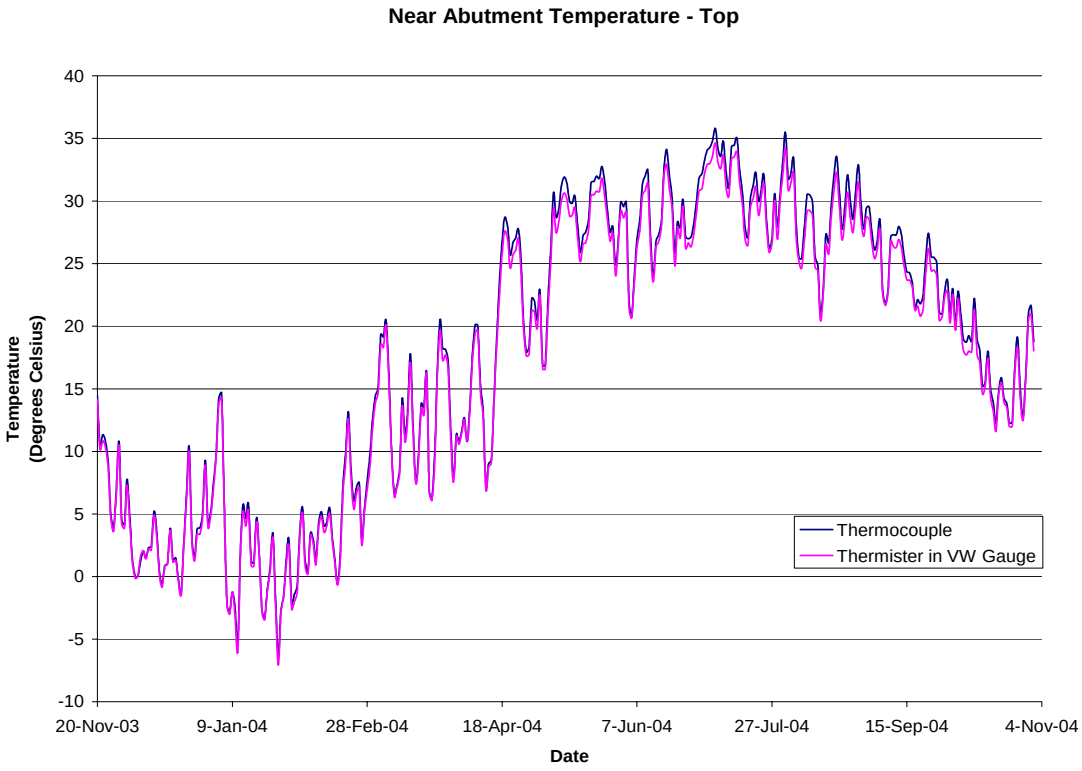

Figure 4.40: Temperature Comparison of Top of Deck at Abutment

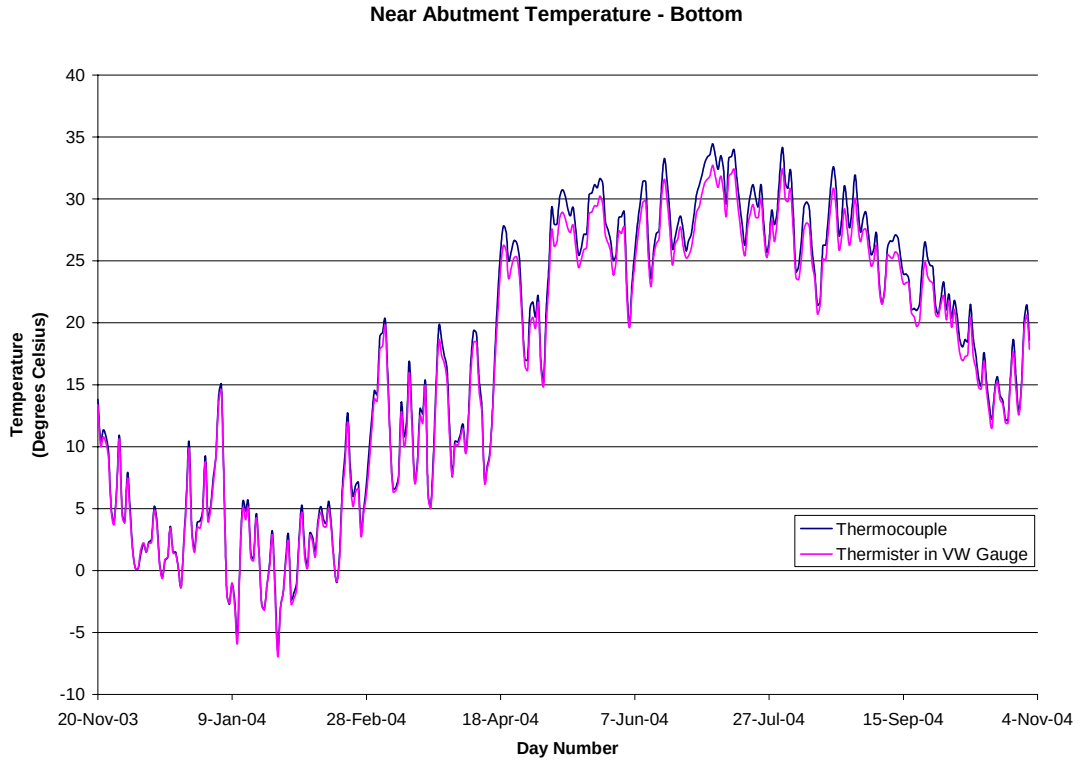

Figure 4.41: Temperature Comparison of Bottom of Deck at Abutment

The trends at midspan are similar to the abutment. Figure 4.42 compares the temperature readings of the two types of instrumentation at midspan at the top of the deck. Figure 4.43 does the same for the bottom of the deck. For both the top and bottom of the deck at midspan, the thermocouple tended to record a slightly higher temperature than the thermisters. The thermister over girder 4 gave higher readings than girder 5. This may be attributed to the parapet being so close to girder 5 and keeping the deck cooler in that location.

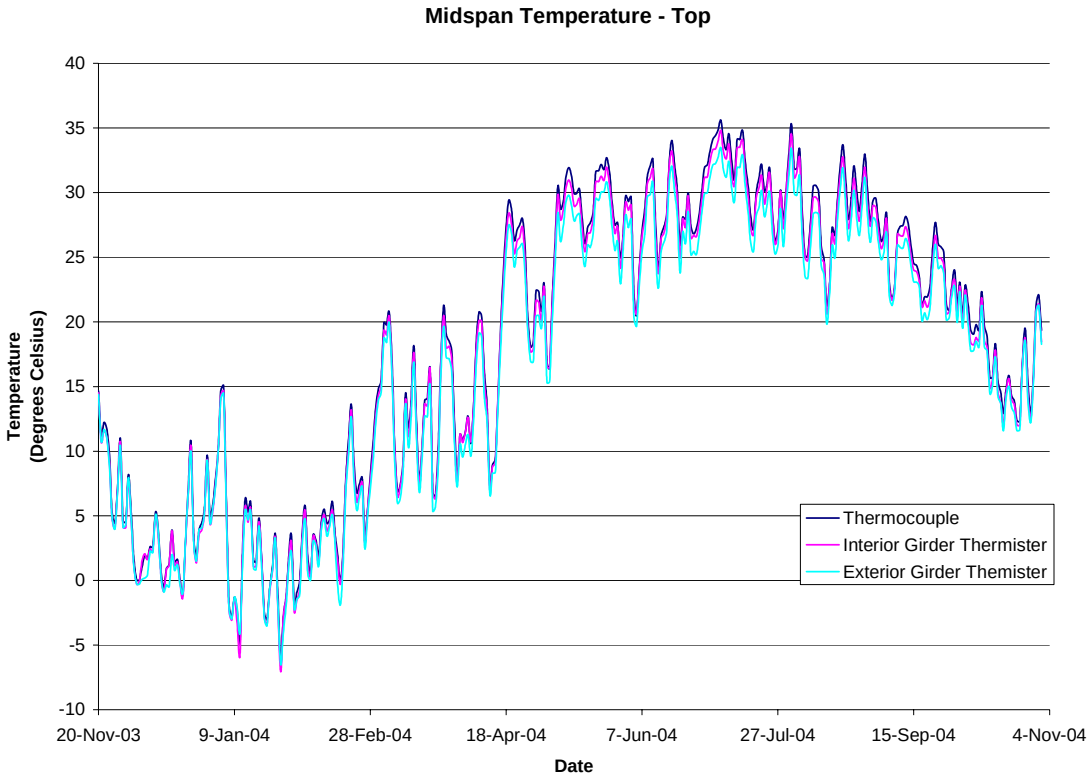

Figure 4.42: Temperature Comparison of Top of Deck at Midspan

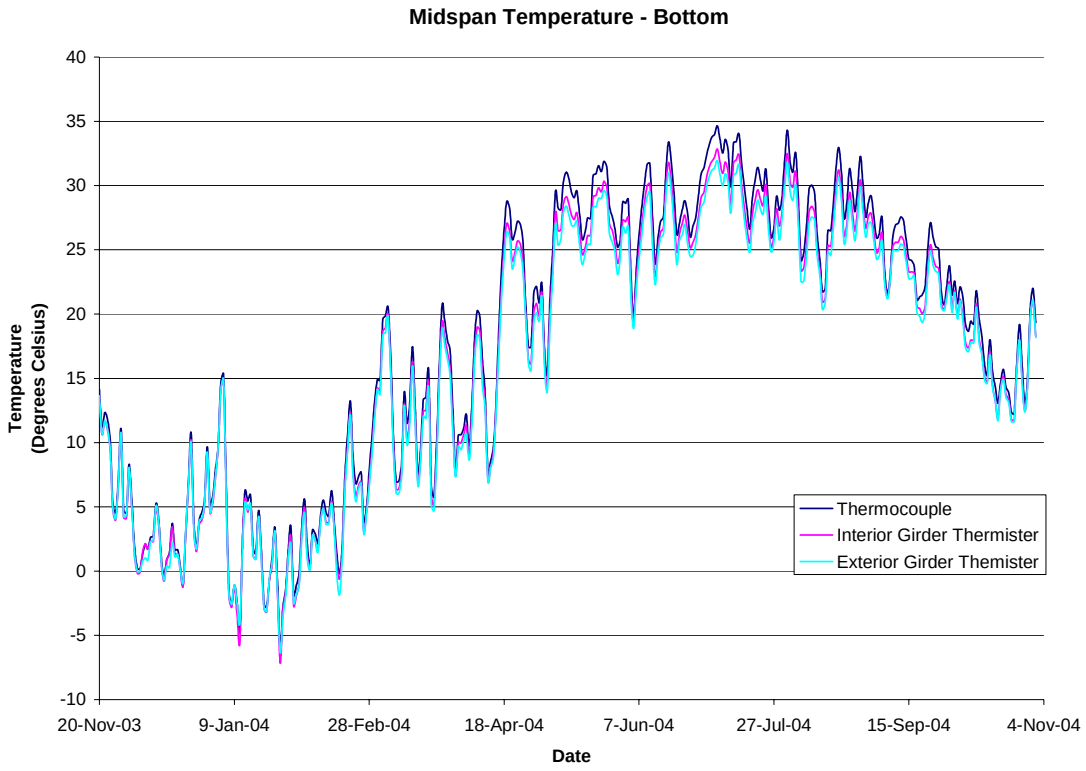

Figure 4.43: Temperature Comparison of Bottom of Deck at Midspan

The temperature readings of the thermocouples and the thermisters correspond well. It can be concluded from the comparisons of the temperature readings that they all are very similar and, therefore, validate each other's accuracy.

4.3.2 GFRP Reinforcing Bar Strains

The readings of the ER strain gauges and VW gauges were recorded every hour. All of the VW gauges worked well throughout the year. However, not all of the ER gauges continued to perform well and some stopped working completely. The progress of the ER strain gauges is shown in Table 4.14. When the status is listed as not continuous that means that the acquisition system was not getting a reading every hour. At some points the system could read a resistance across the strain gauge, but not every hour. When the status is "not working" it means that no readings could be recorded by the data acquisition system. The gauges that had problems are in bold print for easier identification. The "N" represents that the given gauge never had the status. For reference, the live load testing was performed on the bridge on day 209.

Table 4.14: ER Strain Gauge Statuses

	Beginning Day of Status	
	Not continuous	Not working
ATME1	**247**	N
ATME3	**150**	N
ATME4	N	N
ATME5	N	N
ATME6	**167**	**344**
ATME7	N	N
ATME8	N	N
ATMI1	N	N
ATMI3	N	N
ATMI6	**79**	N
ATMI7	N	N
ATA2	**29**	N
ATA4	N	N
ATA6	**93**	**166**
AL1	N	N
AL2	N	N
AL3	N	N

Both of the original data sets recorded for the ER strain gauges and VW gauges had to be adjusted to get the true change in strain. For the ER strain gauges, the readings recorded were voltages that needed to be converted to strain. This voltage was used in the following equation to calculate the corresponding strain:

$$\Delta\varepsilon = \frac{\frac{4000 \times zeroedvoltage}{GF}}{1 - 2(zeroedvoltage/1000)} \qquad \textbf{Equation 4-9}$$

where $\Delta\varepsilon$ is the change in strain in the GFRP bar measured in microstrain, *zeroedvoltage* is the reading minus the initial reading, and *GF* is the gauge factor which in this case is 2.1. Due to a difference in sign convention, the signs of the original recorded voltages were reversed before applying Equation 4-9. The VW gauges needed to be corrected for temperature fluctuations. A VW gauge reads strain by plucking a tiny wire in the gauge and recording the wire's frequency. Changes in temperature can cause the wire to slacken or tighten which can result in inaccurate strain readings. To account for this, the original reading was adjusted with the following equation:

$$\Delta\varepsilon = (R_1 - R_0)B + (T_1 - T_0)(C_1 - C_2) \qquad \textbf{Equation 4-10}$$

where R_1 is the recorded strain, R_0 is the initial recorded strain, B is the average batch calibration factor indicated on the VW strain gauge calibration report that comes with the gauges (in this case B=0.9668), T_1 is the recorded temperature, T_0 is the initial recorded temperature, C_1 is the coefficient of expansion of steel (12.2 με/°C), and C_2 is the coefficient of expansion of concrete (an average of 10.4 με/°C).

Figure 4.44 through Figure 4.47 show the strains recorded by each group of ER strain gauges, ATME, ATMI, ATA, and AL. For comparison, the corresponding VW strain is included in the plots where applicable.

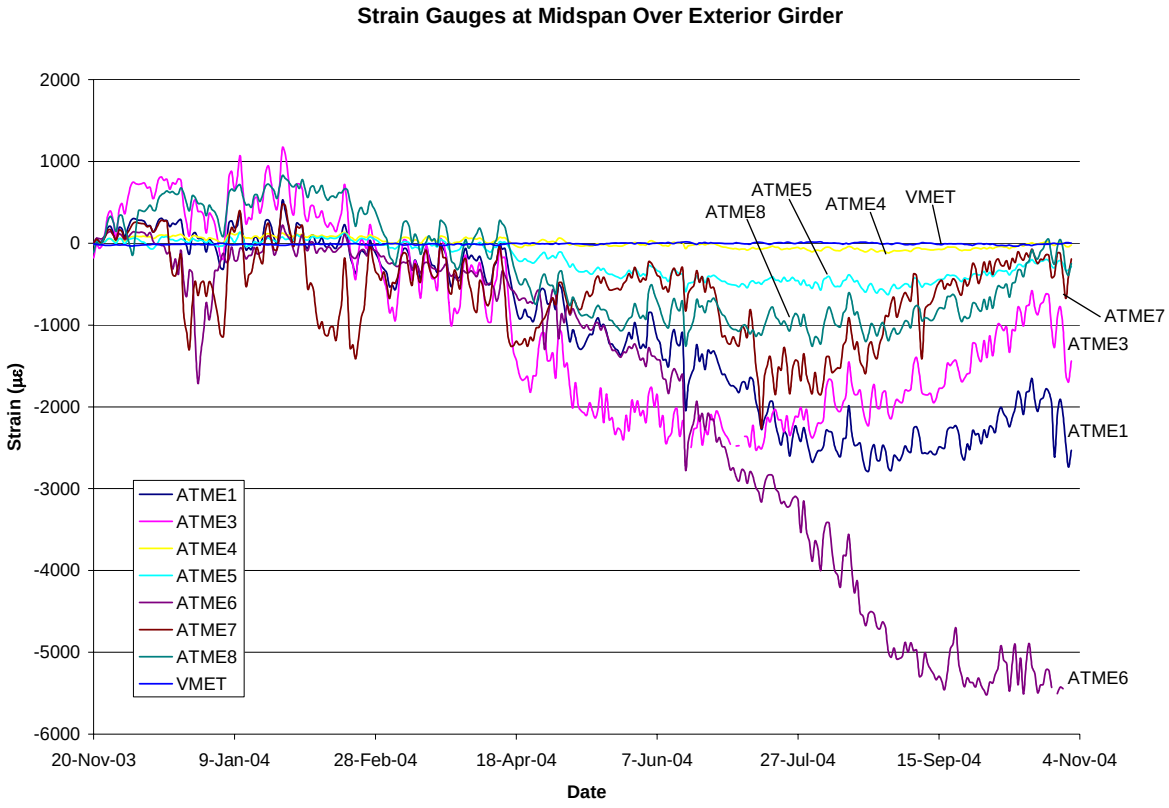

Figure 4.44: Transverse Strain Gauges at Midspan over Exterior Girder

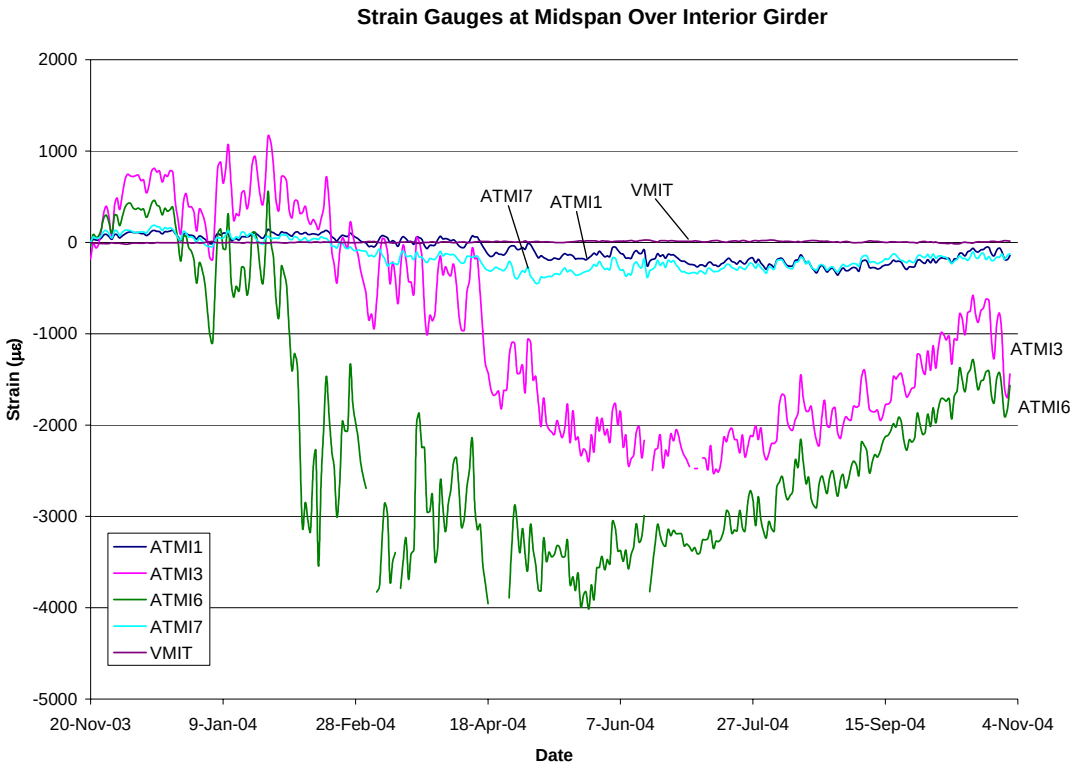

Figure 4.45: Transverse Strain Gauges at Midspan over Interior Girder

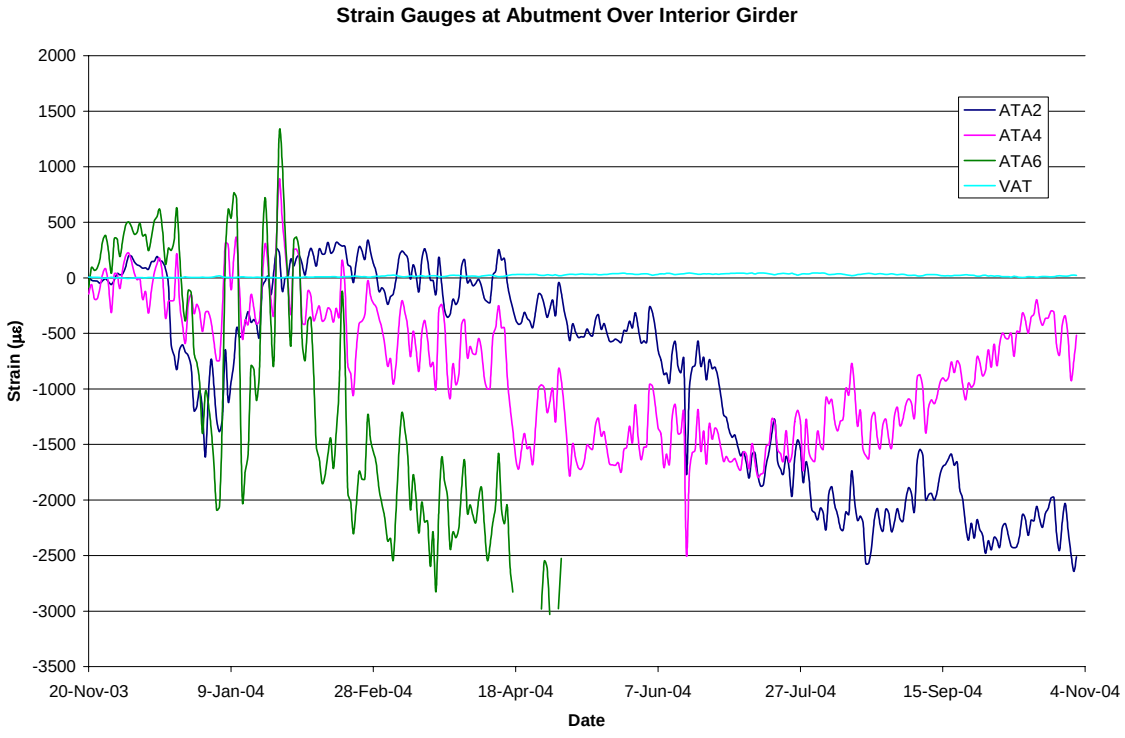

Figure 4.46: Transverse Strain Gauges at Abutment over Interior Girder

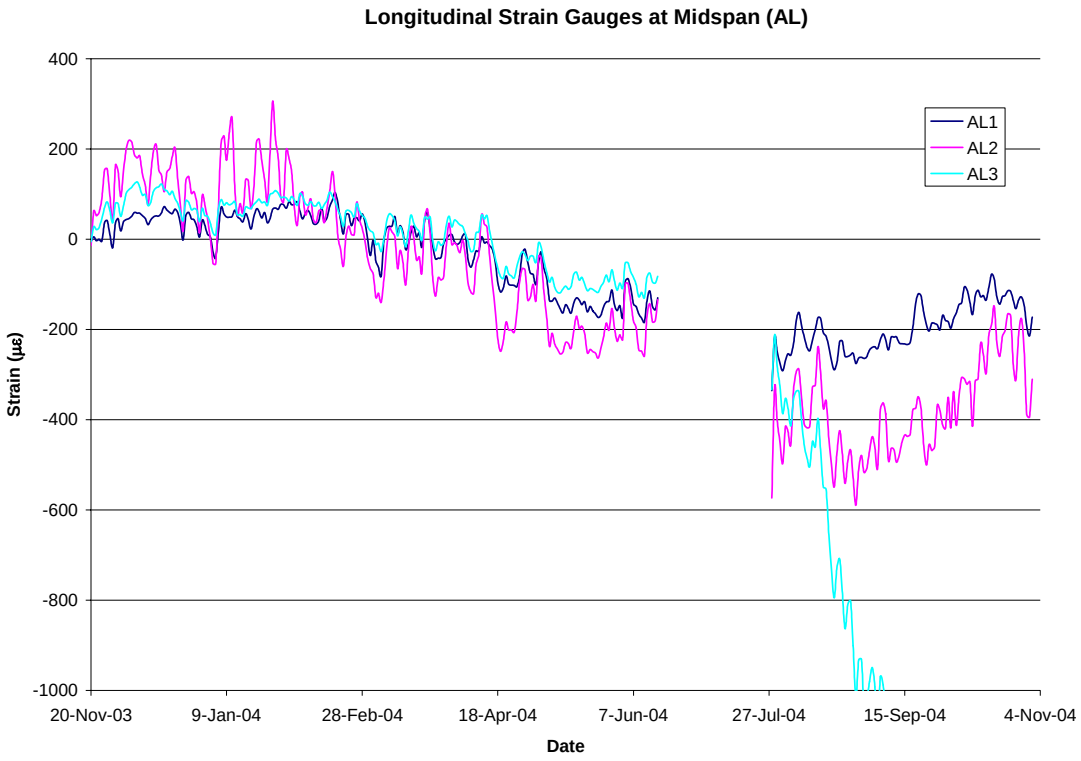

Figure 4.47: Longitudinal Strain Gauges at Midspan

The strains measured by the VW gauges were much smaller than the ER strains. Many of the ER strains increased by large proportions as the year progressed. There was drift in some of the gauges causing them to slowly have increasingly higher readings. Any breaks in the data represent a day where the gauge provided no readings due to an error or malfunction in the gauge. An exception was the breaks in the AL readings in Figure 4.47; they were due to an error in rewiring after the live load testing in June. All of the transverse gauges followed a similar pattern of an increase in compression for the first 100 to 150 days, and then tension for the rest of the year. The ATME gauges followed a similar trend, but many of them started to drift in the later months, especially ATME6. Of the gauges in that group, ATME4 returned the most reasonable results. ATMI3 and ATMI6 followed a similar trend but had very high strains. ATMI1 and ATMI7 had the most reasonable results of the ER strain gauges at the midspan over girder 4. All of the ER strain gauges at the abutment indicated high strains. ATA6 stopped working completely after drifting to about 3000 με. The longitudinal gauges at midspan had strains that were a little more reasonable but still seemed higher than

expected. AL3 had strain readings that increased in tension at a rapid rate, most likely due to drift in the gauge.

In order to find the strain the VW gauges adjusted for temperature, Equation 4-10 was applied to the readings recorded in the field. However, the coefficient of thermal expansion of the concrete bridge deck, C_2, was unknown. An average value for concrete was noted previously, 10.4 με/°C. Depending on the type of coarse aggregate in the concrete mix, the coefficient can vary greatly. In Table 1.3.1 of the *PCI Design Handbook* (1999), the values for concrete with limestone aggregate range from 3.4 to 5.1 με/°F (6.1 to 9.2 με/°C). For concrete with quartz sands and gravels as aggregate, the coefficient ranges from 6.0 to 8.7 με/°F (10.8 to 15.7 με/°C). This large variation in the C_2 value can drastically change the resulting calculated strains. The adjusted strain using different C_2 values for the VW gauge located at the top of the deck at the abutment is illustrated in Figure 4.48.

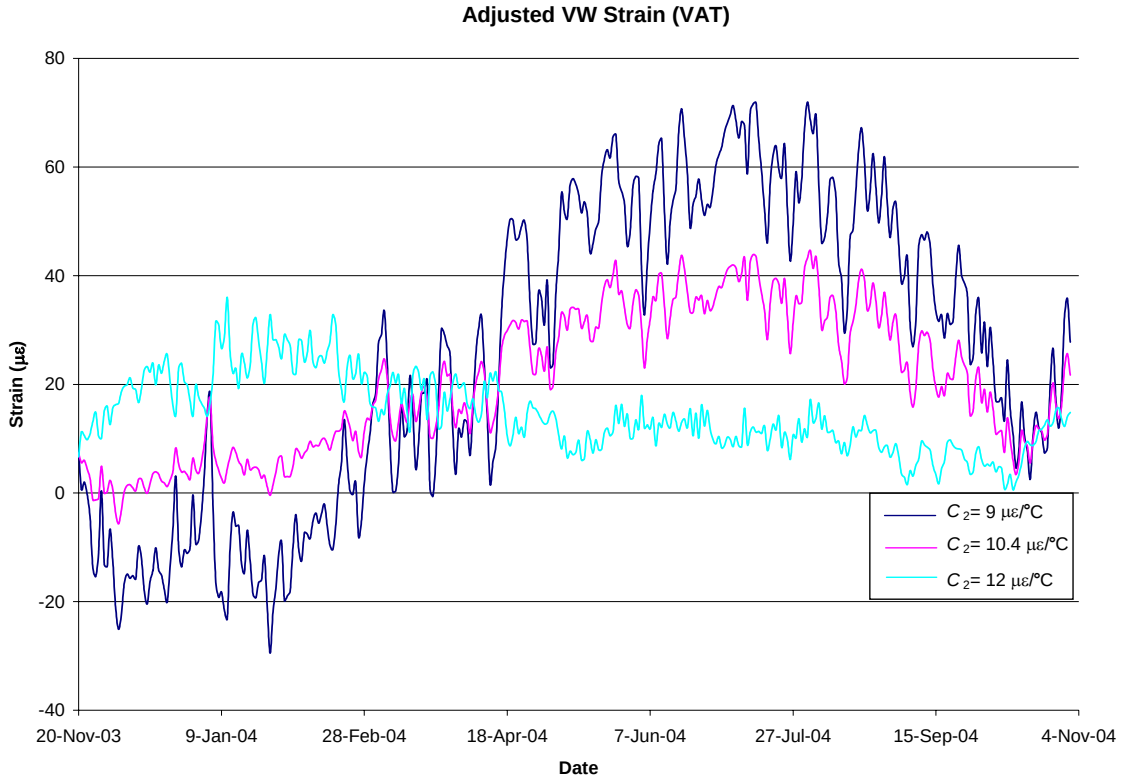

Figure 4.48: VW Gauge Strain for Varying Concrete Thermal Coefficients

Figure 4.41 shows that with smaller C_2 values, the adjusted strains increase. This is because the difference between the coefficient of the vibrating wire in the gauge and the concrete coefficient is increasing. If the C_2 value exceeds the C_1 value, the general trend of tension and compression is reversed. Since the thermal coefficient is unknown, the average value of 10.4 με/°C is used for the calculations in this thesis.

Figure 4.49 and Figure 4.50 show the strain readings of the VW gauges for the year. Since the strains are only relative to the initial strain, a positive strain may not mean the concrete is in tension since the actual initial strain is unknown. However, the increase or decrease in strain can be observed. All of the VW gauges show a similar trend of slowly increasing in tension and around the end of July becoming more compressive. The strains at the abutment followed the same pattern of changes and were about 30 με apart in the beginning of testing and the difference slowly increased to about 50 με. For the gauges over girder 4, the top of the deck experienced a slightly greater increase in strain at the abutment than at the midspan. The reverse was true for the bottom of the deck, with the midspan having a greater change in strain than at the abutment. The bottom of the deck at the same location was mostly in compression. The bottom of the deck at midspan over girder 5 followed the same pattern as the bottom at girder 4 except it did not experience as much compression. It would make sense that less compression was experienced by the gauges at girder 5 since there is less restraint at the exterior girder than at the interior girder. The top of the deck at the midspan over the interior and exterior girders experienced the same strain changes. Again, please note the magnitudes and even the trends of tension and compression could be different if the actual concrete coefficient of thermal expansion were not the 10.4 με/°C used.

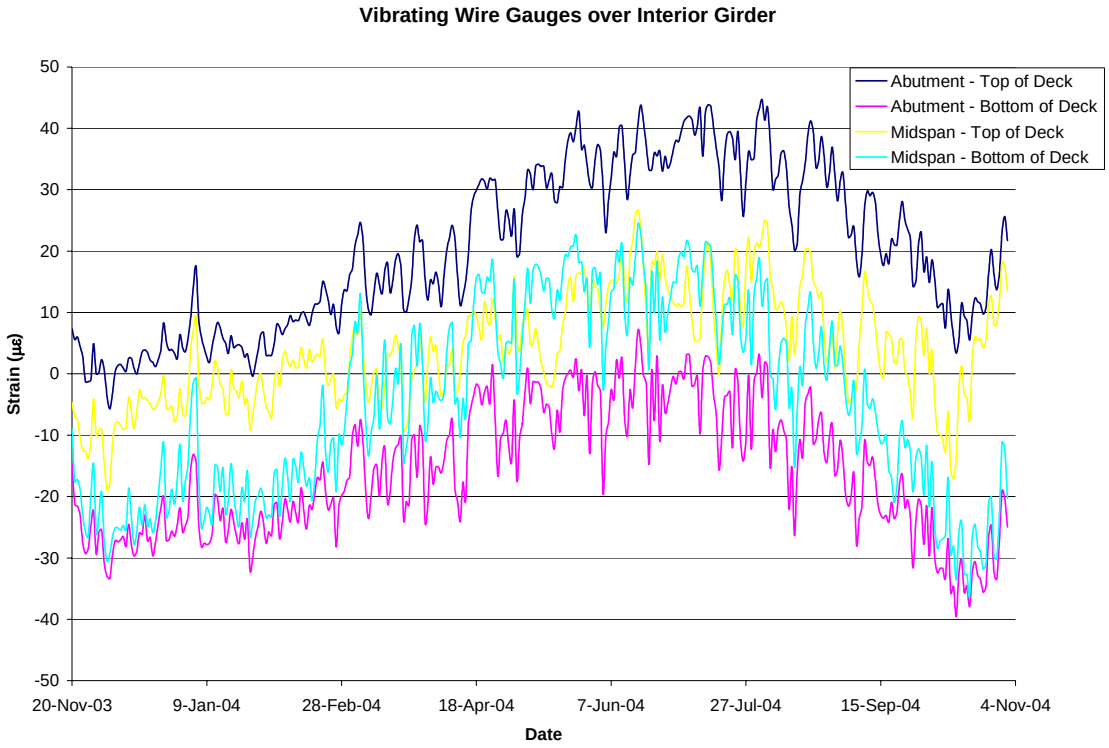

Figure 4.49: VW Gauges over Interior Girder

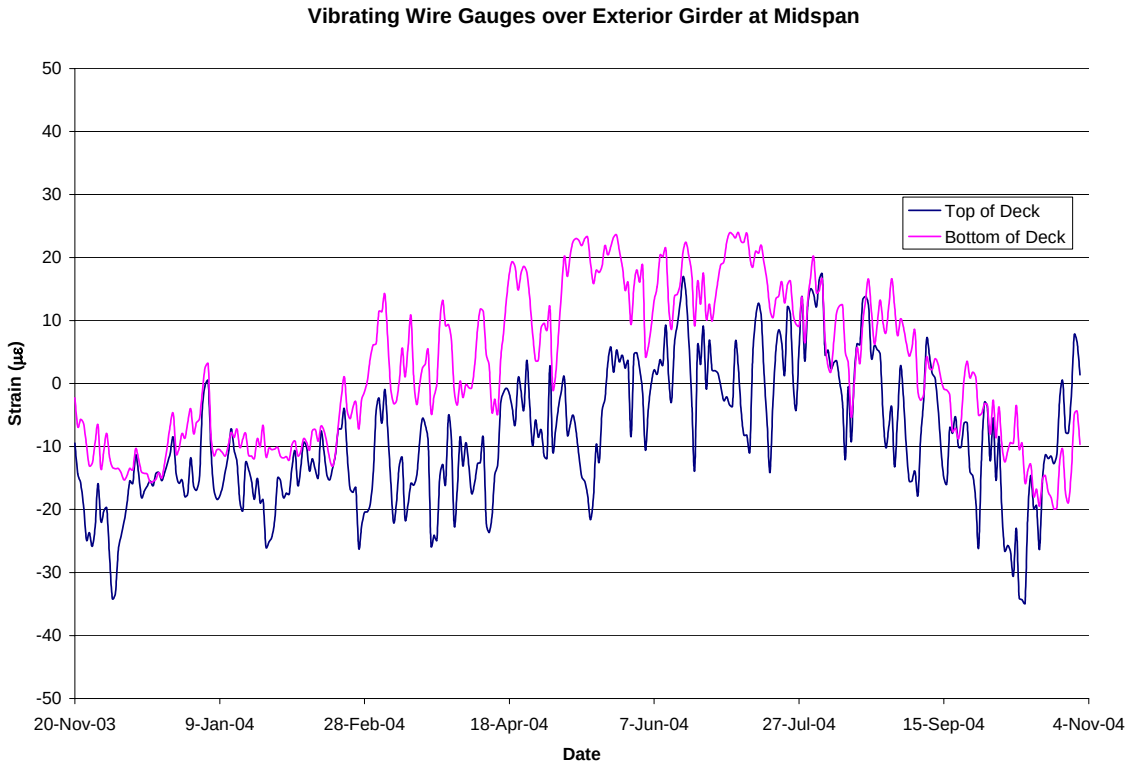

Figure 4.50: VW Gauges over Exterior Girder

Over the year, the strains measured by the VW gauges fluctuated. Table 4.15 shows the difference between the maximum and minimum strains experienced through the year of testing. The table includes the differences from both the raw data and from the average daily data. The strain differences show that at the gauged locations over the interior girder, the bottom of the deck experienced more change in strain than the top. However, at midspan over the exterior girder, the top of the deck experienced more change in strain than the bottom. Comparing the two data sets used for determining the differences in strain demonstrates how averaging data can at times skew the results. With the strains of each day averaged to one point, the variation of the strain was decreased.

Table 4.15: Yearly VW Gauge Strain Differences (με)

	Abutment Interior		Midspan Interior		Midspan Exterior	
	Top	Bottom	Top	Bottom	Top	Bottom
Raw Data	74	91	65	105	88	73
Daily Average	50	47	46	61	52	44

Figure 4.51 compares the strain changes recorded by the ER strain gauge and the VW gauges. ATME4 was used for this comparison since it was the gauge with the least amount of strain variation, and, therefore, the most accurate of the ER strain gauges. The graph shows the hourly strain readings for two 5-day periods taken out of the year of monitoring. The two weeks shown are the first week and then a week about 100 days before the end of the monitoring. Daily fluctuation in strain occurs mainly from temperature changes. During both weeks, the VW gauges varied about 25 με. The ER strain gauge varied about 100 με. However, over the months in between the strain had shifted down approximately 100 με. The ER strain gauge and the VW gauge have opposite trends. When the strain from the ER gauge is decreasing, the VW gauge is showing an increase or more tensile strain. This could indicate that the assumed concrete thermal coefficient was too low. If the coefficient were higher, the two gauges would follow the same trend.

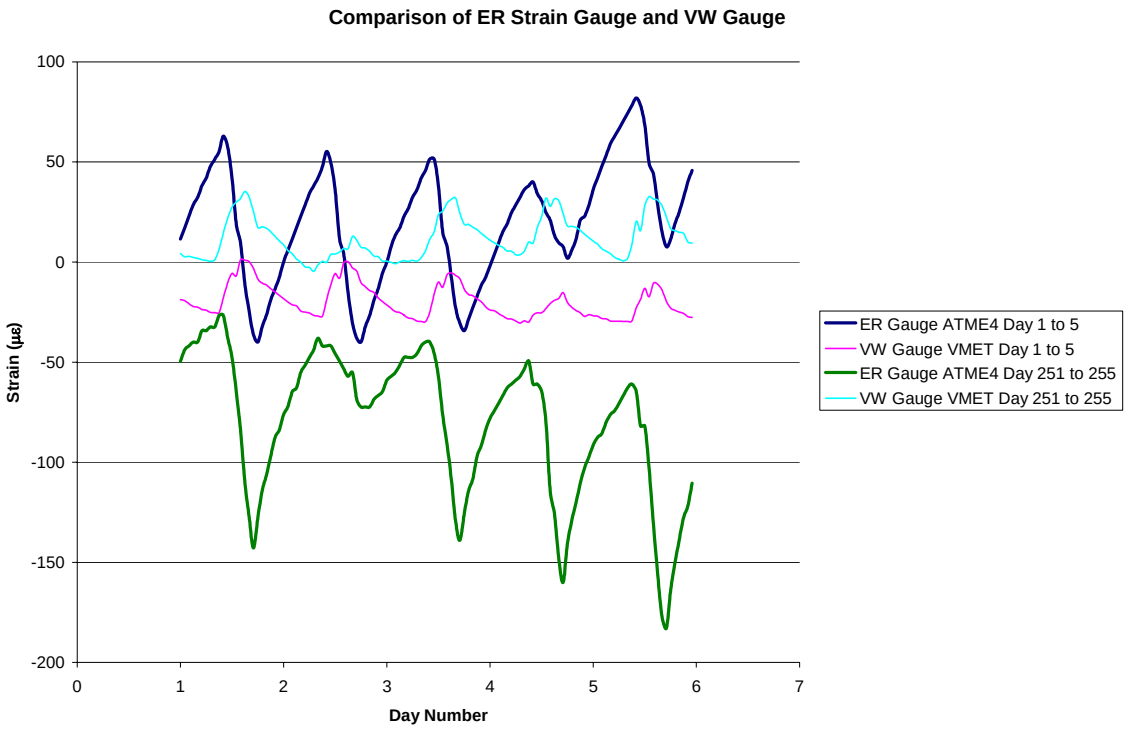

Figure 4.51: Daily Comparison of ER Strain Gauge and VW Gauge at Midspan

Figure 4.52 shows a worse case of how the ER strain gauges were not as reliable as VW gauges. This ER gauge went from fluctuating about 250 με in a day to 1500 με. It also shifted about 1500 με. The breaks in the later readings of the ATA2 gauge were when the gauge was not operating correctly and did not provide a reading. Again, the VW gauge was much more consistent, yet followed an opposite pattern of fluctuating strain.

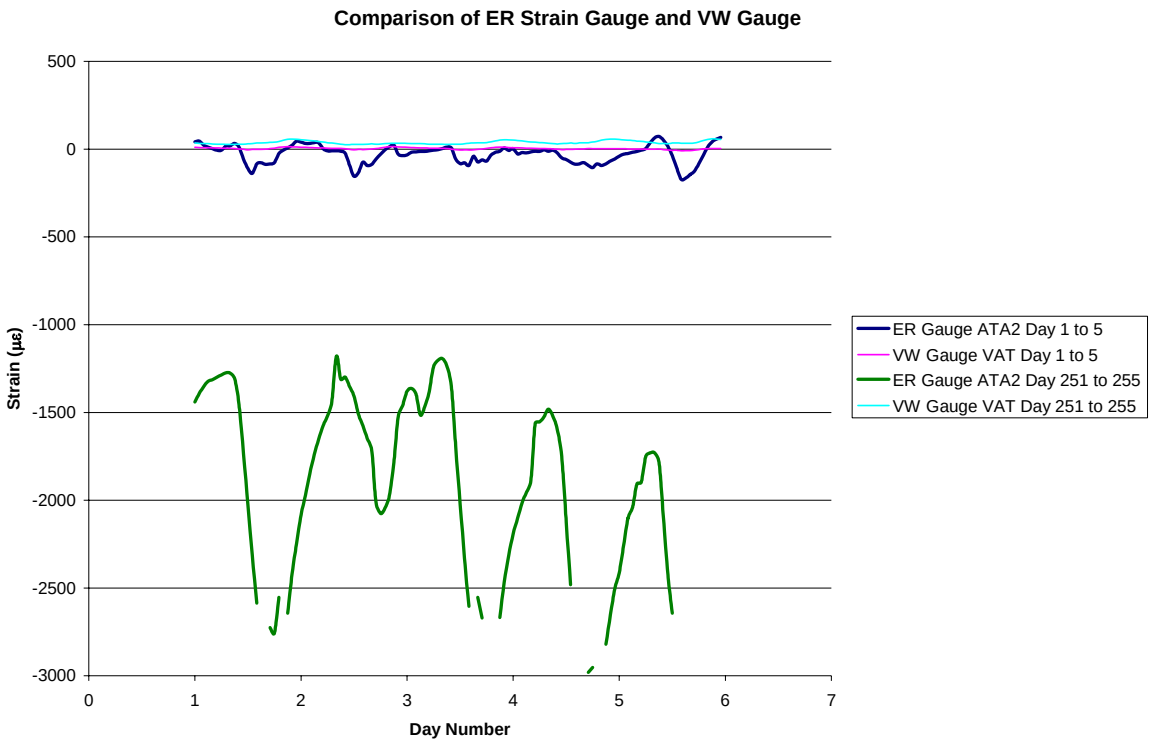

Figure 4.52: Daily Comparison of ER Strain Gauge and VW Gauge at Abutment

From comparing the results of the ER strain gauges and the VW gauges, it can be concluded that the ER strain gauges lose accuracy rapidly over time and should not be used for long-term monitoring of a bridge deck. However, the ER gauges may be useful in determining general trends in the strain changes but not necessarily the magnitude of those changes. To get a better idea of the pattern that the ER gauges and VW gauges followed for the year of monitoring, Figure 4.53 compares two gauges at the same location. Notice that the ER strain gauges and VW gauges are plotted on a different scale to better compare the general strain changes.

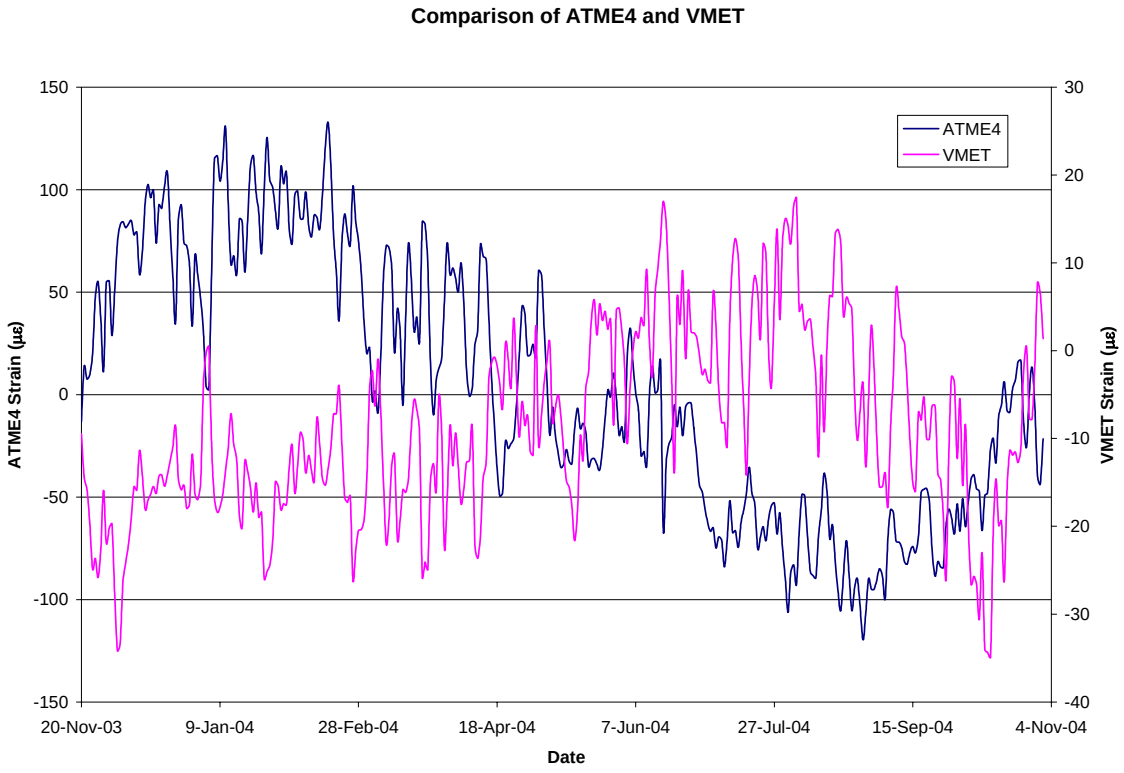

Figure 4.53: Comparison of ATME4 and VMET

4.3.3 Relationship Between Temperature and Strain

From the plots of the daily fluctuations of strain, it appears that temperature plays a role in affecting the strain in the GFRP reinforcing bars and in the concrete. Figure 4.54 shows the relationship between the thermister temperature and ER strain at midspan over the exterior girder. Figure 4.55 shows how the VW strain compares to the temperature at the same location. The ER strain is inversely proportional to the temperature. Therefore, when the temperature increases the strain becomes more compressive. This trend makes sense if the deck is restrained from movement. As the temperature rises, the deck wants to expand. If the deck is restrained, it cannot expand creating compressive stresses in the deck. The VW gauges show that the strain increases with increased temperature. The deck would expand with the temperature rises if it were unrestrained, but the VW gauge would not indicate that increased tension since the readings are adjusted for thermal expansion. There must be an error in the concrete thermal coefficient used to calculate the adjusted strain or an error in the VW gauge itself or its installment.

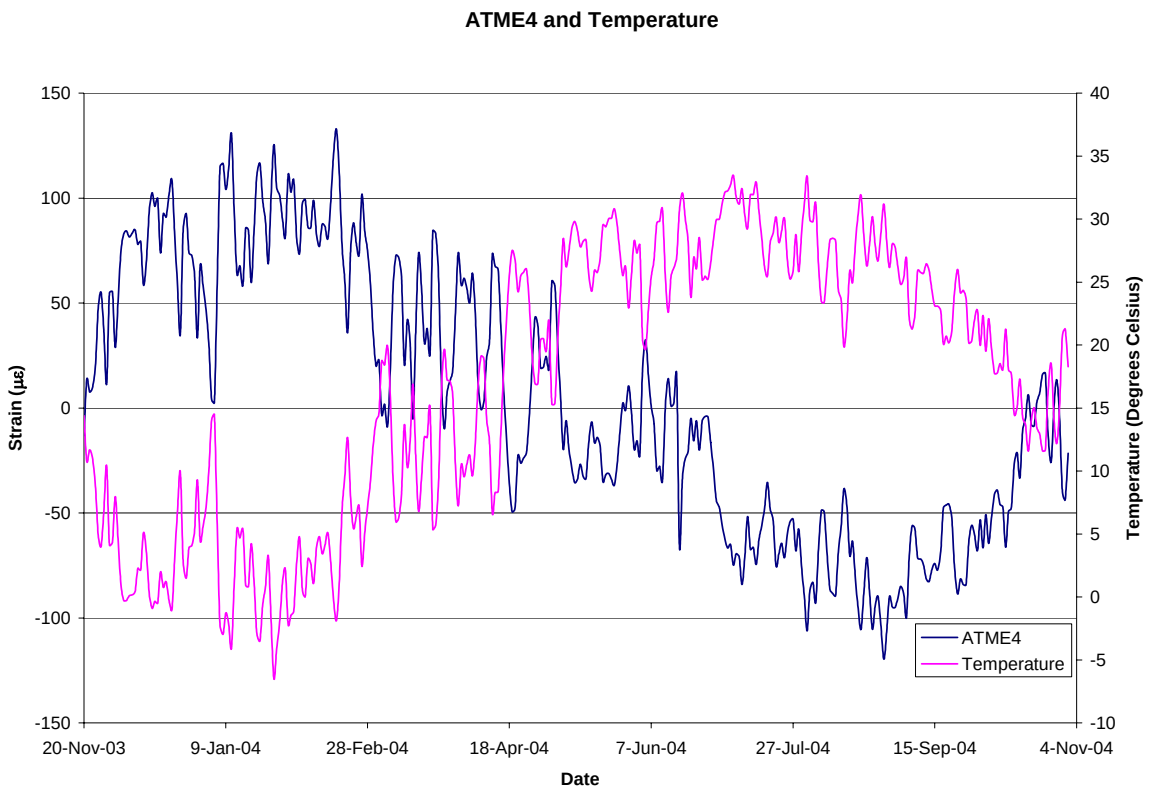

Figure 4.54: Comparison of ER Strain and Temperature

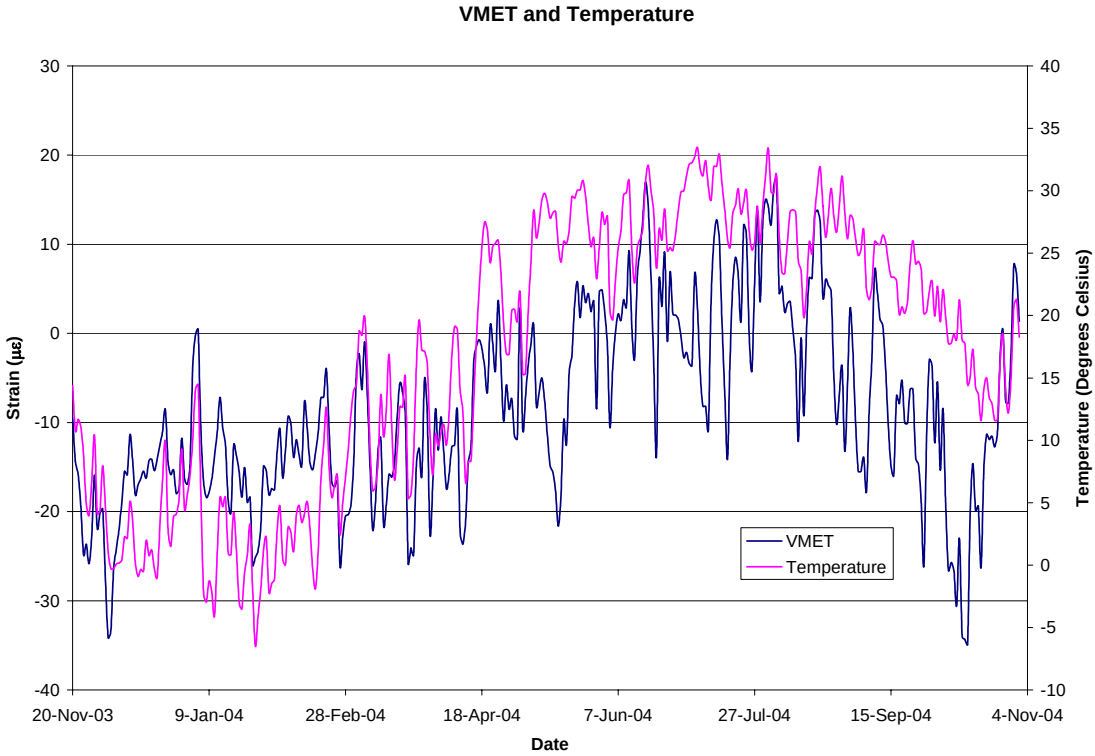

Figure 4.55: Comparison of VW Strain and Temperature

Figure 4.56 shows that the VW strain changes lagged behind the temperature changes. This means that after the temperature had reached its lowest point and was starting to increase, the VW gauge strains were still decreasing. The ER gauges lined up with the temperature better than the VW as shown in Figure 4.57. Note that the strain axis for the ER gauge has been reversed for a better comparison.

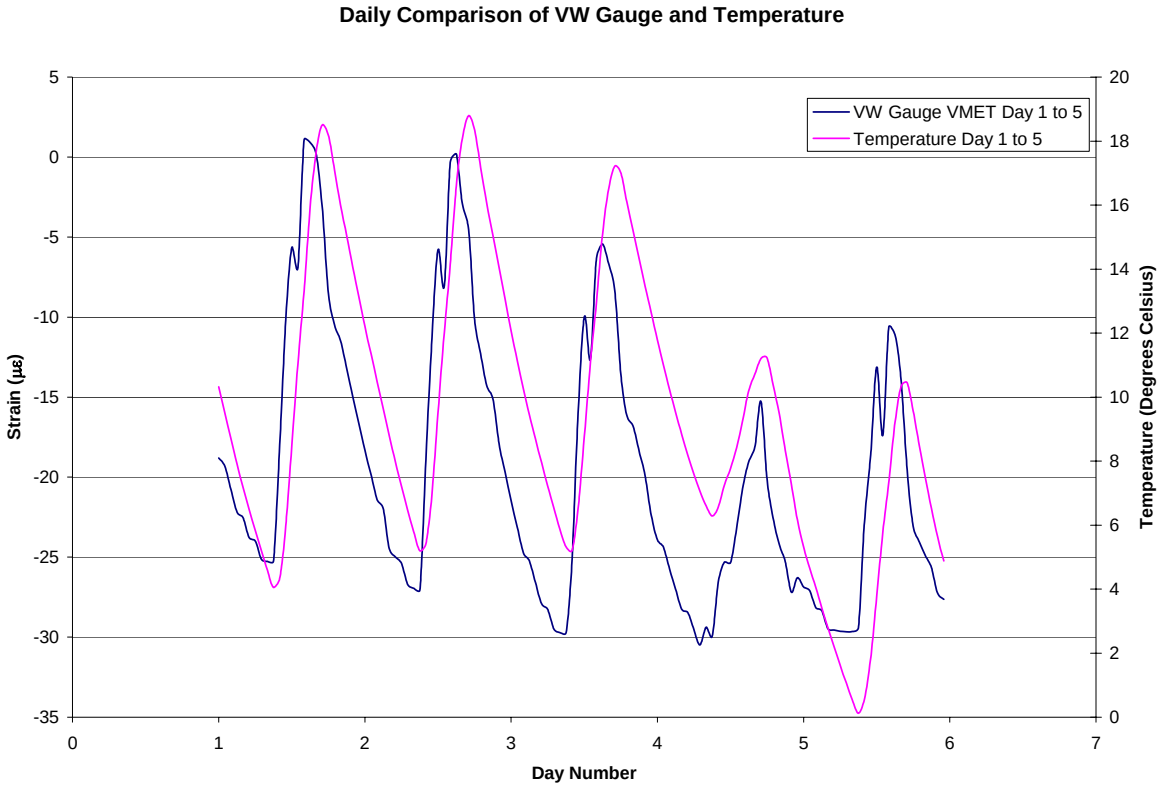

Figure 4.56: Daily Comparison of VW Gauge Strain and Temperature

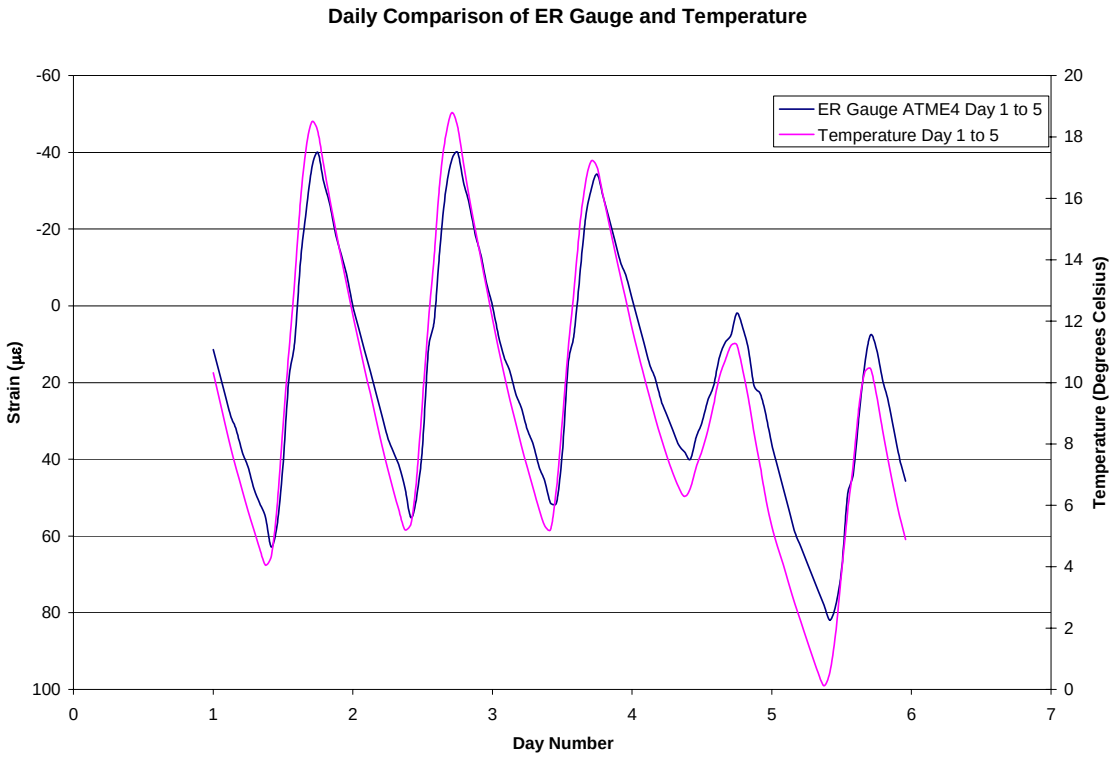

Figure 4.57: Daily Comparison of ER Gauge Strain and Temperature

The main reason for monitoring the strains in the bridge deck for a year was to determine if the strains in the concrete are consistent, perhaps indicating if the GFRP is performing adequately. To determine this, two days with similar average temperatures were chosen and their corresponding average strains were compared. Table 4.16 and Table 4.18 show two samples of the long-term strain changes in the VW gauges, and Table 4.17 and Table 4.19 show the changes in the ER gauges. In Table 4.16 and Table 4.17 there were 184 days between the two dates. Table 4.18 and Table 4.19 had 237 days between the two dates.

Table 4.16: Comparison of VW Gauge Strains after 184 Days

		30-Apr-04		31-Oct-04		
		Avg. Temp (°C)	Avg. Strain (με)	Avg. Temp (°C)	Avg. Strain (με)	Δε (με)
VW Strain Gauge	VAT	21.1	25.4	21.0	25.6	**0.3**
	VAB	20.4	-11.6	20.6	-20.2	**-8.6**
	VMIT	21.5	3.2	21.4	17.6	**14.4**
	VMIB	20.8	5.3	21.0	-12.3	**-17.6**
	VMET	20.5	-11.5	21.3	6.6	**18.1**
	VMEB	20.1	9.5	21.1	-4.4	**-13.9**

Table 4.17: Comparison of ER Gauge Strains after 184 Days

		30-Apr-04		31-Oct-04		
		Avg. Temp (°C)	Avg. Strain (με)	Avg. Temp (°C)	Avg. Strain (με)	Δε (με)
ER Strain Gauge	ATA2	21.1	-282	21.0	-2642	**-2360**
	ATA4		-1117		-745	**372**
	ATA6		-3030		-	**N/A**
	ATMI1	21.5	-76	21.4	-187	**-112**
	ATMI3		-533		-751	**-218**
	ATMI6		-3398		-1827	**1571**
	ATMI7		-353		-144	**208**
	ATME1	20.5	-731	21.3	-2734	**-2003**
	ATME3		-1434		-1698	**-264**
	ATME4		19		-44	**-63**
	ATME5		-177		-327	**-150**
	ATME6		-743		-	**N/A**
	ATME7		-734		-404	**329**
	ATME8		-517		-390	**127**

Table 4.18: Comparison of VW Gauge Strains after 237 Days

		1-Mar-04		24-Oct-04		
		Avg. Temp (°C)	Avg. Strain (με)	Avg. Temp (°C)	Avg. Strain (με)	Δε (με)
VW Strain Gauge	VAT	11.8	13.5	12.0	10.7	**-2.8**
	VAB	11.3	-17.4	11.9	-34.6	**-17.3**
	VMIT	12.7	-3.0	12.0	5.5	**8.6**
	VMIB	12.2	-4.2	11.7	-31.0	**-26.8**
	VMET	12.1	-19.2	11.7	-11.2	**8.0**
	VMEB	11.8	3.9	11.6	-19.7	**-23.6**

Table 4.19: Comparison of ER Gauge Strains after 237 Days

		1-Mar-04		24-Oct-04		
		Avg. Temp (°C)	Avg. Strain (με)	Avg. Temp (°C)	Avg. Strain (με)	Δε (με)
ER Strain Gauge	ATA2	11.8	-122	12.0	-1978	**-1856**
	ATA4		-365		-310	**55**
	ATA6		-1897		-	**N/A**
	ATMI1	12.7	14	12.0	-56	**-70**
	ATMI3		-175		-532	**-357**
	ATMI6		-2417		-1410	**1007**
	ATMI7		-89		-155	**-65**
	ATME1	12.1	-269	11.7	-1819	**-1549**
	ATME3		-314		-636	**-323**
	ATME4		35		17	**-18**
	ATME5		-7		-214	**-208**
	ATME6		-165		-5221	**-5056**
	ATME7		-454		-147	**306**
	ATME8		202		47	**-155**

The VW gauges had much more consistent results than the ER gauges. The VW gauges located in the bottom of the deck all became more compressive over time. The VW gauged near the top of the deck mostly became more tensile over time. The strain differences over time were less for the VW gauges than for the ER gauges but were significant when compared to the strain changes over the year of monitoring. For example, the gauge VMIB had a strain reading difference of 26.8 με, but the strain only varied 61 με over the year. The ER gauges had larger strain differences and the changes were not consistent within each group. Also, for the ER gauges, the larger time period between the compared readings did not always result in a larger difference in strain. The sampling used may not be completely representative of each case, especially since each day's temperatures and strains were averaged. However, it does indicate that the ER gauges are not reliable in their results and that the VW gauges' strains have increased over the year of monitoring.

Chapter 5 - Conclusions and Recommendations

5.1 Introduction

The intention of this research was to investigate the durability of GFRP and to gather information to determine if GFRP is a good material to be used as reinforcement in bridge decks. To accomplish this aim, three objectives were met. The first objective was to perform a live load test on the Gills Creek Bridge and see any changes that may have occurred since the first test from a year prior. The second objective was to perform two live load tests on the concrete slab installed at the weigh station along I-81 and determine any changes between the two test dates. The third objective was to monitor the Gills Creek Bridge for approximately one year to examine how GFRP bars' performance varies over time. This chapter presents the conclusion drawn from completing these three objectives.

5.2 Conclusions from Live Load Testing

5.2.1 Gills Creek Bridge

The live load testing of the Gills Creek Bridge provided valuable insight on the change in strain of GFRP bars and how the changes affect factors of design such as girder distribution factors and dynamic load allowances.

5.2.1.1 Strains and Stresses in the GFRP Reinforcement

The stresses calculated from the quasi-static and dynamic tests all showed that the transverse GFRP bars were experiencing more compression during the 2004 live load test than during the initial test. The highest tensile stresses occurred at the interior girder at the abutment during the dynamic test. The transverse bars experienced a tensile stress of 0.075 ksi, or 75 psi. This is well below the ACI 440 specified allowable tensile stress of 13.9 ksi and far less than the bar's measured tensile strength in the lab of 109 ksi. The largest compressive stress of -0.13 ksi or -130 psi occurred at the interior girder at midspan during the dynamic test. ACI 440 does not specify an allowable compressive stress for FRP because creep rupture is not a problem in compression. The stress recorded in this case is so small that it can be assumed that the concrete can carry the stress.

From the stresses calculated, it can be concluded that the top mat of transverse GFRP reinforcement was designed to be more than adequate to handle the applied stresses. The design parameters for bridge decks reinforced with GFRP should be made less conservative if stresses were the controlling factor. Serviceability issues, such as cracking, may be a design consideration as well. There were no cracks on the bridge deck upon visual inspection; however, a more thorough crack study should be performed.

No comparisons could be made between Span A and Span C since not enough of the ER strain gauges were operable in Span C.

5.2.1.2 Girder Distribution Factors

The girder responses measured using the deflectometers, ER strain gauges, and WIM gauges showed that Span A had greater deflections and girder strains for both the quasi-static and dynamic tests. The largest responses resulted from the dynamic tests. The greatest deflection was 0.11 in. at Span A. The maximum ER strain and WIM strain were 145 με and 104 με, respectively. The ER strain gauges and WIM gauges followed the same pattern, but for all causes the strain readings of the WIM gauges were lower than the ER strain gauges. In Span A, the highest responses were in the girder closest to the truck orientation.

The girder distribution factors calculated from the 2004 live load testing were not significantly different from the initial testing. There was no clear trend of an increase or decrease in GDF values between the two test dates. For the interior truck orientation, the different methods used to calculate the GDF values resulted in conflicting trends of increasing or decreasing since 2003. In Span A, the largest factor was S/10.0 measured by the ER strain gauges in 2004. In Span C, the largest factor was S/9.7 measured by the WIM gauges in 2004. Both of these values are well below the limits specified by the AASHTO Standard Specification and the AASHTO LRFD Specification of S/7.0 and S/7.4, respectively. For the exterior orientation, the 2004 Span A results were slightly lower than in 2003, and the Span C results indicated a slight increase in the distribution factors. In Span A, the largest factor was S/8.0 measured by the ER strain gauges in 2003. Span C had a maximum factor of S/8.1 measured by the WIM gauges in 2004. Again, these values were less than the AASHTO Standard and AASHTO LRFD design limit of S/6.5 calculated using the lever rule. From these comparisons, it can be

concluded that the bridge was designed conservatively with respect to transverse load distribution and that no significant changes in the distribution of load were seen after one year of service.

When comparing the distribution factors for Span A and Span C, the two spans distribute the load similarly. In 2004 for the interior truck orientation, the values calculated for Span A ranged from S/10.0 to S/11.2. For Span C, the distribution factors were from S/9.7 to S/12.3. For the exterior truck orientation, the values for Span A ranged from S/8.3 to S/9.6 and for Span C were between S/8.1 to S/8.6. These differences are minimal. Therefore, it can be concluded that the span reinforced with GFRP bars is distributing the transverse load the same as the span reinforced with epoxy-coated steel bars. Note that the deck was uncracked at the time of both live load tests, and that cracking could cause the loads to be redistributed.

5.2.1.3 Dynamic Load Allowance

The dynamic load allowance results show that the impact factors increased between 2003 and 2004. Using the deflection data for Span A, the impact factors increased from 0.36 to 0.52 when traveling northbound, and from 0.18 to 0.37 when traveling southbound. For Span C, the northbound values increased from 0.11 to 0.36. However, the soundbound values decreased from 0.22 to 0.18. Many of the 2004 values were above the AASHTO Standard Specification design value of 0.29 and the AASHTO LRFD Specification design value of 0.33. Using the ER strain data, similar trends were seen, but the impact factors were smaller. For Span A, the live load tests carried out in 2003 resulted in negative values of -0.84 traveling northbound and -0.87 traveling southbound. These were erroneous results from malfunctioned gauges, so they cannot be compared to the 2004 values. In 2004, Span A had impact factors of 0.53 traveling northbound and 0.31 traveling southbound. For Span C, the northbound value increased from 0.06 to 0.12 and the soundbound value decreased from 0.23 to 0.22. The Span A results were higher than the AASHTO design values. The WIM gauges were only installed in the 2004 testing. The impact factors calculated using their data was at Span A traveling northbound, 0.62, and southbound, 0.34. At Span C, the values were 0.13 traveling northbound and 0.23 traveling southbound.

The increase in impact factors over just one year is alarming. Dynamic load allowances can be increased by a change in the riding-surface roughness, profile differences in the approaches, or a difference in the suspension of trucks. However, no significant changes in the roadway or approaches were seen upon visual inspection and the same truck was used for both live load sessions. The differences between the impact factors from Span A and Span C indicate that the GFRP-reinforced span demonstrated poorer performance than the steel-reinforced span. Although the impact factors were above the design values, there was no cracking or compromising of the structure seen during testing. The highest stress seen in the girders was 4.62 ksi, less than 10% of the tensile strength of the girders. Additional live load tests must be performed to see if the impact factors continue to increase and to determine if the GFRP-reinforcement is playing a role in the increase.

5.2.1.4 Comparison of Electrical Resistance Strain Gauges and Weigh-in-motion Strain Gauges

Like the results from 2003, the WIM gauges had similar strain readings to the ER strain gauges at the girders further from the load. However, in the girders closest to the load, the strains from the WIM gauges were much less than those from the ER gauges. The same types of differences were seen in both the quasi-static and dynamic tests from both dates of testing. It can be concluded that WIM gauges are not adequate to record accurate strains in place of ER strain gauges. Future tests using WIM gauges and ER strain gauges in tandem may allow researchers to calibrate the WIM gauges to produce similar results to the ER strain gauges.

5.2.2 I-81 Weigh Station Slab

The live load testing of the I-81 weigh station slab provided valuable insight into the performance of GFPR bars when subjected to heavy truck traffic. The strains in the GFRP bars increased over time. When comparing the increase in strains in the GFRP and steel bars, the GFRP bars experienced a much greater increase in strain between the two test dates. Higher strains resulted from a decrease in stiffness over time. The higher stiffness of steel agrees with past research indicating GFRP is more flexible than steel. Converting the strains to stresses showed that the GFRP bars had far less stress in them than the allowable. The maximum stress in the GFRP bars was 3.30 ksi, which is much

smaller than the ACI 440's allowable GFRP tensile stress of 13.9 ksi. It can be concluded that although the GFRP bars were more flexible than the steel bars, the GFRP was performing adequately as the top mat of reinforcement in the weigh station deck.

5.3 Long-Term Monitoring Conclusions

5.3.1 Temperatures

The temperatures in the bridge's concrete deck were taken by thermocouples and thermisters within the VW gauges. Both the thermocouples and the thermisters reported very similar temperatures. As expected the temperatures at the top of the deck typically were a little higher than at the bottom. At the locations where the middle temperature was recorded, the middle temperature was always in-between the top and bottom temperatures. By comparing the two sources of temperature data, it can be concluded that the instrumentation is recording an accurate deck temperature.

5.3.2 GFRP Reinforcing Bar Strains

The GFRP reinforcing bars strains were measured by ER strain gauges and VW gauges. Of the original 27 ER gauges, 17 of them were operable at the time of installation of the long-term data acquisition system. Over one year of testing, 6 gauges had times during which they did not take readings due to a malfunction in the gauge. Two of those 6 gauges stopped working completely by the end of the year. From this, ER gauges showed that they do not have a long lifespan when used in the field. Additionally, the ER gauges were installed in four groups. Aside from the AL group with a gauge over girders 1, 3, and 5, the gauges within each group were relatively close together. The ER gauges within each group did not have similar readings as expected. Many of the strains reported by the gauges appeared to drift, often into the thousands of microstrain. Due to the inconsistency of the readings and the frequency that the ER strain gauges were becoming inoperable, it was concluded that the data from the ER strain gauges could not be used alone in determining the long-term health of the GFRP reinforcing bars and bridge deck. They could, however, be useful in determining trends in the strain changes.

The VW gauges reported much smaller and consistent strains than the ER gauges. Over the year, the greatest variation in the VW strain gauge readings was 107 με at the

midspan over girder 4. This variation was much lower than that of the ER strain gauges. Since the concrete coefficient of thermal expansion was not measured for the deck, the VW gauges results were not as reliable as expected. For the continued long-term monitoring performed on the Gills Creek Bridge, only the strains from the VW gauges should be considered along with the trends shown by the operable ER gauges.

5.3.3 Relationship Between Temperature and Strain

The strains in the bridge deck were directly proportional to the change in temperature according to the VW gauges. As the temperature increased, the strains in the deck became more tensile. The ER gauges indicated the opposite, that the strains are inversely proportional to temperature. The use of a different concrete thermal coefficient may indicate that the VW gauges are reading strains following a similar pattern as the ER gauges. Both gauges followed the temperature changes closely showing that temperature is primary controlling factor of the strains in concrete and in the GFRP reinforcement bars when the bridge deck is restrained.

5.4 Recommendations for Future Research

This research is another step towards understanding the performance and durability of GFRP reinforcement bars. The use of GFRP bars in concrete bridge decks is still a new concept. Before GFRP can be accepted as a reliable and cost effective material, more research is required. Some recommendations for future research involving GFRP reinforcement are presented in this section.

The monitoring of the Route 668 Bridge should be continued. Changes in strain and temperature over the years of service would indicate the performance of the GFRP bars. The performance of the bridge deck when cracking begins to occur should be examined. Also, with continued monitoring, the durability of the testing instruments can be determined. In future projects, fiber optic sensors should be used to track the change in strain of the GFRP bars since they are more reliable than ER strain gauges. Like the Route 668 Bridge, similar spans reinforced with GFRP and steel should be monitored together to see how the two materials compare. Long-term monitoring of bridges in service is the best way to determine the durability of GFRP bars.

Furthermore, additional live load tests should be completed throughout the bridge's life. After one year of service, no cracking was detected. Later live load tests could address the concern with cracking of the deck and the expected increase in flexibility of GFRP. Specifically, the dynamic load allowances should be observed to ensure that the impact factors are not continuing to increase with time.

The validity of the WIM gauges is another issue that should be investigated further. The ease of installation of WIM gauges makes them an attractive replacement for ER strain gauges. However, additional live load tests need to be performed to confirm if they are acceptable for this kind of application.

Future live load tests should also include the use of multiple trucks. With the use of multiple trucks, the girder distribution factors for two or more lanes loaded can be evaluated and compared to the AASHTO design standards.

The monitoring of the I-81 weigh station slab should be continued as well. Changes in strain and temperature over the years of service would indicate the performance of the GFRP bars. After testing of the current slab, a slab reinforced entirely with steel with the same dimensions should be tested and monitored to see any differences in performance.

Finally, future live load tests on the weigh station slab should be run. The strains caused by known truck loads could be recorded and compared to the previous tests. Also, the effects of cracking can be determined.

Hopefully with future research, the dependability of GFRP bars as reinforcement in concrete bridge decks will be verified leading to an increase in the ease of construction, improvement of the durability of bridge decks, and a reduction in maintenance costs.

References

AASHTO, *AASHTO LRFD Bridge Design Specification*, Second Edition, 1998, Washington, DC.

AASHTO, *AASHTO Standard Specifications for Highway Bridges*, 17th Edition, 2002, Washington, DC.

ACI Guide for the Design and Construction of Concrete Reinforced with FRP Bars, ACI 440.1R-03 (2003), American Concrete Instititute Committee 440, Farmington Hills, MI.

Amico, R., "Shear Strength of GFRP Reinforced Bridge Decks and Strength Degradation of GFRP Reinforcement Bars," M.S. Thesis, Virginia Polytechnic Institute and State University, Blacksburg, VA, 2005.

Benmokrane, B. and El-Salakawy, E., "Serviceability of Concrete Bridge Deck Slabs Reinforced with Fiber-Reinforced Polymer Composite Bars," *ACI Structural Journal*, Vol 101, No. 5, 2004, pp. 727-736.

Benmokrane, B., El-Salakawy, E., Desgagné, G., and Lackey, T., "FRP Bars For Bridges," *Concrete International*, Vol. 26, No. 8, 2004, pp. 84-90.

Bhise, Vikrant S., "Strength Degradation of GFRP Bars," M.S. Thesis, Virginia Polytechnic Institute and State University, Blacksburg, VA, 2002.

Bice, J., Phelan, R., Vann, W., and Bradberry, T., "Instrumentation of a FRP Reinforced Bridge Deck for Long Term Monitoring and Live Load Testing," *Proceedings from the Sixth International Conference on Short and Medium Span Bridges*, Canadian Society for Civil Engineering, Montreal, Canada, 2002.

Bradberry, T. E., "FRP-Bar-Reinforced Concrete Bridge Decks," *Transportation Research Board Proceedings, 80th Annual Meeting*, TRB, Washington, DC, 2001.

Chong, K., "Durability of Composite Materials and Structures," *Durability of Fibre Reinforced Polymer (FRP) Composites for Construction – Proceedings of the first International Conference (CDCC)*, 1998, pp. 1-12.

Clarke, J. and Sheard, P., "Designing Durable FRP Reinforced Concrete Structures," *Durability of Fibre Reinforced Polymer (FRP) Composites for Construction – Proceedings of the first International Conference (CDCC)*, 1998, pp. 13-24.

Dejke, V., *Durability of FRP Reinforcement in Concrete*, Goteborg, Sweden, Reproservice, Chalmers, 2001.

Elbadry, M., Abdalla, H., and Ghali, A., "Effects of temperature on the behaviour of fiber reinforced polymer reinforced concrete members: experimental studies," *Canadian Journal of Civil Engineering*, Vol. 27, No. 5, 2000, pp. 993-1004.

Gentry, T., Bank, L., Thompson, B., and Russell, J., "An Accelerated-test-based Specification for Fiber Reinforced Plastics for Structural Systems," *Durability of Fibre Reinforced Polymer (FRP) Composites for Construction – Proceedings of the second International Conference (CDCC)*, 2002, pp. 13-24.

Hall, T. and Ghali, A., "Long-term deflection prediction of concrete members reinforced with glass fibre reinforced polymer bars," *Canadian Journal of Civil Engineering*, Vol. 27, No. 5, 2000, pp. 890-898.

Harlan, M., "Field Test of a Bridge Deck with Glass Fiber Reinforced Polymer Bars as the Top Mat of Reinforcement," M.S. Thesis, Virginia Polytechnic Institute and State University, Blacksburg, VA, 2004.

Nanni, A., Bakis, C., and Mathew, J., "Acceleration of FRP Bond Degradation," *Durability of Fibre Reinforced Polymer (FRP) Composites for Construction – Proceedings of the first International Conference (CDCC)*, 1998, pp. 45-56.

Porter, M. and Barnes, B., "Accelerated Durability of FRP Reinforcement for Concrete Structures," *Durability of Fibre Reinforced Polymer (FRP) Composites for Construction – Proceedings of the first International Conference (CDCC)*, 1998, pp. 191-202.

PCI Design Handbook, Precast/Prestressed Concrete Institute, Fifth Edition, 1999.

Vijay, P., GangaRao H., and Kalluri, R., "Hygrothermal Response of GFRP Bars under Different Conditioning Schemes," *Durability of Fibre Reinforced Polymer (FRP) Composites for Construction – Proceedings of the first International Conference (CDCC)*, 1998, pp. 243-252.

Ziemian, R. and McGuire, W., MASTAN2 Version 1.0, 2000.

Appendix A – Route 668 Bridge Calculations

A.1 Composite Section Analysis

Section Properties

Bridge Properties	
Span Length =	45.0 ft
Girder Spacing =	6.50 ft
# of Beams =	5
Girder Properties	Steel I-beams: W27x94
Area =	27.7 in^2
Flange width (b_f) =	9.99 in.
Flange thickness (t_f) =	0.745 in.
Web thickness (t_w) =	0.49 in.
Depth (d)=	26.9 in.
I_{xx} =	3,270 in^4
c_1 =	13.45 in.
c_2 =	13.45 in.
S_t =	243 in^3
S_b =	243 in^3
E_s =	29000 ksi
Deck Slab Properties	
Thickness (t_s) =	8.0 in.
Structural thickness =	7.5 in.
f'_c =	4000 psi
E_c =	3605 ksi
Haunch Properties	
Thickness =	1.5 in.
Width =	9.99 in.

Composite Properties of Interior Girder

Effective Flange Width

Minimum of the following:	
0.25*(span length)	135.0 in.
12*(avg. thickness of slab) + greater of web thickness or ½ width of top flange of girder	101.0 in.
avg. spacing of adjacent girders	78.0 in.

b_{eff} = 78.0 in. controls

Modular Ratio Between Deck and Beam Material:

$n=E_c/E_s$= 0.1243

Deck

b_{tr} = 0.1243(78) = 9.696 in.

Haunch

b_{tr} = 0.1243(9.99) = 1.242 in.

Composite Section

Component	A (in^2)	y_b (in.)	Ay_b (in^3)	d (in.)	Ad^2 (in^4)	I_o (in^4)	$I = I_o + Ad^2$ (in^4)
Beam	27.70	13.45	372.57	13.55	5088.66	3270	8358.66
Deck 7.5" x b_{tr}	72.72	32.15	2338.00	5.15	1925.89	340.88	2266.77
Haunch 1.5" x b_{tr}	1.86	27.65	51.51	0.65	0.78	0.35	1.13
Totals	102.28 in^2		2762.07 in^3			I_c =	10,626.6 in^4

y_{bar} = 27.0 in. (y_{bar} is in the web)

h_c = 26.9 + 1.5 + 7.5 = 35.9 in.

y_{tg} = 35.9 - 27.0 - 7.5 - 1.5 = -0.10 in.

y_{tc} = 35.9 - 27.0 = 8.90 in.

$S_{bc} = I_c/y_{bar}$ = 394 in^3

$S_{tc} = (1/n)*(I_c/y_{tc})$ = 9609 in^3

A.2 Calculation of Girder Distribution Factors

Distribution Factors for Interior Girder

AASHTO LRFD Bridge Design Specification 1998

Requirements to use Equations 4-3 and 4-5:

3.5' = S = 16'	S =	6.50 ft	***OK***
4.5" = t_s = 12"	t_s =	7.5 in.	***OK***
20' = L = 240'	L =	45 ft	***OK***
N_b > 3	N_b =	5 beams	***OK***

1 lane loaded

$$g = 0.06 + \left[\left(S/14 \right)^{0.4} \left(S/L \right)^{0.3} \left(\frac{K_g}{12\,Lt_s^{\,3}} \right)^{0.1} \right]$$ = 0.441

K_g =	104,226 in^4	longitudinal stiffness parameter = $n*(I+Ae_g^2)$
e_g = 32.15 - 13.45 =	18.70 in.	distance between c.g. of beam and slab
$n = E_s/E_c$ =	8.04	

g = 0.441 lanes per beam
g = S/D = 6.5/D = 0.441
D = 6.5/0.441 = 14.7
g = S/14.7 per lane load
g = S/7.35 per wheel line

Distribution Factors for Exterior Girder

AASHTO LRFD Bridge Design Specification 1998
AASHTO Standard Specifications for Highway Bridges 2002

1 lane loaded
Use lever rule.

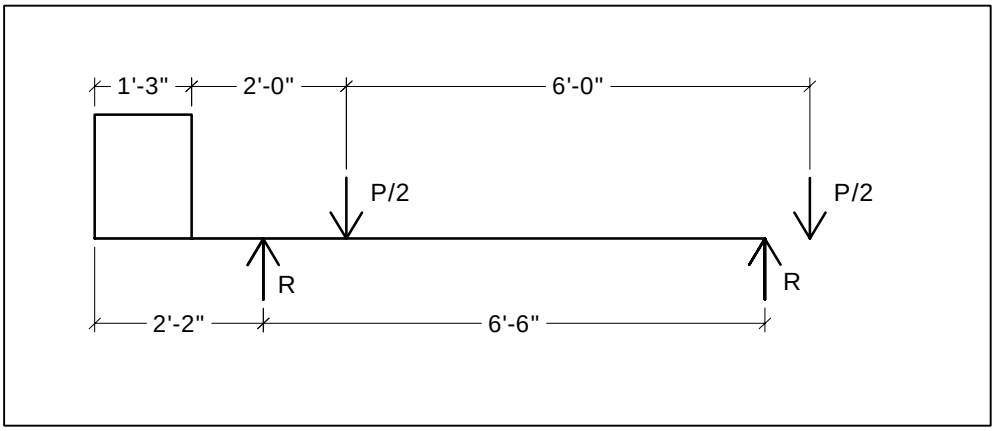

Sum Moments at first interior girder
-R(6.5) + P/2(5.4167) = 0
R = 0.417P

g = 0.417m = 0.417(1.2) = 0.500 lanes per beam
m = multiple presence factor = 1.2

D = (S/g)(1/2) = (6.6/5.0)(1/2) = 6.5
g = S/6.5 per wheel line

Table A.1: GDF Results for Span A Interior Configuration Tests from ER Strain Gauges

Span A - Interior Truck Configuration								
	Static Data				Dynamic Data			
Girder #	ε_{favg} (με)	GDF_{max}	GDF_{min}	GDF_{avg}	ε_{favg} (με)	GDF_{max}	GDF_{min}	GDF_{avg}
G1	21.4	0.082	0.041	0.059	19.4	0.086	0.023	0.045
G2	56.2	0.139	0.131	0.135	58.2	0.141	0.112	0.122
G3	83.6	0.227	0.197	0.211	91.5	0.208	0.186	0.199
G4	114.4	0.325	0.309	**0.316**	135.8	0.323	0.275	0.303
G5	105.0	0.289	0.270	0.279	144.8	0.347	0.302	**0.331**
				Σ = 1.000				Σ = 1.000

Table A.2: GDF Results for Span C Interior Configuration Tests from ER Strain Gauges

Span C - Interior Truck Configuration								
	Static Data				Dynamic Data			
Girder #	ε_{favg} (με)	GDF_{max}	GDF_{min}	GDF_{avg}	ε_{favg} (με)	GDF_{max}	GDF_{min}	GDF_{avg}
G6	19.1	0.052	0.043	0.048	21.4	0.065	0.050	0.057
G7	44.8	0.127	0.114	0.120	41.3	0.129	0.107	0.115
G8	77.8	0.222	0.211	0.216	68.2	0.203	0.190	0.197
G9	111.3	0.318	0.309	**0.313**	103.4	0.295	0.281	0.290
G10	108.9	0.311	0.288	0.303	115.3	0.360	0.329	**0.341**
				Σ = 1.000				Σ = 1.000

Table A.3: GDF Results for Span A Exterior Configuration Tests from ER Strain Gauges

Span A - Exterior Truck Configuration				
	Static Data			
Girder #	ε_{favg} (με)	GDF_{max}	GDF_{min}	GDF_{avg}
G1	8.4	0.040	0.000	0.023
G2	41.2	0.105	0.088	0.095
G3	67.5	0.177	0.154	0.167
G4	117.6	0.336	0.315	0.324
G5	136.1	0.407	0.371	**0.390**
			Σ = 1.000	

Table A.4: GDF Results for Span C Exterior Configuration Tests from ER Strain Gauges

Span C - Exterior Truck Configuration				
	Static Data			
Girder #	ε_{favg} (με)	GDF_{max}	GDF_{min}	GDF_{avg}
G6	9.7	0.024	0.014	0.020
G7	32.3	0.092	0.087	0.090
G8	60.8	0.176	0.170	0.173
G9	111.8	0.325	0.318	0.322
G10	134.6	0.403	0.387	**0.395**
			Σ =	1.000

Table A.5: GDF's and D-values for Span A from ER Strain Gauges

			Span A						
			GDF's (per axle)			Denominator "D" (per wheel)			
Truck Config.	Type	# Passes	Min	Max	Avg.	Min	Max	Avg.	Comb. Avg.
Interior	Quasi-Static	5	0.309	0.325	0.316	10.5	10.0	10.3	10.0
	Dynamic	6	0.302	0.347	0.331	10.8	9.4	9.8	
Exterior	Quasi-Static	5	0.371	0.407	0.390	8.8	8.0	8.3	8.3

Table A.6: GDF's and D-values for Span C from ER Strain Gauges

			Span C						
			GDF's (per axle)			Denominator "D" (per wheel)			
Truck Config.	Type	# Passes	Min	Max	Avg.	Min	Max	Avg.	Comb. Avg.
Interior	Quasi-Static	5	0.309	0.318	0.313	10.5	10.2	10.4	10.0
	Dynamic	6	0.329	0.360	0.341	9.9	9.0	9.5	
Exterior	Quasi-Static	5	0.387	0.403	0.395	8.4	8.1	8.2	8.2

Table A.7: GDF Results for Span A Interior Configuration Tests for WIM Gauges

Span A - Interior Truck Configuration								
	Static Data				Dynamic Data			
Girder #	ε_{favg} (με)	GDF_{max}	GDF_{min}	GDF_{avg}	ε_{favg} (με)	GDF_{max}	GDF_{min}	GDF_{avg}
G1	16.8	0.061	0.056	0.058	22.8	0.083	0.041	0.063
G2	45.9	0.171	0.163	0.165	53.2	0.173	0.101	0.145
G3	74.5	0.271	0.268	0.270	86.2	0.278	0.241	0.254
G4	65.7	0.238	0.232	0.236	79.0	0.247	0.205	0.228
G5	74.8	0.277	0.268	**0.272**	103.9	0.319	0.301	**0.309**
			Σ =	1.000			Σ =	1.000

Table A.8: GDF Results for Span C Interior Configuration Tests from WIM Gauges

Span C - Interior Truck Configuration								
	Static Data				Dynamic Data			
Girder #	ε_{favg} (με)	GDF_{max}	GDF_{min}	GDF_{avg}	ε_{favg} (με)	GDF_{max}	GDF_{min}	GDF_{avg}
G6	11.6	0.043	0.033	0.037	12.8	0.059	0.012	0.045
G7	41.0	0.135	0.128	0.131	36.1	0.135	0.107	0.125
G8	69.9	0.229	0.222	0.225	58.3	0.211	0.199	0.204
G9	91.7	0.297	0.289	0.293	79.1	0.285	0.255	0.267
G10	97.2	0.325	0.303	**0.314**	99.6	0.394	0.339	**0.359**
			Σ =	1.000			Σ =	1.000

Table A.9: GDF Results for Span A Exterior Configuration Tests from WIM Gauges

Span A - Exterior Truck Configuration				
	Static Data			
Girder #	ε_{favg} (με)	GDF_{max}	GDF_{min}	GDF_{avg}
G1	6.2	0.022	0.020	0.021
G2	33.0	0.130	0.129	0.129
G3	61.5	0.239	0.237	0.238
G4	66.5	0.260	0.257	0.259
G5	90.1	0.354	0.351	**0.353**
			Σ =	1.000

Table A.10: GDF Results for Span C Exterior Configuration Tests from WIM Gauges

Span C - Exterior Truck Configuration				
	Static Data			
Girder #	ε_{favg} (με)	GDF_{max}	GDF_{min}	GDF_{avg}
G6	3.5	0.014	0.010	0.012
G7	29.3	0.100	0.099	0.100
G8	54.6	0.189	0.185	0.187
G9	87.8	0.299	0.297	0.298
G10	117.3	0.406	0.401	**0.403**
			Σ =	1.000

Table A.11: GDF's and D-values for Span A from WIM Gauges

			Span A						
			GDF's (per axle)			Denominator "D" (per wheel)			
Truck Config.	Type	# Passes	Min	Max	Avg.	Min	Max	Avg.	Comb. Avg.
Interior	Quasi-Static	5	0.268	0.277	0.272	12.1	11.8	12.0	11.2
	Dynamic	6	0.301	0.319	0.309	10.8	10.2	10.5	
Exterior	Quasi-Static	5	0.351	0.354	0.353	9.3	9.2	9.2	9.2

Table A.12: GDF's and D-values for Span C from WIM Gauges

			Span C						
			GDF's (per axle)			Denominator "D" (per wheel)			
Truck Config.	Type	# Passes	Min	Max	Avg.	Min	Max	Avg.	Comb. Avg.
Interior	Quasi-Static	5	0.303	0.325	0.314	10.7	10.0	10.4	9.7
	Dynamic	6	0.339	0.394	0.359	9.6	8.2	9.1	
Exterior	Quasi-Static	5	0.401	0.406	0.403	8.1	8.0	8.1	8.1

Appendix B – I-81 Weigh Station Slab Calculations

B.1 Calculation of Cracked Moment of Inertia

Using data from tested cylinders, f'c is the 28-day compressive strength in psi
f'c = 7998 psi

For normal weight concrete, $E_c = 57*f'_c{}^{0.5}$
E_c = 5097 ksi
Length = 15.25 ft
Avg slab thickness (h) = 7.25 in.

All calculations are per one foot of slab.
A_f (#6 bars at 4") = 1.32 in^2 #6 bar = 0.44 in^2
A_s (#6 bars at 8") = 0.66 in^2

E_f = 6300 ksi
E_s = 29000 ksi
d' = 2.00 in.
d = 5.75 in.

$f_r = 7.5*f'_c{}^{0.5}$ = 670.72 psi
$n_f = E_f/E_c$ = 1.24
$n_s = E_s/E_c$ = 5.69

Uncracked Transformed Section

Area = $A_f*(n_f-1) + A_s*(n_s-1) + 12*h$ = 90.4 in^2
$NA_{bot} = [A_s*(n_s-1)*(h-d) + A_f*(n_f-1)*(h-d') + 6h^2]/Area$ = 3.56 in.
NA_{top} = 3.69 in.
$c_f = NA_{top} - d'$ = 1.69 in.
$I = 1/12*12"*h^3 + 12h*(NA_{bot}-h/2)^2 + A_s*(n_s-1)*(NA_{top}-d)^2 + A_f*(n_f-1)*(NA_{top}-d')^2$ = 395.47 in^4
For 5' slab,

A =	**452.03 in^2**
I =	**1977.34 in^4**

Cracked at Top Transformed Section

Assume the Neutral Axis is below the steel, making the FRP be in tension.

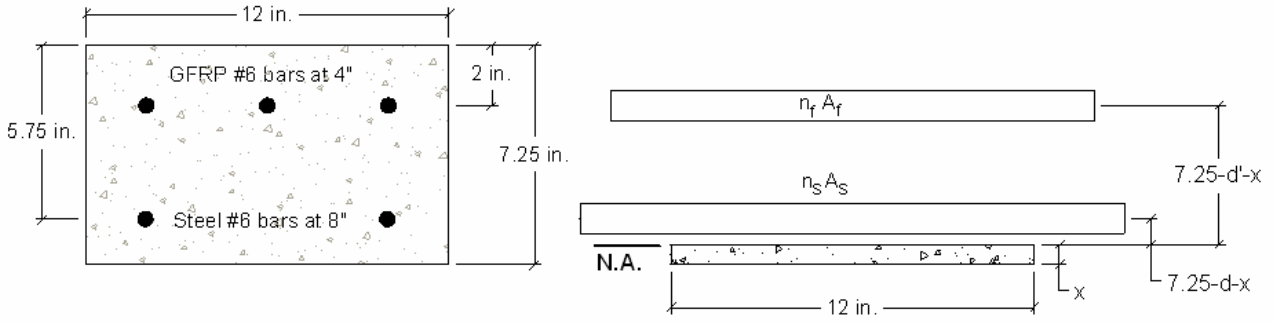

The concrete is in compression at the bottom:

$$12 \cdot x \cdot \left(\frac{x}{2}\right) = n_f \cdot A_f \cdot (7.25 - dprime - x) + n_s \cdot A_s \cdot (7.25 - d - x)$$

To find x, the coefficients to the polynomial were found:

$A*x^2 + B*x + C = 0$

A= 12/2 = 6

$B = A_f*n_f + A_s*n_s$ = 5.386

$C = A_f*n_f*(d'-7.25) + A_s*n_s*(d-7.25)$ = -14.1971

$$x = \frac{-B + \sqrt{B^2 - 4 \cdot A \cdot C}}{2 \cdot A}$$ = 1.154 in. < 1.5 in. Steel is above the neutral axis, therefore assumption was correct.

$x = NA_{cr}$ = 1.154 in.

$c_f = 7.25 - NA_{cr} - d'$ = 4.10 in.

$I_{cr} = NA_{cr}^3 + 3*NA_{cr}^3 + A_f*n_f*(7.25-NA_{cr}-d')^2 + A_s*n_s*(7.25-NA_{cr}-d)^2$

I_{cr} = 33.97 in^4

For 5' slab,

c_f =	**4.10 in.**
I_{cr} =	**169.84 in^4**

Cracked at Bottom Transformed Section

Assume the Neutral Axis is above the FRP, making the FRP be in tension.

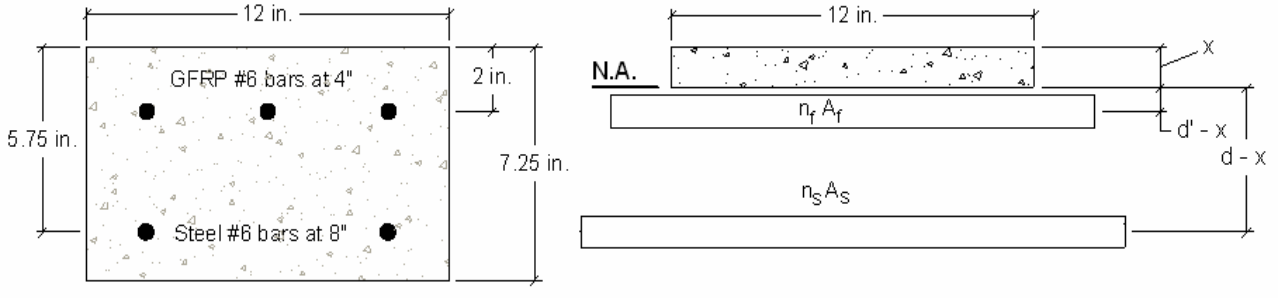

The concrete is in compression at the top:

$$12 \cdot x \cdot \left(\frac{x}{2}\right) = n_f \cdot A_f \cdot (dprime - x) + n_s \cdot A_s \cdot (d - x)$$

To find x, the coefficients to the polynomial were found:

$A*x^2 + B*x + C = 0$

A= 12/2 = 6

$B = A_f*n_f + A_s*n_s$ = 5.386

$C = -A_f*n_f*d' - A_s*n_s*d$ = -24.853

$$x = \frac{-B + \sqrt{B^2 - 4 \cdot A \cdot C}}{2 \cdot A}$$ = 1.635 in. < 2.0 in. FRP is below the neutral axis, therefore assumption was correct.

$x = NA_{cr}$ = 1.635 in.

$c_f = d' - NA_{cr}$ = 0.36 in. Positive since below the neutral axis

$I_{cr} = NA_{cr}^3 + 3*NA_{cr}^3 + A_f*n_f*(NA_{cr}-d')^2 + A_s*n_s*(NA_{cr}-d)^2$

I_{cr} = 81.28 in^4

For 5' slab,

c_f =	**0.36 in.**
I_{cr} =	**406.41 in^4**

B.2 Analysis of Design Truck

E_C = 5097 ksi

A = 452.03 in^2

L = 15.25 ft

Uncracked, I= 1977.34 in^4

Cracked, I_{cr} = 169.84 in^4

Even gauges location (measured from left end): 7.292 ft

Odd gauges location (measured from left end): 7.958 ft

Stress = Mc/I

			Even Gauges				
Distance from centerline (ft)	Location of left tire measured from left end (ft)	Location of right tire measured from left end (ft)	Moment (ft-k)	Uncracked Stress (ksi)	Cracked Stress (ksi)	Uncracked Strain (με)	Cracked Strain (με)
0	1.625	7.625	-1.47	0.0151	0.4255	2.40	67.54
1	2.625	8.625	-10.09	0.1036	2.9205	16.45	463.57
2	3.625	9.625	-14.93	0.1533	4.3214	24.34	685.93
3	4.625	10.625	-15.99	0.1642	4.6282	26.06	734.63

			Odd Gauges				
Distance from centerline (ft)	Location of left tire measured from left end (ft)	Location of right tire measured from left end (ft)	Moment (ft-k)	Uncracked Stress (ksi)	Cracked Stress (ksi)	Uncracked Strain (με)	Cracked Strain (με)
0	1.625	7.625	-1.89	0.019	0.547	3.08	86.83
1	2.625	8.625	-6.81	0.070	1.971	11.10	312.87
2	3.625	9.625	-13.29	0.136	3.847	21.66	610.58
3	4.625	10.625	-15.99	0.164	4.628	26.06	734.63

Appendix C – CR23X Micrologger Programs for Long-term Monitoring

C.1 Gills Creek Bridge

File Name: LONGTERM

```
;{CR23X}
;
*Table 1 Program
  01: 10800     Execution Interval (seconds)

1:  Panel Temperature (P17)
 1: 1        Loc [ PTemp     ]


2:  Thermocouple Temp (DIFF) (P14)
 1: 6        Reps
 2: 21       10 mV, 60 Hz Reject, Slow Range
 3: 3        DIFF Channel
 4: 1        Type T (Copper-Constantan)
 5: 1        Ref Temp (Deg. C) Loc [ PTemp     ]
 6: 2     -- Loc [ Therm1_1  ]
 7: 1.0      Mult
 8: 0.0      Offset

3:  Do (P86)
 1: 41       Set Port 1 High

4:  Beginning of Loop (P87)
 1: 0        Delay
 2: 17       Loop Count

5:  Do (P86)
 1: 72       Pulse Port 2

6:  Delay w/Opt Excitation (P22)
 1: 1        Ex Channel
 2: 0        Delay W/Ex (units = 0.01 sec)
 3: 1        Delay After Ex (units = 0.01 sec)
 4: 5000     mV Excitation

7:  Full Bridge (P6)
 1: 1        Reps
 2: 21       10 mV, 60 Hz Reject, Slow Range
 3: 1        DIFF Channel
 4: 1        Excite all reps w/Exchan 1
```

```
 5: 5000     mV Excitation
 6: 8     -- Loc [ StrainGag ]
 7: 1.0      Mult
 8: 0.0      Offset

8:  End (P95)

9:  Do (P86)
 1: 51       Set Port 1 Low

10:  Do (P86)
 1: 43       Set Port 3 High

11:  Beginning of Loop (P87)
 1: 0        Delay
 2: 6        Loop Count

12:  Do (P86)
 1: 74       Pulse Port 4

13:  Excite-Delay (SE) (P4)
 1: 1        Reps
 2: 15       5000 mV, Fast Range
 3: 3        SE Channel
 4: 2        Excite all reps w/Exchan 2
 5: 100      Delay (units 0.01 sec)
 6: 2500     mV Excitation
 7: 25    -- Loc [ Thermist1 ]
 8: .001     Mult
 9: 0.0      Offset

14:  Polynomial (P55)
 1: 1        Reps
 2: 25    -- X Loc [ Thermist1 ]
 3: 25    -- F(X) Loc [ Thermist1 ]
 4: -104.78  C0
 5: 378.11   C1
 6: -611.59  C2
 7: 544.27   C3
 8: -240.91  C4
 9: 43.089   C5

15:  Vibrating Wire (SE) (P28)
 1: 1        Reps
 2: 4        SE Channel
 3: 2        Excite all reps w/Exchan 2
```

```
 4: 4        Starting Freq. (units = 100 Hz)
 5: 10       End Freq. (units = 100 Hz)
 6: 500      No. of Cycles
 7: 500      Rep Delay (units = 0.01 sec)
 8: 31    -- Loc [ Vibwir1   ]
 9: 3194     Mult
10: 0.0      Offset

16:  End (P95)

17:  Do (P86)
 1: 53       Set Port 3 Low

18:  Do (P86)
 1: 10       Set Output Flag High (Flag 0)

19:  Real Time (P77)
 1: 1110     Year,Day,Hour/Minute (midnight = 0000)

20:  Sample (P70)
 1: 7        Reps
 2: 1        Loc [ PTemp     ]

21:  Sample (P70)
 1: 17       Reps
 2: 8        Loc [ StrainGag ]

22:  Sample (P70)
 1: 6        Reps
 2: 25       Loc [ Thermist1 ]

23:  Sample (P70)
 1: 6        Reps
 2: 31       Loc [ Vibwir1   ]

*Table 2 Program
  02: 0.0000    Execution Interval (seconds)

*Table 3 Subroutines

End Program
```

C.2 I-81 Weigh Station Slab

File Name: NICKSLAB

```
;{CR23X}
;
*Table 1 Program
  01: 3600        Execution Interval (seconds)

1:  Panel Temperature (P17)
 1: 1        Loc [ PTemp     ]


2:  Thermocouple Temp (DIFF) (P14)
 1: 6        Reps
 2: 21       10 mV, 60 Hz Reject, Slow Range
 3: 3        DIFF Channel
 4: 1        Type T (Copper-Constantan)
 5: 1        Ref Temp (Deg. C) Loc [ PTemp     ]
 6: 2     -- Loc [ Therm1_1  ]
 7: 1.0      Mult
 8: 0.0      Offset

3:  Do (P86)
 1: 41       Set Port 1 High

4:  Beginning of Loop (P87)
 1: 0        Delay
 2: 13       Loop Count

5:  Do (P86)
 1: 72       Pulse Port 2

6:  Delay w/Opt Excitation (P22)
 1: 1        Ex Channel
 2: 0        Delay W/Ex (units = 0.01 sec)
 3: 1        Delay After Ex (units = 0.01 sec)
 4: 5000     mV Excitation

7:  Full Bridge (P6)
 1: 1        Reps
 2: 21       10 mV, 60 Hz Reject, Slow Range
 3: 1        DIFF Channel
 4: 1        Excite all reps w/Exchan 1
 5: 5000     mV Excitation
 6: 8     -- Loc [ StrainGag ]
 7: 1.0      Mult
 8: 0.0      Offset

8:  End (P95)
```

```
9:  Do (P86)
 1: 51       Set Port 1 Low

10:  Do (P86)
 1: 10       Set Output Flag High (Flag 0)

11:  Real Time (P77)
 1: 1110     Year,Day,Hour/Minute (midnight = 0000)

12:  Sample (P70)
 1: 7        Reps
 2: 1        Loc [ PTemp     ]

13:  Sample (P70)
 1: 13       Reps
 2: 8        Loc [ StrainGag ]

*Table 2 Program
  02: 0.0000    Execution Interval (seconds)

*Table 3 Subroutines

End Program
```

Appendix D – CR23X Micrologger Wiring Diagram for Gills Creek Bridge

D.1 Multiplexer 1 → Campbell

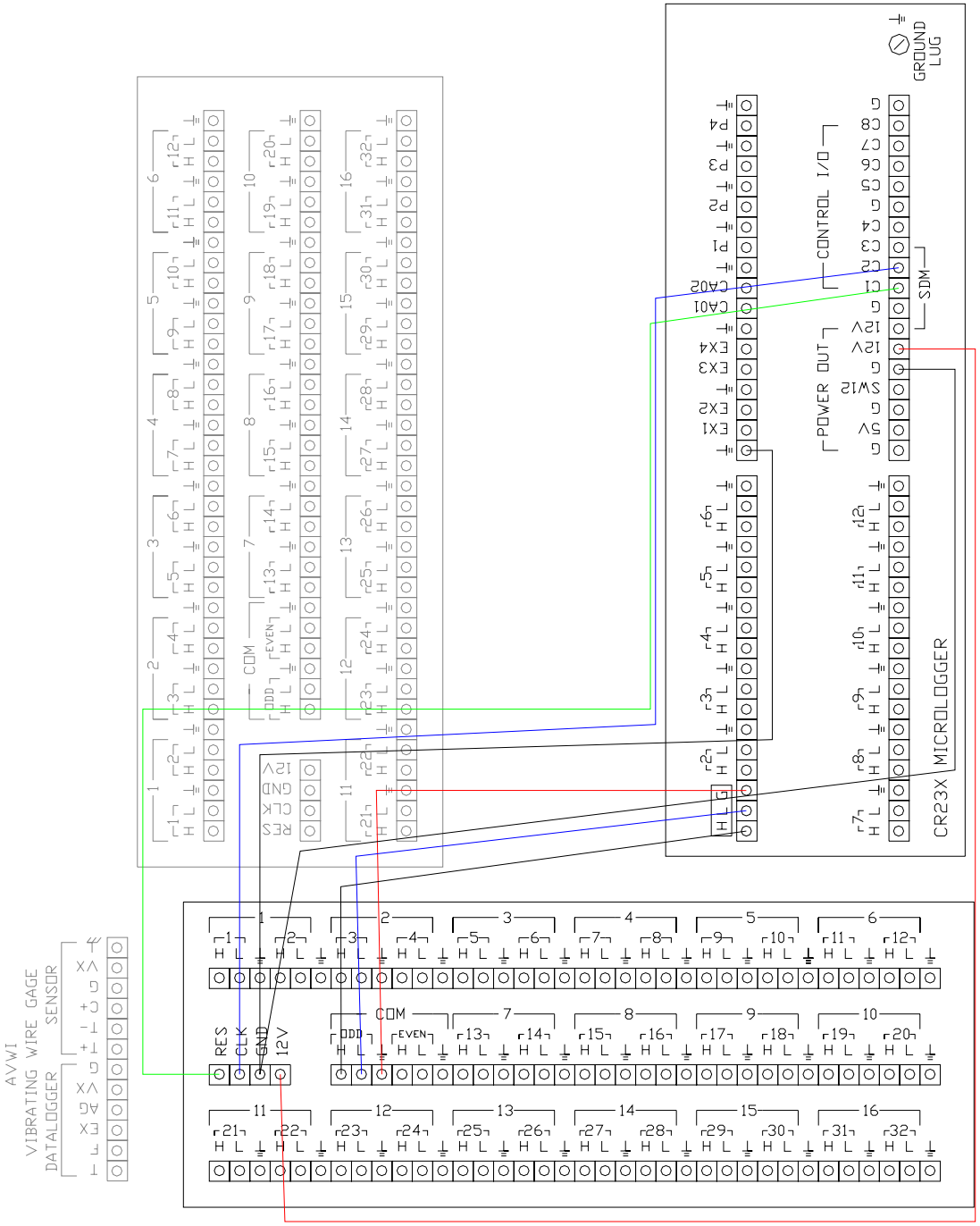

D.2 Multiplexer 2 → Campbell

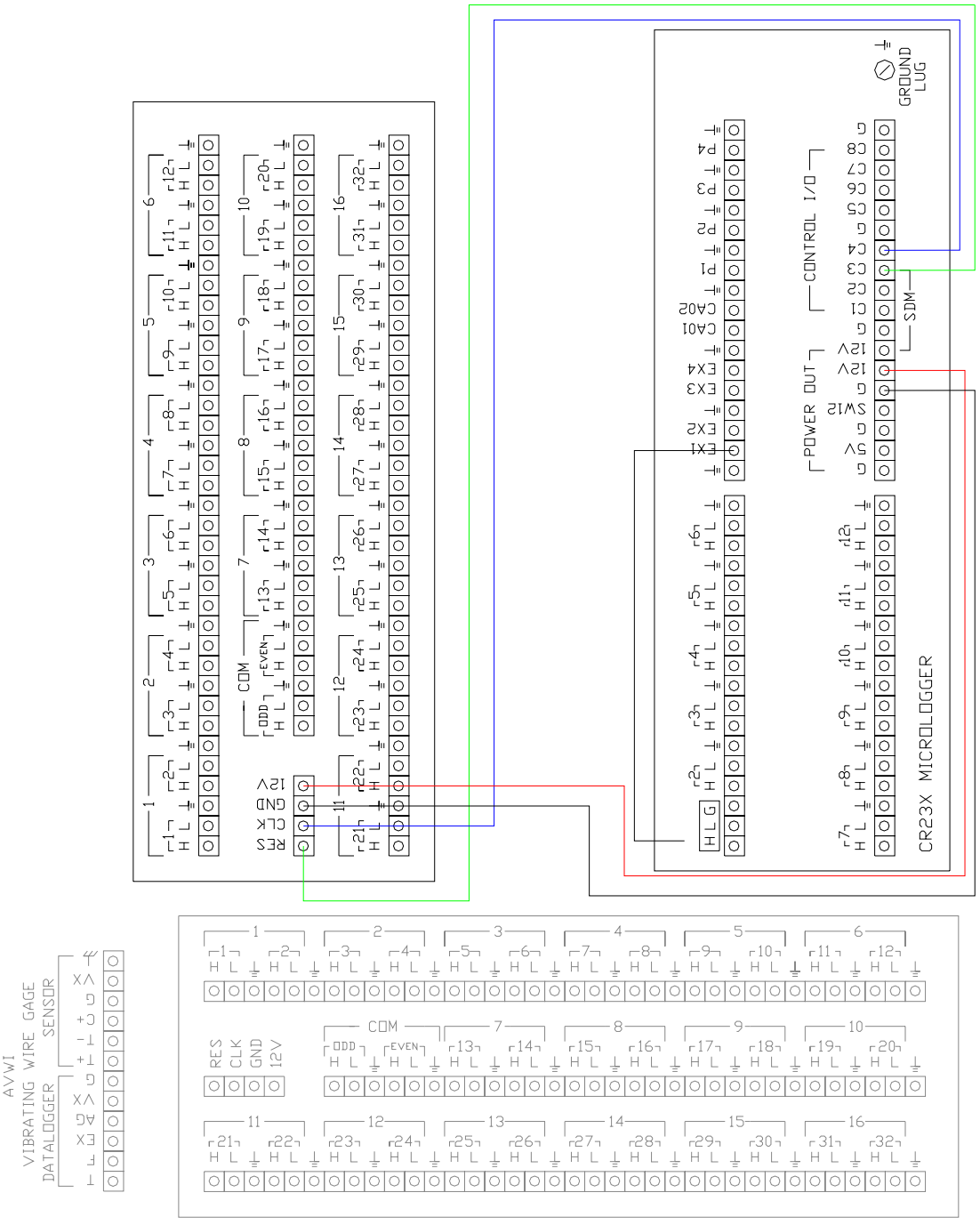

D.3 AVWI Vibrating Wire Gage Connections

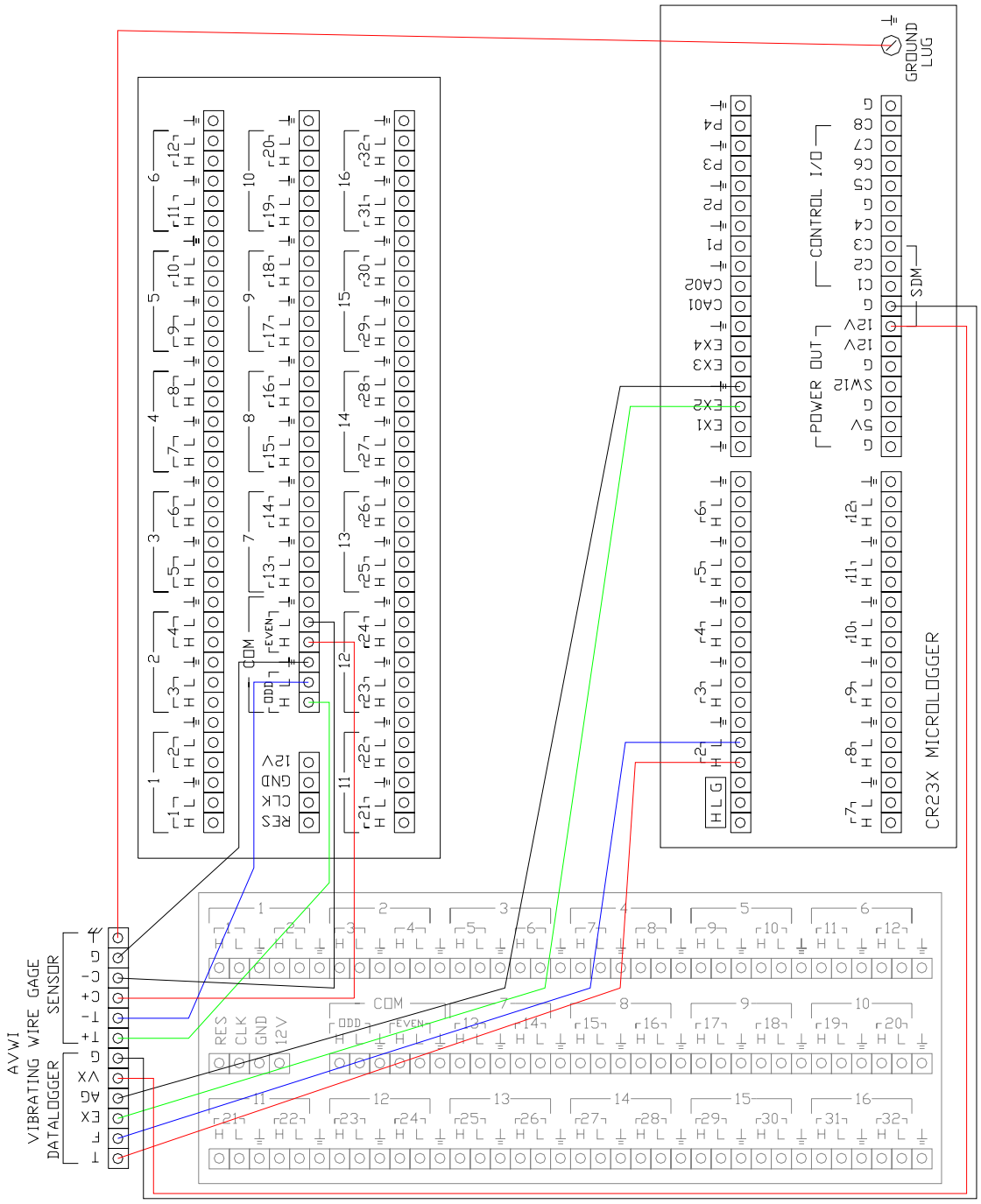

Vita

Kimberly Phillips was born to Carlton and Elberta Phillips on February 26, 1981 in Harrisburg, PA. She was raised in Harrisburg and graduated from Central Dauphin High School in May 1999. She then attended Bucknell University in Lewisburg, PA from 1999 to 2003, where she received her Bachelor of Science degree in Civil and Environmental Engineering, graduating *magna cum laude*. She earned her Master of Science degree in Civil Engineering with an emphasis in Structural Engineering at Virginia Polytechnic Institute and State University in December 2004. Kimberly Phillips accepted a position in December 2004 as a civil engineer with Bechtel Corporation at their Frederick, MD office. She is licensed as an Engineer In Training in the state of Pennsylvania.